# Increasing Soil Compaction Efficiency

An experimental study on biogenic gas formation as a pre-treatment on silt sand mixtures

John Koes

Delft University of Technology

**TU**Delft

# Increasing Soil Compaction Efficiency

An experimental study on biogenic gas formation as a pretreatment on silt sand mixtures

by

## John Koes

to obtain the degree of Master of Science
at the Delft University of Technology,
to be defended publicly on 11 October, 2022 at 10:00 AM.

An electronic version of this thesis is available at `http://repository.tudelft.nl/`.
Cover Image: Preliminary test set up. Photo by: John Koes

**Boskalis**  **TU**Delft

# Acknowledgements

# Abstract

This study aimed to evaluate the field scale potential of Microbially Induced Desaturation (MID) to improve the compactibility of silty sands. Conventional soil compaction techniques for saturated silty sands often require either high compaction effort or even fail to reach aspired relative densities. This thesis is a follow-up study based on the promising small scale results of Stals 2020. The proposed solution consists of a two-stage method in which, firstly, a soil sample was desaturated by means of Microbially Induced Desaturation (MID) through denitrification and, secondly, dynamically compacted. The objective of this, and previous, research was to assess whether biogenic gas formation could be used as a pretreatment to increase the effectivity of soil compaction techniques. Tests with a height of 1m and 2.5m were developed, opposed to the previous 15cm small scale tests. Series of tests were conducted on a silt-sand mixture of 16% fines. Each series was compacted with both a different compaction method and energy input. The investigated scale effects included: the desaturation stage, bubble growth, bubble distribution, gas migration and final degree of compaction. All treated soils were able to desaturate to, and even below the optimum water content. In this research the in-situ shear strength was linked to swelling and bubble production. Based on a qualitative inspection, the gas distribution in the sample was found to be homogeneous over depth. In order to estimate swelling and venting of the sample during the desaturation stage, a model was produced based on a saturation dependent gas conductivity. It was suggested that a continuous gas phase was responsible for the highest amounts of compactive strain. With a non-intrusive compaction method, more compactive energy led to faster, but not more, release of gas. All 2.5m tests ended with a residual amount of gas. A 1m test series, consisting of three tests resulted in higher degrees of compaction for the treated tests opposed to the untreated tests. The final relative density of the treated tests was at least two times higher than the final relative density of the untreated test. A 2.5m test, which included surcharge, had a final RD 2.8 times higher opposed to a similar untreated test without surcharge. Taking into account the uncertainties of the results, it was concluded that a field trial is feasible.

# Contents

# Nomenclature

## Abbreviations

| Abbreviation | Definition |
|---|---|
| Ac | Calcium Acetate |
| AEV | Air Entry Value |
| ASTM | American Society for Testing and Materials |
| BB | Big Bag |
| CDC | Cofra Dynamic Compaction |
| CRR | Cyclic resistance ratio |
| EC | Electrical Conductivity |
| Nit | Calcium Nitrate |
| OWC | Optimum Water Content |
| PVD | Prefabricated Vertical Drain |
| TEA | Technological Economical Assessment |
| SOP | Standard Operating Procedure |
| VWC | Volumetric Water Content |

## Symbols

| Symbol | Definition | Unit |
|---|---|---|
| $c_u$ | Undrained Shear Strength | [kPa] |
| $C_u$ | Uniformity coefficient | [-] |
| $C_z$ | Coefficient of curvature | [-] |
| $D$ | Grain Diameter | [m] |
| $e$ | Void ratio | [-] |
| $G$ | Shear modulus | [kPa] |
| $G_s$ | Specific particle density grains | [-] |
| $LL$ | Liquid Limit | [-] |
| $n$ | Porosity | [-] |
| $PI$ | Plasticity Index | [-] |
| $PL$ | Plastic Limit | [-] |
| $p_c$ | Capillary Pressure | [kPa] |
| $p_n w$ | Pressure, non wetting phase | [kPa] |
| $p_w$ | Pressure, wetting phase | [kPa] |
| $Q$ | Discharge | [L/s] |
| $RD$ | Relative density | [-] |
| $S_g$ | Gas saturation | [-] |
| $S_w$ | Water saturation | [-] |
| $w$ | Gravimetric Water content | [kg/kg] |
| $t$ | Time | [s] |
| $V$ | Volume | [kg/m$^3$]] |
| $v$ | Velocity | [m/s] |
| $\rho_s$ | Grain Density | [kg/m$^3$] |
| $\rho_w$ | Water Density | [kg/m$^3$] |
| $\rho_{wet}$ | Wet Density of soil | [kg/m$^3$] |
| $\rho_{dry}$ | Dry Density of soil | [kg/m$^3$] |

| Symbol | Definition | Unit |
|--------|-----------|------|
| $\rho_s$ | Density | [kg/m$^3$] |
| $\Theta$ | Volumetric water content | [-] |
| $\sigma$ | Soil Stress | [kPa] |
| $\mu$ | Dynamic Viscosity | [kg/(ms)] |

# List of Figures

# List of Tables

# 1

# Introduction

Mankind strives to ensure safety of infrastructure and buildings. The overall design of a certain structure depends on the interplay between the structure itself and the soil properties. On one hand a structural engineer can make design choices with respect to the building in such a way that the design is safe with the given soil properties. On the other hand many design possibilities for the structural engineer may present itself by improving the present soil conditions. Soil improvement techniques have been used by the Romans as early as 100AD (Nicholson, 2014). Presently, as urban space becomes more scarce, technical developments in soil improvement techniques are of great relevance in the building sector. One soil improvement technique is compaction. This research focuses on a way to improve the effectivity of soil compaction by means of a biological pretreatment. Moreover a two stage method is proposed in which, firstly, the soil is desaturated towards the optimum water content before, secondly, the compaction stage is initiated.

## 1.1. Problem statement

The reasons for soil compaction are often well defined. The densification process of compaction aims to acquire enhanced values of shear strength and stiffness. Furthermore, future settlements will decrease. According to Nicholson 2014, the main variables that will affect the degree of compaction are:

- Type of soil
- Method of compaction
- Compactive effort
- Moisture content

Dynamic compaction is most suitable for loose sands (Nicholson 2014). Often with low initial relative densities of 15% to 25%. Furthermore the book states that the best results are acquired when the soil is well drained in combination with a low saturation. The distinction is made between shallow (roughly 0 to 5 m depth) and deep densification (5-15 m). The most efficient way to compact this kind of soils is with the aid of vibrations Nicholson 2014. In figure 1.1 the range of application for deep vibro compaction is further illustrated in figure 1.1.

In practice the ideal situation for this compaction method is not always present. Problems arise when saturated homogeneous soil layers with more than 10 to 15% fines are present (Andrag 2017). In this case, due to lower permeabilities, compaction techniques are not effective as the soil behaves undrained (Raju and Sondermann 2005). Thereby generating pore pressures instead of rearranging the soil skeleton. Ultimately resulting in lower densities than aspired.

Since vibrocompaction is relatively cost effective in contrast to the use of stone columns and other replacement techniques, new ways are developed to increase the range of situations in which this technique can be applied.
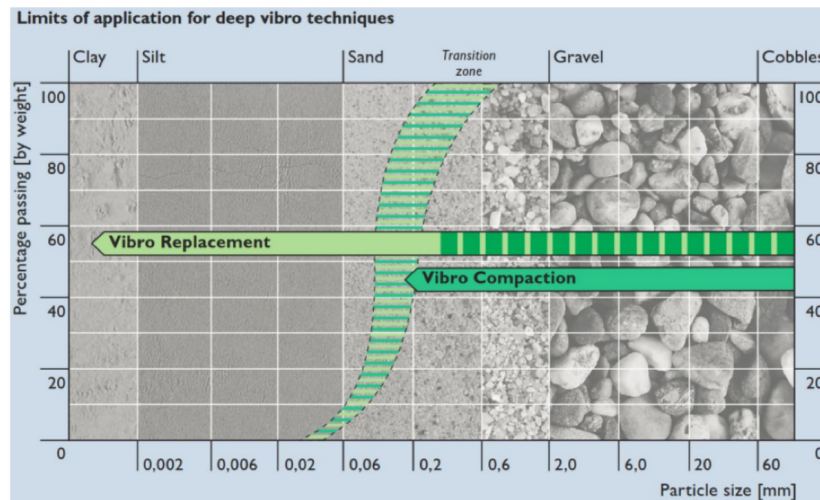
Figure 1.1: Range of soil improvement techniques Keller n.d.

## 1.2. Proposed solution

As previously mentioned, fully saturated homogeneous soil bodies with low permeabilities can be problematic to densify. For fine grained soils, with approximately 20% fines the optimum water content (OWC) is found at a saturation of approximately 80% (figure 2.7). Therefore, it was proposed to desaturate the soil first before the compaction stage will be initiated. Desaturation will be done by providing nutrients to microbes that are naturally present in the soil. The described process of desaturating a soil body using microbes is known as Microbially induced desaturation (MID).

A field trial is planned that includes, at least, three phases. First, the nutrients will be provided to the soil by means of an injection/extraction set up. This injection system will make use of already in place prefabricated vertical drains (PVD's). The second stage comprises of converting the nutrients into biogenic gas. A soil body with a thickness of order magnitude 5m is aimed to be desaturated to the OWC. The produced gas present in the soil body will aid during the final stage, the compaction phase. The soil will be compacted by means of dynamic compaction or vibroflotation.

## 1.3. Objectives

This research presents a series of experimental studies to determine the feasibility of the planned field trial. In order to make the carryover towards practice, a test set up that was representative of in situ conditions needed to be devised. This was done by scaling up the lab tests performed by Stals 2020.

Scaling up and the assessment whether the proposed method also works out on a larger scale is the main objective of this thesis. This research can be seen as an intermediate step between lab testing and field testing. In the end the results will act as a guide towards the pilot in the field. Scaling up the tests leads to the following research targets.

## Degree of compaction

The first target of the research is the same as previous research namely the achieved degree of compaction. The focus will be set on a homogeneous silty sand sample with 10 to 20% fines. To test this, a reproducible placement technique must be devised so that a homogeneously mixed sample is produced. The research target will be to focus on how the degree of compaction changes over time for treated and untreated samples. The main parameters considered will be both the dry density and the resulting relative density of the sample. The results can be used to determine the response of homogeneously mixed silty sand layers when the proposed solution is applied.

## Gas behaviour

A parameter that will change due to scale effects is the overburden. In previous research by Stals 2020 the samples were only 15 cm high. Even then the gas was mostly found in the top of the sample. This phenomenon was also found in samples of Pham 2017. Scaling up the test will increase the overburden pressure. In order to determine whether MIDP can be used in field conditions, the relationship between the overburden and the resulting gas behaviour in the sample will be researched. As the pressure will have an effect on the gas solubility (Henry's law) and the occupied volume of the gas (Ideal gas law). On the other hand, during the compaction phase the overburden will have an influence on the degree of compaction. Compaction methods such as vibroflotation require a certain degree of overburden to work properly. These results will be of importance to determine the feasibility of the method in the field. More specifically how the gas will behave during both the desaturation and compaction stage.

## Compactive effort

The soil will be compacted. When scaling up the test, the method of compaction will change as well. A compaction technique must be devised so that the energy input of the compaction method is comparable to compaction methods in the field. The amount of energy put in the system must be analysed to determine which compaction method is most applicable for the proposed solution. This will be done taking note of the power of the compaction method in combination with the total time of the compaction stage. The product of the two is described as compactive effort.

## Feasibility and recommendations regarding a field trial

In the end the results of this research targets will be combined to make an assessment whether the proposed method is feasible in the field. Whether something is feasible or not depends on a combination of technological achievability and the resulting costs of the proposed method.

A cost-benefit analysis, comparing different solutions will be made. This will include various aspects such as costs of nutrients, but also compactive effort; compactive effort being the combination of required time and energy input. In this research the soil is mixed with nutrients, meaning that The effect of injection/extraction of nutrients is not taken into account. The expected problems of injection/extraction of the nutrients will be touched briefly upon based on literature.

## 1.4. Research questions

The main objective of this research is to determine the feasibility of MIDP being a solution for compaction of silty sands. The means to acquire this objective is to scale up the lab tests performed by Stals 2020.

Naturally the main research question of this thesis remains the same as in Stals 2020.

- Can MIDP be used as a pretreatment to increase the compactability of silty sands?

Scaling up the tests leads to scale effects. The secondary research question, with its corresponding subquestions becomes.

- What are the scale effects, scaling up from previous work?
  (i) What is the relationship between the overburden and the resulting gas distribution?
  (ii) What are the respective gas behaviour mechanisms during gas production ànd gas migration?
  (iii) What is the effect of the overburden on the compaction method?
  (iv) What is the effect of different amounts of compactive effort on treated silty sands mixtures in terms of degree of compaction?

## 1.5. Hypothesis

Scaling up the tests leads to differences in the input conditions. The hypothesis highlights these differences and presents the expected outcome for the desaturation stage and the compaction stage.

### Desaturation stage

Andrag 2017, hypothesised what would happen to treated soil samples. It was stated that during gas formation the soil will desaturate. Additionally, the density will either increase, path (AC), stay the same ,(path AB), or decrease (path AE) (figure 1.2, left). Moreover, it was hypothesised that the desaturation would follow path AB and during the compaction stage the density would go up as the saturation would also go up (path BC).
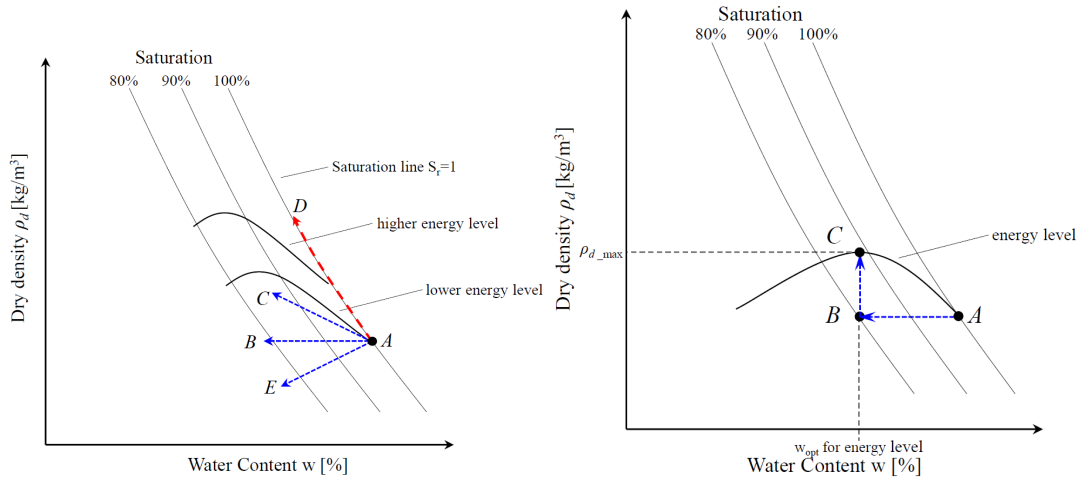


Figure 1.2: Hypothesis, proposed in Andrag 2017

Small scale tests performed by Stals 2020 actually found that neither was the case (figure 1.3). Based on the results it was found that all samples swelled during gas formation, corresponding to path AE in figure 1.2. Furthermore, during compaction not only the saturation and density increased, in all tests of Stals 2020 the water content also decreased.
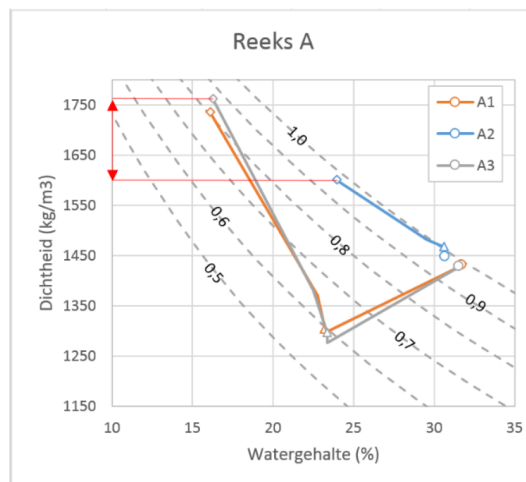


Figure 1.3: Course of gas formation and compaction process of treated (A1,A3) and untreated (A2) samples from: Stals 2020

Scaling up the test will lead to a higher overburden on top, creating a larger stress opposed to the upward force created by gas production. For treated samples it is expected that swelling will take place to a certain degree. However, the swelling will mostly occur at the top of the sample where the gas pressure of produced gas is greater than the overburden pressure. It is hypothesised that a gradient of swelling over the depth of the sample is present, this is illustrated in figure 1.4
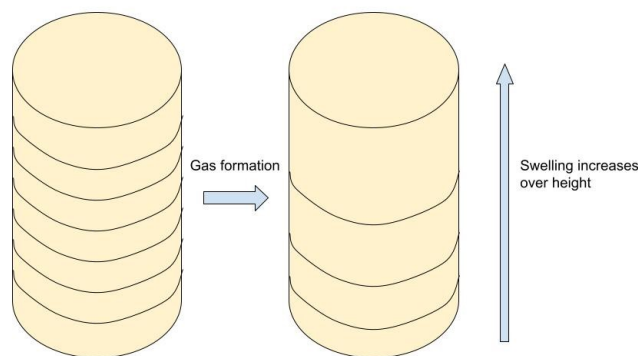
Figure 1.4: Hypothesis regarding swelling, a scehmatic of a soil sample that undergoes gas formation. The top of the right sample has experienced more strain than the bottom.

A larger overburden will result in higher pressures in the sample. Based on Henry's law (2.8) it is expected that a gradient in gas volume over depth is present. Where most of the produced gas volume will be found at the top of the sample, decreasing as the pressure increases.

It is expected that the the average path of a treated sample follows a similar course as the results by Stals 2020. However, in the desaturation phase, the total volume change caused by swelling will be less. Additionally, the degree of saturation after the first phase will be higher as less gas was able to desaturate the soil.

Compaction stage

The travelling distance of fluids will be larger. Gas produced at the bottom of the sample has to travel further. In the results of Stals 2020, the samples were not able to return to a fully saturated state. It is expected that increasing the travelling distance will add to this effect, resulting in an even lower saturation after compaction.

After desaturation it is expected that during compaction, higher amounts of compactive effort, be it in terms of extra time or more energy, will result in a higher saturation closer to full saturation of 1. The reason being that higher amounts of energy will allow for more pathways for the gas to escape.

## 1.6. Scope of work

This research focuses on the following topics.

- A review of literature regarding the current state of microbially induced soil improvement techniques and conventional soil improvement techniques.
- A review of literature regarding gas migration in porous media
- Phase I: The development of a new test set up and a corresponding methodology. Elaborating and scaling up on previous research and tests (Pham 2017; Andrag 2017; Hopman 2018; Stals 2020)
- Phase II: The development of another new test set up and a corresponding methodology. Scaling up again based upon Phase I.
- An analysis on the results and a discussion on the effects of scaling up the proposed method
- A discussion on possible mechanisms for both gas formation and gas migration in the soil sample
- An assessment on the feasibility of the proposed solution for a field trial

# 2

# Review of literature

In order to get an insight of the current state of the research, a literature study was carried out. Thereby the starting point of this thesis is made clear. Additionally, the variables that play a role for the research questions are studied.

## 2.1. Denitrification

Denitrification is a process that reduces nitrate to nitrogen. Biological denitrification involves microorganisms that are the driving factor for the reduction of nitrate (Pham 2017). In anoxic environments microbes consume nitrate in addition to a dissolved organic carbon source for growth and self maintenance (Pham 2017). The most common dissolved carbon source is calcium acetate. The nitrate source is often calcium nitrate, which is also used as fertilizer in agriculture. Using these compounds as nutrients the growth of the biomass, also described as the anabolic reaction, is denoted in Young et al. 2021 as:

$$0.73C_2H_3O_2^- + 0.2NO_3^- + 0.28H_2O \rightarrow CH_{1.8}O_{0.5}N_{0.2} + 0.45HCO_3^- + 0.48OH^- \tag{2.1}$$
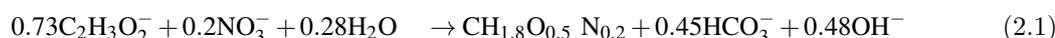
The generation of energy, also described as the catabolic reaction, is given by: Young et al. 2021:

$$C_2H_3O_2^- + 1.6NO_3^- \rightarrow 0.8\,N_2(\,g) + 2HCO_3^- + 0.2H_2O + 0.6OH^- \tag{2.2}$$
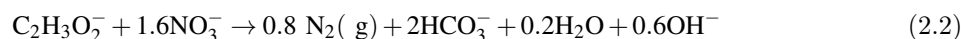
Together they make up for the metabolic reaction. Presented in figure 2.1. The stoichiometry of this metabolic reaction depends on the growth rate of the microbes. In this research the maximum growth rate will be held as a standard.
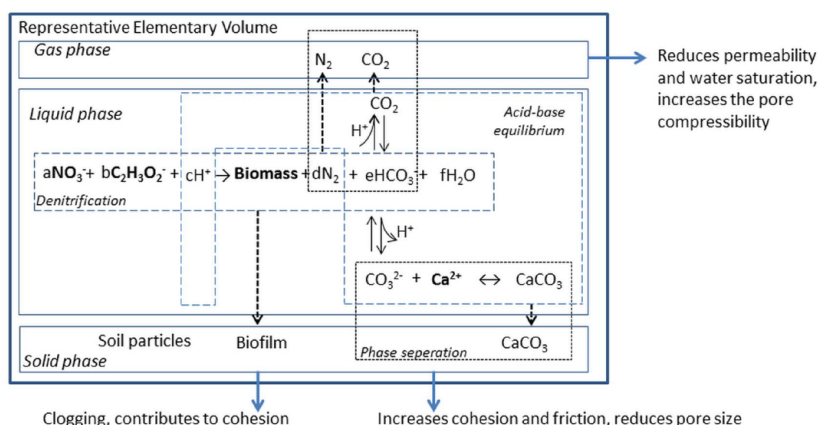


Figure 2.1: "Calcium carbonate precipitation and its potential impact on a unit volume of soil." (Pham, 2017)

The stoichiometry for peak growth was determined by Pham 2017 and is presented as:

$$1.21C_2H_3O_2^- + 0.97NO_3^- + 0.76H^+ \rightarrow 1CH_{1.8}O_{0.5}N_{0.2} + 1.41HCO_3^- - +0.39N_2 + 0.59H_2O \tag{2.3}$$
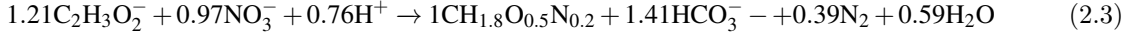
During the reaction bicarbonate ($HCO_3^-$) is produced, which is alkaline. Due to the provided nutrients, dissolved calcium ions are present. Calcium ions and bicarbonate may precipitate as calcium carbonate ($CaCO_3$) (Young et al. 2021).

$$Ca^{2+} + HCO_3^- \rightarrow CaCO_3(\text{ s}) + H^+ \tag{2.4}$$

The acid may react with some of the remaining bicarbonate to carbonic acid. This compound is relatively unstable, ultimately leading to the production of carbon dioxide and water.

$$HCO_3^- + H^+ \rightarrow H_2CO_3 \rightarrow CO_2(\text{ g}) + H_2O \tag{2.5}$$
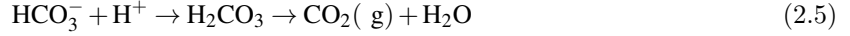
The produced acid buffers the pH. This is of great relevance, as fluctations in the pH may lead to nitrate not fully being converted. All intermediate products, nitrite ($NO2^-$), nitrous oxide ($NO$) and nitrous dioxide ($N_2O$), are harmful to the environment and living organisms Pham 2017. Furthermore, nitrite inhibits microbial growth, resulting in less gas being produced. The stepwise denitrification of nitrate is presented in (2.6).

$$NO_3^- \rightarrow NO_2^- \rightarrow NO \rightarrow N_2O \rightarrow N_2 \tag{2.6}$$

Biogenic gas formation focuses on gas production to desaturate the soil. In figure 2.1 this is illustrated as the "gas phase", consisting of nitrogen $N_2$ and carbon dioxide $CO_2$.

## 2.2. Applications of MIDP

### Liquefaction mitigation

Liquefaction is a phenomenon in which the soil behaves like a liquid. It may occur when soils in saturated conditions experience cyclic loads. This causes pore pressure generation. Pore pressures will increase over time if they cannot dissipate quickly enough. In equation (2.7) (Terzaghi, Peck, and Mesri 1996?) it can be seen that as pore pressures keep increasing effective stress of the soil approaches zero, provided that the effective stress remains the same.

$$\sigma_{total} = \sigma_p + \sigma_{eff} \tag{2.7}$$

The loss of effective stress results in a drastic decrease of shear strength. The soil behaves essentially as a liquid and severe consequences may present itself. Risks include loss of bearing capacity and slope failure.

One of the ways to mitigate liquefaction is by desaturation. More specifically microbially induced desaturation (MID) can be used. The in-place gas is able to dampen the forces and thereby, decreasing the amount of pore pressure generated. Thereby the the cyclic resistance ratio (CRR) increases. The CRR is a measure of liquefaction resistance. Studies have shown that the CRR for sandy soils may increase significantly due to desaturation (Tsukamoto et al. 2002,Arab, Shahrour, and Lancelot 2011, Yang, Savidis, and Roemer 2004,Okamura and Soga 2006).

Earthquakes are known to produce cyclic loads and are thus a cause for liquefaction. Therefore liquefaction mitigation plays an important role for earthquake sensitive areas. The advantage of MID is that it can provide a non-intrusive, relatively easy way to mitigate liquefaction and thereby increase the safety for existent structures.

### Reduction of permeability

Decreasing the permeability has many applications. A no flow boundary may be required to reduce seepage, below for example dikes. Khodadadi et al. 2017.

The desaturation process itself leads to the hydraulic conductivity being lower. However this is a reversible process as the soil may become fully saturated again and have the same conductivity characteristics.

Aside from gas production, in figure 2.1 it can be seen that the denitrification process also leads to extra biomass being produced. Furthermore, when multiple flushes of MID are injected and/or are catalysed

using urease, carbonates precipitate (MICP). The produced biomass and precipitated carbonates may clog the pores of a soil body. This way, the permeability can be reduced. The advantage is that this is an irreversible permeability reduction Pham 2017.

### Increasing soil compactibility

As described in the proposed solution 1.2 MID can be used to increase soil compactibility. Multiple research has been conducted on the matter (Andrag 2017, Hopman 2018 and Stals 2020).

Both Andrag 2017 and Hopman 2018 showed that desaturation to a water saturation of 80% was possible. Both researches made use of a rowe cell to investigate whether "The same degree of compaction can be achieved with less compaction effort" or similarly "A higher degree of compaction with the same amount of compaction effort". Andrag 2017; Hopman 2018 found that the way compaction effort is put in the system is of great relevance. It was concluded that for static loading the proposed two stage method does not lead to significant increase in compaction efficiency. Inconclusive results were found and it was suggested to move from a static compaction method to a dynamic compaction method.

Stals 2020, made use of a set up that consisted of 15cm high cylinders. A dynamic compaction method was implemented by means of a vibratory table. Contrary to the Rowe cell, this new set up did lose the ability to pressurize the sample.

dynamic loading did lead to higher degrees of compaction Stals 2020. This result is in correspondence with Nicholson 2014 who states that vibrations are the most effective way to compact soils.
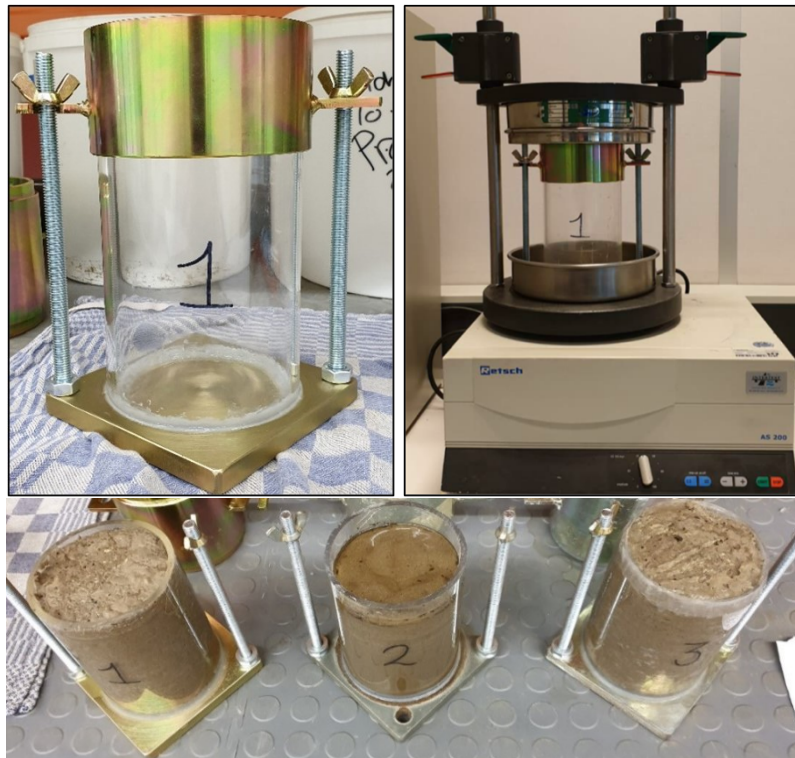


Figure 2.2: Experimental set up by Stals 2020

In figure 2.3 the dry density over time was plotted against the corresponding water content. From right to left the following stages are described: The initial deposited state (1). For treated test the desaturation stage was accompanied with swelling of the samples (2). After the desaturation stage both untreated and treated samples were compacted (3). It can be seen that, with the same compactive effort, a higher final density of treated tests was achieved opposed to untreated tests. The difference in final density is denoted as the profit of the proposed solution (4).
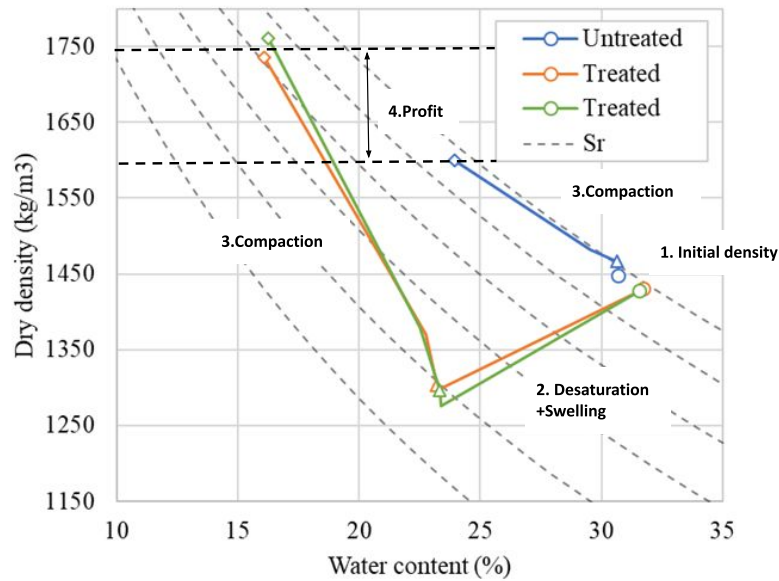
Figure 2.3: Dry density vs water content over time for one untreated test and two treated tests. The dashed lines correspond to saturation contours (from: Stals 2020, edited)

In the experiments it was shown that the final relative density of treated soils after compaction could be as high as a factor two times higher, opposed to untreated soils. This factor was described as the improvement ratio. The fine fraction played a major role for this parameter. It was found that the optimum range for which the treatment yielded the best results was from 10% fines to approximately 20% fines (figure, 2.4). Below this range, conventional compaction techniques suffice and above this range the proposed method was not effective.
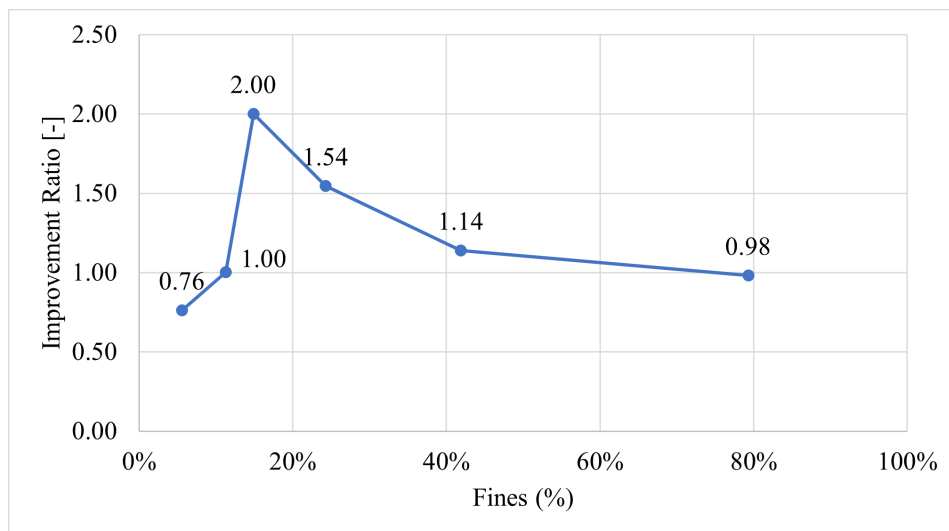


Figure 2.4: "Ratio between the relative densities of treated and untreated samples for different fines percentages" Stals 2020
.

## 2.3. Gas behaviour in porous media

### Gas nucleation and bubble growth

Initially the soil skeleton is assumed to be fully saturated. As mentioned during the reaction nitrogen is produced. This is produced in a dissolved state first, with the concentration of gas increasing over

time. The concentration of dissolved gas is dependent on the amount of Nitrogen produced by MIDP. A prerequisite for bubbles to nucleate is that the concentration of dissolved gas reaches a supersaturation state, accordingly with Henry's law (equation 2.8).

$$K_h = \frac{C_g}{p_g} \tag{2.8}$$

With $K_h$ being Henry's constant, $C_g$ the dissolved gas concentration in liquid phase and $p_g$ the partial pressure in the gas phase.

Whether a bubble nucleates is dependent on the pressure difference. The pressure difference can can be expressed as an energy barrier that needs to be exceeded to nucleate a bubble. The energy barrier originates from the surface tension of pore water. Which in term is related to the La-place pressure equation:

$$\Delta p = \frac{2\sigma}{r} \tag{2.9}$$

With

$\Delta p$:     The excess pressure in $Pa$
$\sigma$:     The surface tension in $N/m$
$r$:     The bubble radius in $m$

In formula 2.9 it can be seen that as the bubble radius (r) increases, the excess pressure decreases (with $\sigma$ held constant). Following this process nucleation happens preferentially at larger pores, resulting in a heterogeneous distribution of gas bubbles throughout the available pore space (Van Kessel and Van Kesteren 2002).
Smaller bubbles and dissolved gas will have a higher pressure than larger bubbles. This pressure difference results in a migration process that leads to smaller bubbles merging with larger bubbles (Kessel 1998). In Mahabadi, Zheng, et al. 2018 this process is called bubble coalescence. Bubble coalescence may even lead to horizontal gas lenses that cause a disconnected wetting phase. When this phenomenon presents itself the whole soil body on top of this lens attains an upward pressure due to buoyancy. As a result a jump in hydraulic pressure may be expected.

As the volume of gas increases over time, two mechanisms are recognized by Kessel 1998:

(i) The bubble deforms the soil matrix, or;
(ii) The bubble moves through the soil matrix without deforming it and with that expulses water out of the soil body.

## Mechanism I, The bubble deforms the soil matrix
If this mechanism applies then Equation (2.9) is adjusted. The required pressure for bubble growth is described in Schotmeyer 1998 and Vesic 1964:

$$\Delta p = \frac{4}{3}c_u \left[ 1 + \ln\left(\frac{G}{c_u}\right) + \ln\left(1 - \left(\frac{r}{r_1}\right)^{-3}\right) \right] \tag{2.10}$$

With:

$\Delta p$     Pressure difference Pa
$c_u$     Undrained shear strength Pa
$G$     Shear modulus Pa
$r(t)$     Bubble radius at a certain moment in time (m)
$r_1$     Initial bubble radius before gas production (m)

As $r \xrightarrow{\cdot} \infty$, formula (2.10) becomes dependent on the shear strength $c_u$ and the shear modulus $G$. However, in Kessel 1998 it is stated that this formula is not accurate for sands because preferential flow through

arise. Principle pathways for the gas or, as Zeng et al. 2021 describes, hydraulic fractures may occur when the gas pressure exceeds the fracturing initiation pressure. Thereby breaking up the soil and creating a vent for the gas to escape. For sands this pressure is considered to be equal to the confining pressure Zeng et al. 2021.

## Mechanism II, Rigid soil skeleton

After a bubble nucleates the pressure of the non-wetting phase increases. The mensicus moves towards the pore throat. During this phase the pressure that is required for the bubble to grow is described as in (2.9).

At a certain moment in time the gas bubble is stuck in a pore. During this phase the gas pressure keeps increasing. At a certain moment in time the gas pressure exceeds a threshold, the air entry value (AEV). When the AEV is exceeded the non-wetting phase "jumps" through the pore throat. Thereby volume of the gas increases and the gas pressure drops accordingly with the ideal gas law. These jumps are known as Haines jumps, summarised in figure 2.5. This mechanism is based on the paper of Young et al. 2021.
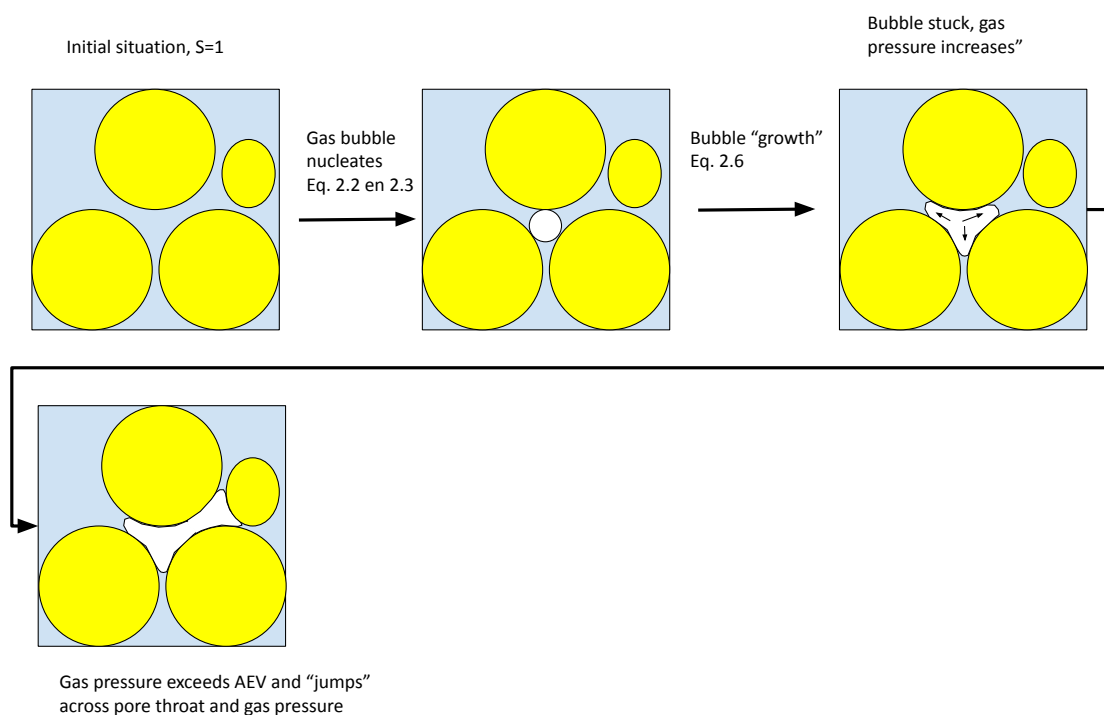


Figure 2.5: Schematic of gas formation and Haines Jumps under the assumption of 'rigid' soil skeleton

As the bubble migrates, simaltaneously, the pore water is driven out. Additionally a plug in the pore throat can be formed by residual liquid of the wetting phase (figure 2.6).
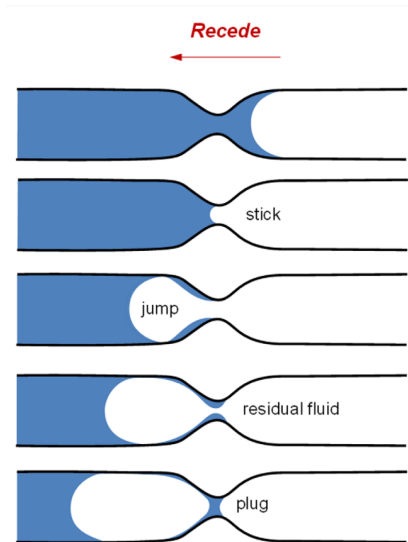
Figure 2.6: Plug forming of residual liquid during gas migration (from Junbong Jang, Sun, and Santamarina 2016

### Gas migration in slurry's and liquefied soils

In slurry's gas bubbles may migrate upwards due to buoyancy. For sludge, the following criterium was set up by Nguyen and Boger 1992:

$$r_{\text{crit}} = f \frac{c_{\text{u}}}{\rho g} \tag{2.11}$$

With:

| | |
|---|---|
| $r_{crit}$ | Critical radius of bubble (m) |
| $f$ | Form factor (-) |
| $\rho$ | Density of the slurry kg/m3 |

It was stated in Kessel 1998 that this mechanism only applies for bubbles with radii of several decimeters, considering an undrained shear strength of 1 kPa. In practice bubbles will have found a way out of the system along preferential flow paths before these bubble sizes can be achieved. In general bubbles for sludges, bubbles with a radius 0.1-1 cm are observed Kessel 1998.

Stoke's law can be applied to determine the settling velocity for a sphere in a viscous liquid.

$$v = \frac{2}{9} \frac{(\rho_p - \rho_{\text{f}})}{\mu} g R^2 \tag{2.12}$$

With:

| | |
|---|---|
| $v$: | The velocity of a sphere |
| $g$: | The gravitational acceleration $(m/s^2)$ |
| $R$: | The radius of the spherical particle (m) |
| $\rho_p$: | The mass density of the particle $(kg/m^3)$ |
| $\rho_f$: | The mass density of the fluid $(kg/m^3$ |
| $\mu$: | The dynamic viscosity (kg/(ms)) |

When a soil liquefies one could simplify gas migration and suppose that the soil behaves as a viscous fluid and gas migration may be simplified using Stoke's law. The advantage is that gas pressures do not have to be determined.

## 2.4. Optimum water content

One of the variables that is of major influence on the compaction process is the water content of the soil. This is elaborated upon by means of the proctor test. The proctor test ensures a standardized compaction energy input. When varying the water content, an optimum water content is observed for which the highest dry density (for that particular energy input) is reached. This is shown in figure 2.7.
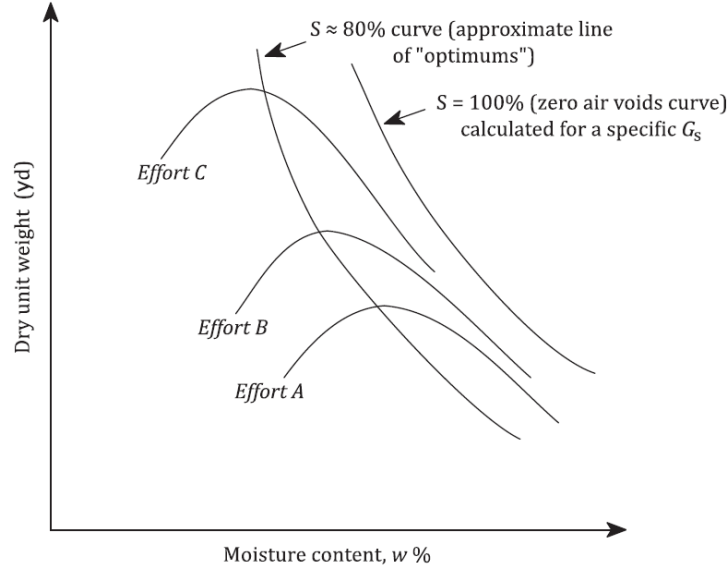


Figure 2.7: Dry unit weight vs moisture content for a sample compacted at three different levels of compaction effort (effort A< effort B< effort C) (from: Nicholson 2014).

The course of the lines can be explained in twofold. Starting on the right hand side, i.e. a fully saturated soil. The pore volume is filled with (almost) in-compressible water which inhibits further compaction of the soil. In this case the water content will be the limiting factor. On the other side of the spectrum the soil can be too dry. According to (Fredlund and Rahardjo 1993) the matric suction is highest at low water contents. In this case this paramater is the limiting factor for the densification process. In figure 2.7 it can be observed that for fine soils the optimum saturation of the soil is around 80%. Nicholson 2014 states that, in general, as the plasticity of a soil increases the maximum dry density and optimum water content also increase.

During the process described above the matric suction, is also described in literature as the capillary pressure. Which is defined as the difference between the wetting, in this case water, and the non-wetting fluids, gas.

$$p_g = p_c + p_w + p_{atm} \tag{2.13}$$

In which:

$p_g$      Gas pressure [kPa]
$p_c$      Capillary pressure [kPa]
$p_w$      Water pressure [kPa]
$p_{atm}$      Atmospheric pressure [kPa]

According with equation (2.13) as the gas pressure comes into contact with the atmosphere the gas pressure ($p_g$) becomes equal to the atmospheric pressure ($p_{atm}$). The capillary pressure then becomes equal to the negative water pressure. In that case the capillary pressure aids in the compaction process. In coarse materials, such as gravels, proctor tests present a less curved and more flat line. Coarse materials have larger pore throats, according with (2.9) this results in lower capillary pressures. Therefore

an optimum water content is not so pronounced.

Based on figure 2.7, it is clearly outlined that a higher dry density can be achieved with equal energy input. This was the starting point for previous studies (paragraph 2.2.

## 2.5. Vibroflotation

Vibroflotation, is able to compact loose granular soils up to 10% fines . The method makes use of an intrusive vibrating needle that produces horizontal vibrations to densify the surrounding soil. Depths of order magnitude of 10's of meters can be compacted, however the first few meters are not compacted effectively due to the lack of overburden. The head of the vibroflot uses water a water jet to liquefy a small portion of the soil around the needle, which makes soil penetration to the maximum desired depth possible. As the vibroflot is held at a certain depth the soil is densifies. Thereby, the power to keep the same frequency of the engine increases. The required power is often measured by means of the oil pressure of the system and it is correlated to the in-situ density. Once the desired density is reached the vibroflot is moved upwards to the next successive depth.
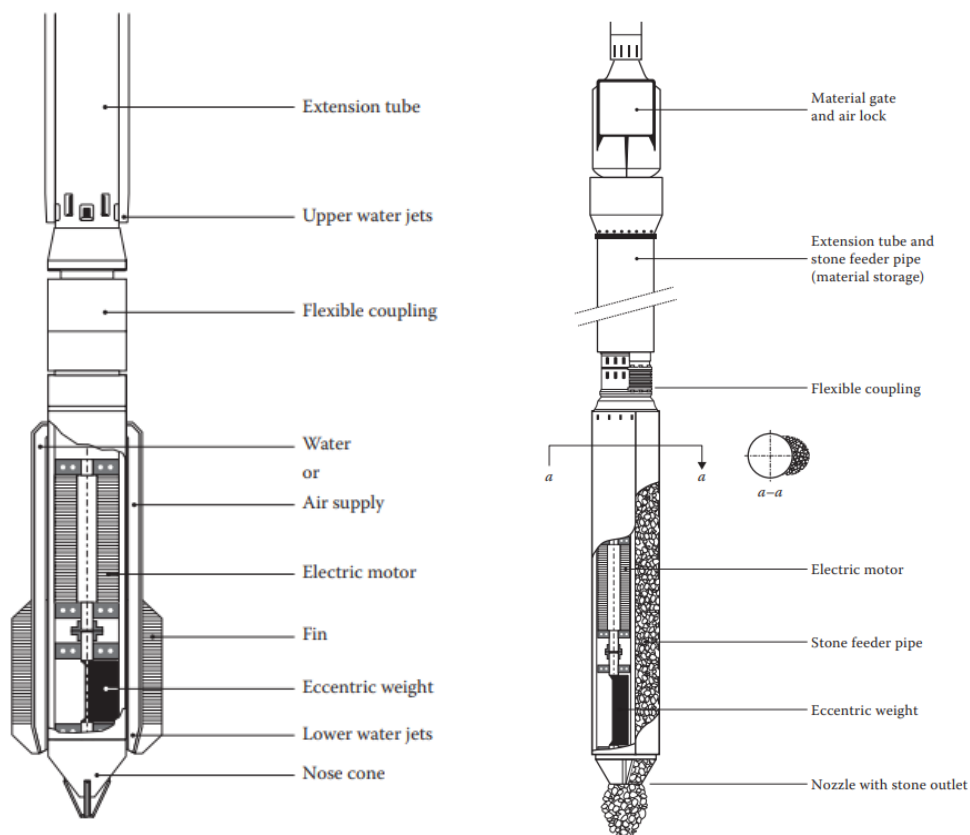


Figure 2.8: Vibroflot and vibroflot used for vibro replacment K. Kirsch and F. Kirsch 2017

Radially, an ideal soil response of granular materials is characterized by four zones. At the vibrating probe the soil is fluidized (1) . As the distance from the vibrating probe increases, the plastic (2), compaction (3) and elastic zone (4) are encountered (figure 2.9).
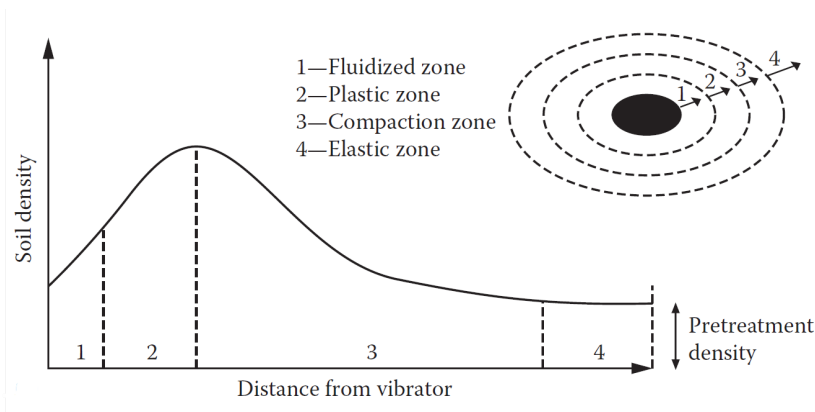
Figure 2.9: Idealised response of granular soils when a depth vibrator is applied. (From:K. Kirsch and F. Kirsch 2017, after Rodger, A.A., Vibrocompaction of cohesionless soils, Internal Report, R.7/79, Cementation Research Limited, Croydon, UK, 1979.)

In figure 2.9 it can be observed that the compaction zone is actually not found at the vibratory probe itself. The rearrangement of the soil skeleton depends on the ability to overcome the shear strength. It was found that the required particle accelelartion to achieve this was 0.5g. Furthermore, K. Kirsch and F. Kirsch 2017 states that the compaction zone is found when the particles reach an acceleration of approximately 1g (figure 2.10)
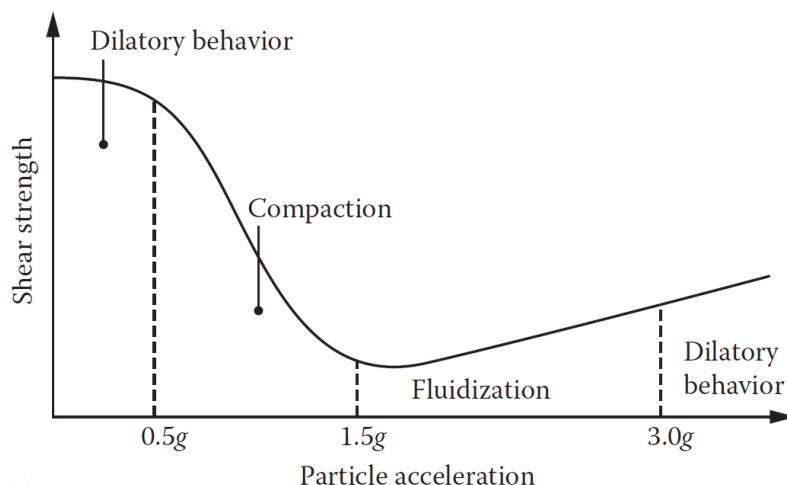


Figure 2.10: Particle acceleration against shear strength from: Nicholson 2014

Due to the cohesive nature of soils with more than 10% fines the vibrations of the depth vibration do not lead to desired results K. Kirsch and F. Kirsch 2017.

## 2.6. Vibroreplacement technique, stone columns

An alternative solution when vibroflotion is not suitable is stone columns. In figure 2.8, right, a schematic of a modified vibroflot is illustrated. Two types of stone column techniques can be used depending on the undrained shear strength.

If the undrained shear strength is around 10-30 kPa. The wet method is often applied, in which the borehole is filled with water. After penetration the probe is completely withdrawn, whereafter the borehole is filled with backfill material. This is top feed of stones is preferably done in batches after which the probe is used to tamp down the columns, increasing the density even more.

If stiffer material is encountered with an undrained shear strength it can be opted to use a dry, bottom feed, method. In this method the vibrator deposits the stones from the tip of the probe (figure 2.8, right).
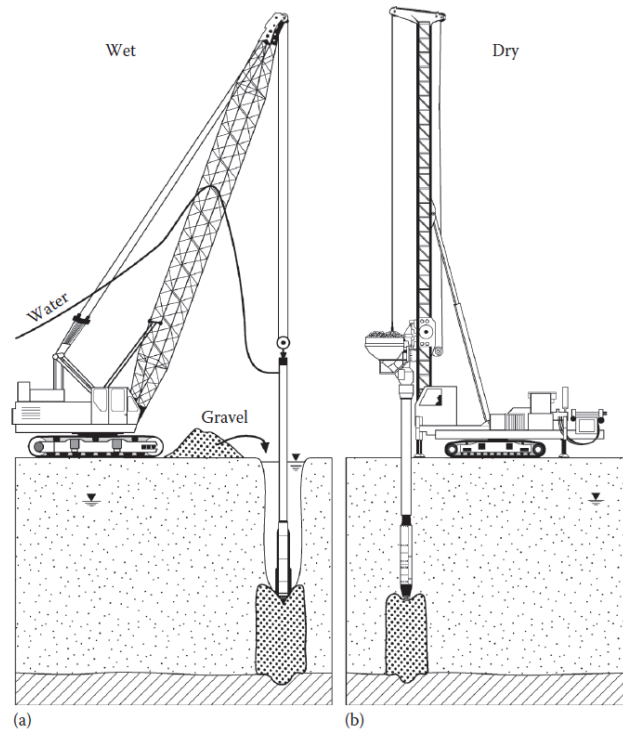
Figure 2.11: Schematic of vibroreplacement by means of stone columns. Figure (a) shows a wet, top feed, method and figure (b) a dry, bottom feed, method K. Kirsch and F. Kirsch 2017

## 2.7. Dynamic compaction & CDC

In practice, soils up to a depth of 7m are commonly dynamically compacted. Dynamic compaction includes dropping a heavy mass repeatedly on a soil mass. It is a relatively cost effective method. Due to the impact of the weight, craters of 2m can be produced (Nicholson 2014). These craters are backfilled with material, this way the soil is densified. Additionally, at depth the soil is also densified. This secondary densification process is due to the stress wave that is produced by the impact of the weight.



Figure 2.12: Menard's "Giga"compactor drops a 200 ton weight. (from Nicholson 2014, picture of Menard)

CDC (Cofra Dynamic Compaction) is a form of impact compaction and consists of a 9 to 16 tonne mass that is repeatedly hydraulically hammered on the surface. CDC is used for granular materials. The produced vibrations are often adjusted so that the hits of the hammer do not result in liquefaction of the soil. The advantage of impact compaction is that the hammer remains in contact with the surface. Creating a controlled and safe work space. The applied depth of is approximately 4-7m (Nicholson 2014).
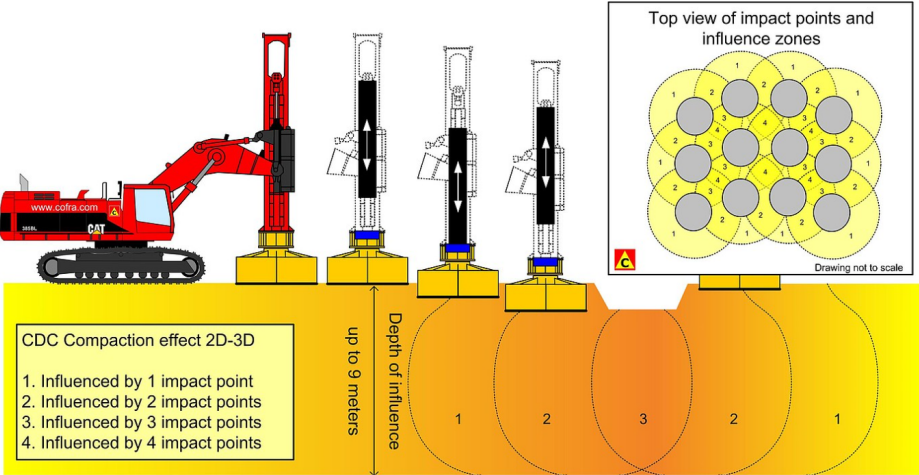


Figure 2.13: Schematic of Cofra Dynamic Compaction (CDC) (from: Cofra n.d.)

# 3

# Material & Soil characterization

This chapter focuses on the test material and characterization thereof. This is done by sieving tests, consistency tests, proctor tests and lastly determination of the maximum and minimum density.

## 3.1. Test Material

The soil was used as a pre-load for a construction site. In order to determine whether the soil was suitable, the fraction of fines was determined by means of a field test. The soil was sampled in a glass jar and mixed with water, the percentage of fines was estimated based on settling speed. Sand was categorised as material that settled after a few seconds. Silt, after approximately 30 seconds and what remained in suspension was determined to be the clay fraction.



Figure 3.1: Sampling of test material by means of a visual settling test, left.
Filling of big bags, middle and right

After the field test it was decided to use the material as the test material. To minimise the effect of heterogeneity the soil was mixed using the crane first. Sequentially ten big bags, corresponding to approximately ten cubic metres of material, were filled.

## 3.2. Grain size distribution

Big bag 6 (label:"BB6") was chosen as the testing bag for the full grain distribution. This was done due to easy access to the big bag. Three samples were taken from the big bag at different elevations in the big bag (up, mid and low). The reason for this approach was that this method of sampling would result

in a conclusion about the variability in a big bag itself. The expectation was set that higher degrees of fines would be found in the lower part of the big bags due to segregation whilst filling the big bags.



Figure 3.2: Sampling of big bag 6 on three different elevations in the big bag, by means of a PVC tube. Due to low cohesion of the soil the pvc tube was hammered in at an angle of roughly 30 degrees from the vertical.

The grain size distribution from $63\mu m - 2000\mu m$ was determined by sieving according to procedure ASTM D6913 (Soil and Rock 2009b) The fraction from $2\mu m - 63\mu m$ was determined using a hydrometer following procedure ASTM7928 ((Soil and Rock 2009a))
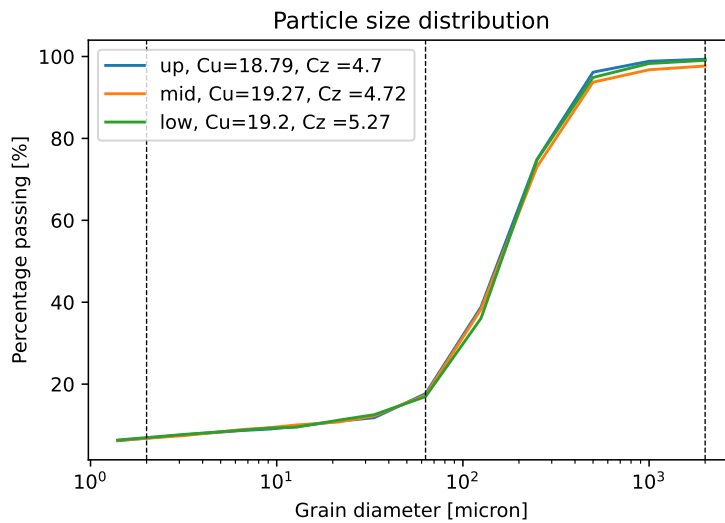


Figure 3.3: Grain size distribution for three samples (up,mid and low), vertical lines represent the boundaries between clay and silt (left), silt and sand (middle) and lastly sand and gravel (right)

The uniformity coefficient and the coefficient of curvature were calculated by:

$$C_u = \frac{D_{60}}{D_{10}} \tag{3.1}$$

$$C_z = \frac{D_{30}^2}{D_{60}D_{10}} \tag{3.2}$$

Table 3.1: Uniformity coefficient and coefficient of curvature for 3 samples

| Sample | Up | Mid | Low |
|--------|------|------|------|
| Cu | 18.79 | 19.27 | 19.20 |
| Cz | 4.70 | 4.72 | 5.27 |

Based on visual inspection of the grain distribution and the high value of $C_u$ it was concluded that the soil was well graded. The percentage of clay was approximately 6.5% for all samples.

Additionally, it was observed that the variability between the samples of BB6 was low. The assumption that the material in every big bag was homogeneous seemed reasonable. On the other hand it should be noted that the sample size was relatively small in comparison to the total amount of soil. For each big bag a sample of around 1 kg was taken, whereas the total mass of a single big bag was approximately 1800 kg. Visual inspection showed that lumps of organic material, clay and rocks were present. The size of these lumps varied between 3 to 15 cm (figure 3.4, right) . The behaviour of the soil mass will be influenced by these lumps, as no gas formation will occur in these lumps. Furthermore, especially the rocks and clay will be difficult to compact with vibrations.



Figure 3.4: Mixed slurry, with lumps of organic material floating on top (left) and encountered rocks in the soil (right)

## 3.3. Fines fraction

Currently, fines are the limiting factor for current vibrocompaction techniques. Therefore it was essential to determine the fines fraction. In total 12 samples were taken, three of which of big bag 6 and 1 of every other big bag. The samples of the other big bags were taken from the top. Although this may not be the most representative sampling method, it was expected that the results will give an insight in the variability between the big bags nonetheless.

The sieving procedure considered sieving each sample through a sieve with an aperture of $63\mu m$. The remaining mass of soil on the sieve was subtracted from the total mass. and the fines fraction was calculated. Figure 3.6 presents the percentage of fines per sample. The maximum and minimum percentage of fines was 18.8% and 13.7 % respectively. It was found that the average degree of fines was 16%. Referring back to the results by Stals 2020 (figure 2.4) it was concluded that with respect to degree of fines the test material was suitable, although 13.7% may be on the low side.

Figure 3.5: Sieving through the 63 $\mu m$ sieve to determine the fines fraction
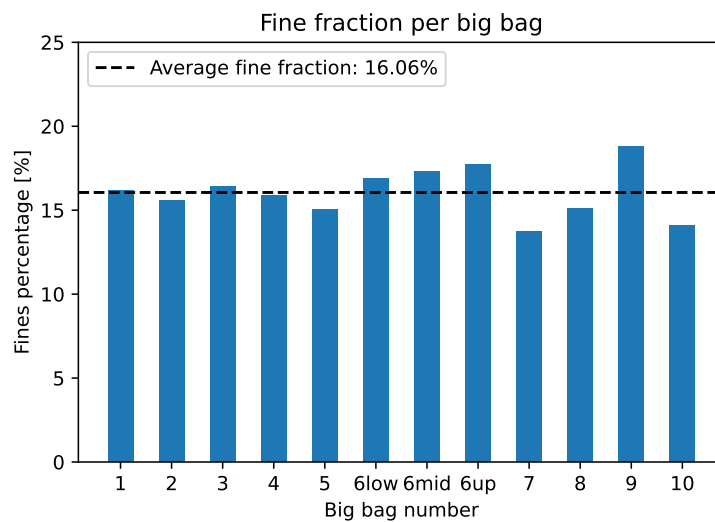


Figure 3.6: Percentage of fines for each sample, including the average percentage of fines

Based on the results presented in figures 3.3, 3.6 it was shown that both the variability in the big bag itself, but also the variability between the big bags falls within reasonable margins. The standard deviation of the fine fraction is calculated to be: $\sigma_{std} = 1.41$

Therefore, as a starting point, the assumption that all material was homogeneous was made. This might be a sensitive assumption, since the sample size was relatively small compared to the entire volume of soil.

## 3.4. Consistency, Atterberger Limits

The Atterberger limits were determined using a falling cone test according to procedure ASTM D4318 using a fall cone apparatus Soil and Rock 2010. It must be noted that the soil was not sieved with a 400 $\mu m$ before starting the test. The fraction of mass above 400 $\mu$ was less than 10% so the effect on the consistency was deemed marginal. The tests were carried out on soil from big bag 6.For this test the average consistency over the entire big bag was desired. As it was not yet known what the variability in each single big bag was, equal parts of bb6up, bb6mid and bb6 low were used.

The shear strength was derived based on the penetration and the mass of the cone (here, 80g).

$$\tau = 0.8 \cdot 9.81 \cdot \frac{m_{cone}}{pen^2} \tag{3.3}$$
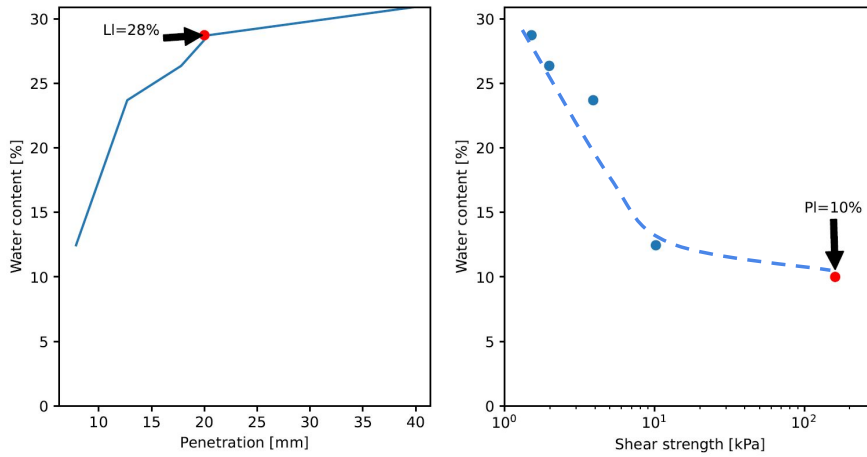
Figure 3.7: Penetration against water content (left) and shear strength against water content for a sample from BB6 (right). Including assumed course of shear strength vs water content.

The liquid limit (*Ll*) corresponds to the water content at a penetration of 20 mm. In this case the liquid limit is found at 28%. The plastic limit is found at a shear strength of 160 kPa. It is expected that the plastic limit was found at a water content of 10%. It should be noted that this an estimated fit. Following equation 3.4, the plasticity index of the soil was estimated to be 18%.

$$PI = Ll = Pl \tag{3.4}$$

Lastly the soil was classified based on the consistency limits based on ASTM D2487 (figure 3.8). It was found that the soil is classified as a low plasticity clay. A low plasticity silt was desired as target soil, however for logistical reasons it was decided to proceed with the soil.
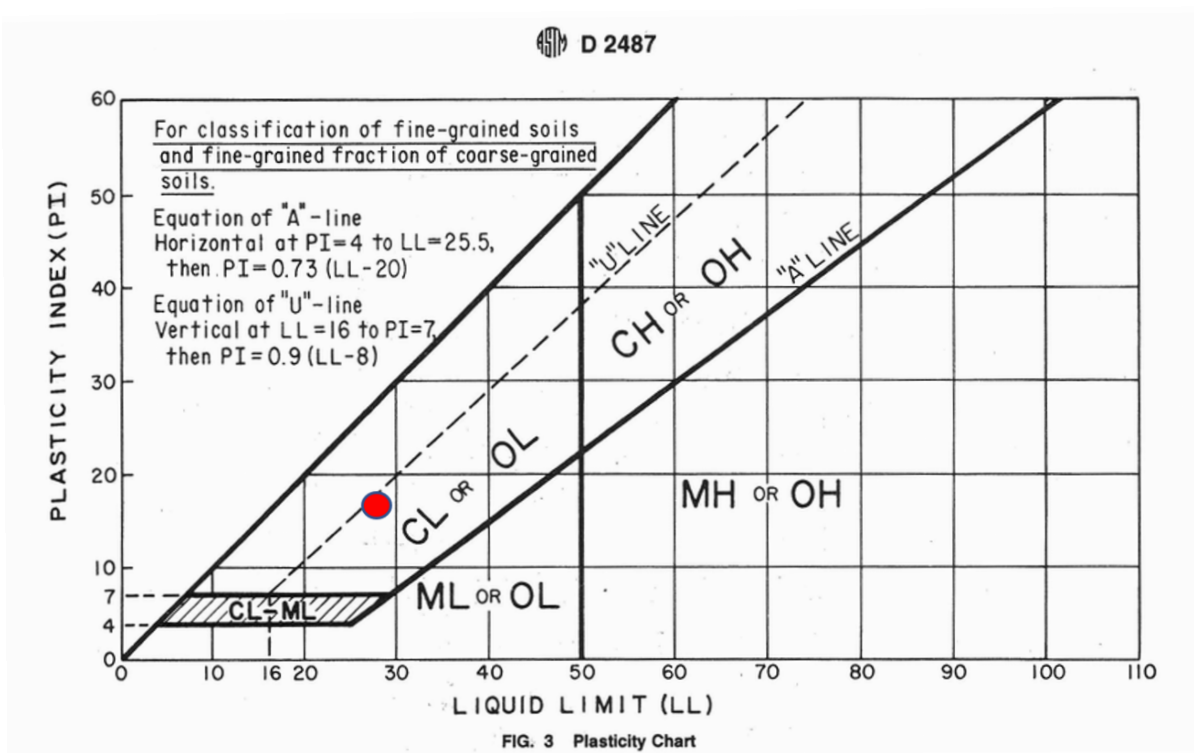


Figure 3.8: Classification of soil using USCS classification chart for fine-grained soils ASTM D2487-17 (2017)

## 3.5. Proctor test

In chapter 2 the optimum water content test was discussed by means of the proctor test. As shown in 3.9, on the y-axis the dry density is plotted and on the x-axis the water content. To give a better insight of the results the saturation lines were also plotted. The saturation lines were plotted based on a rewritten formula of Andrag 2017.

$$w = \frac{(S_{0-1} - 1) * (1 - \frac{\rho_{dry}}{\rho_s}) - \frac{\rho_{dry}}{\rho_s} + 1}{\rho_{dry} - 1} \tag{3.5}$$

In this formula a specific saturation value, for example S=0.5 was taken. Then, for a range of dry densities (in figure 3.9 1600 $kg/m^3$ to 1850 $kg/m^3$) the corresponding water contents were calculated, accordingly with 3.5. With the dry density and the water contents known, the saturation contour was plotted. Sequentially, the following value for the saturation was taken and this process was repeated. In essence, the above describes a nested loop where for every saturation value say (0.5 to 1) and for every dry density (1600 $kg/m^3$ to 1850 $kg/m^3$) the water contents were calculated. In future plots plotted saturation lines were calculated with the same approach.
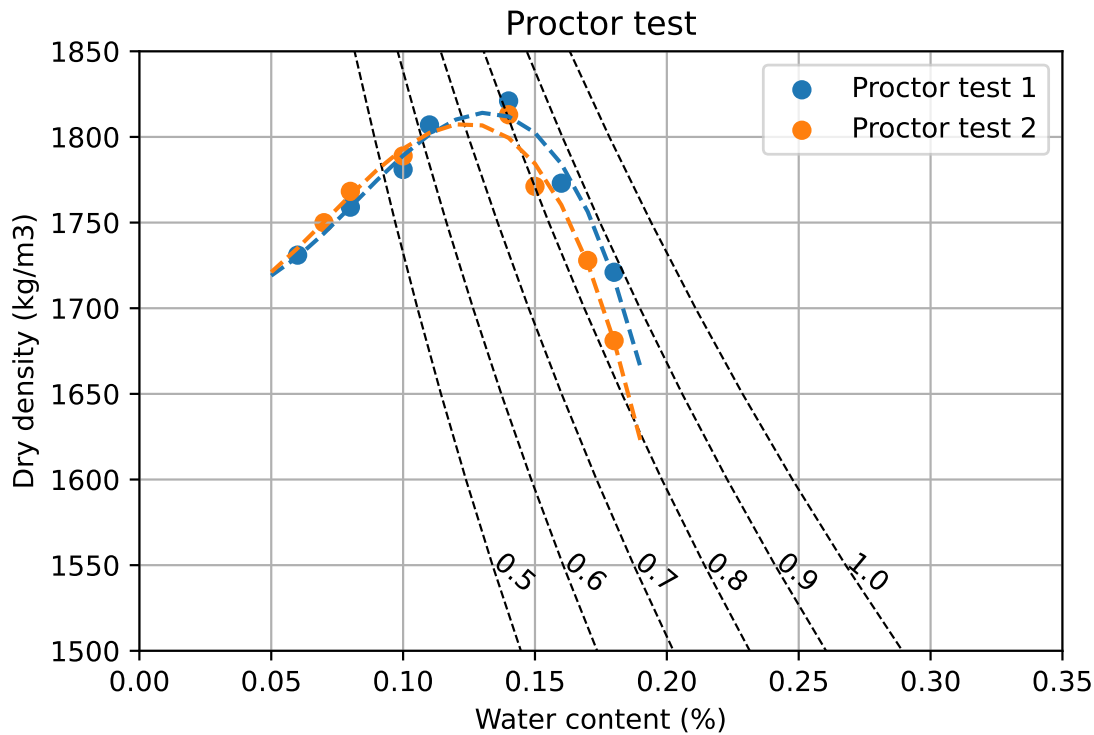


Figure 3.9: Proctor test, plotted with saturation lines

In figure 3.9 two identical standard proctor tests are presented. The tests were performed according to the following procedure. First a layer with a size of 1/3 of the sample ($\approx 40mm$) was deposited. Sequentially, a hammer of 2.5 kg was dropped 25 times from a height of 30 cm. This was repeated three times making up for the whole sample. The water content was increased and the procedure repeated to obtain at least data points.

Figure 3.9 showed that, based on proctor test 1, the maximum dry density was $1809 kg/m^3$ at an optimum water content (OWC) of 13% (proctor test 1). The optimum saturation was found at 75%. This value corresponds to the expected optimum water saturation of 80% (figure 2.7).

## 3.6. Maximum and minimum density

For the maximum and minimum density the following procedure was adopted. A cylinder was filled with oven dried soil sample of 816.86g. First the minimum density was acquired as follows. The cylinder was shaken so that the grains were well distributed. Starting with the cylinder upside down, it was gradually tilted to an upright position, depositing the soil with as little energy as possible. The volume was determined and the density calculated. After determining the minimum density the cylinder was shaken again. The maximum density was calculated by putting the cylinder on a vibrating table without a top load. This process was repeated 8 times (table 3.2

Table 3.2: Maximum and minimum density

| test # | $\rho_{max}[kg/m^3]$ | $\rho_{min}[kg/m^3]$ |
|--------|----------------------|----------------------|
| 1      | 1586                 | 1276                 |
| 2      | 1602                 | 1286                 |
| 3      | 1618                 | 1286                 |
| 4      | 1634                 | 1385                 |
| 5      | 1667                 | 1339                 |
| 6      | 1634                 | 1350                 |
| 7      | 1650                 | 1350                 |
| 8      | 1650                 | 1350                 |

The maximum density was found in test 5, being $1667 \, kg/m^3$. The minimum density was found in test 1, $1276 \, kg/m^3$. Due to the fact that the maximum density was not compacted including a top-load, but only with the vibrating table, one could argue that the maximum density found in this test is not representative for the compaction technique this soil will undergo during the actual test. Therefore, the maximum density of $1809 \, kg/m^3$ based on the performed proctor tests was used as the maximum density.

## 3.7. Hyprop & Ksat

In order to determine the water retention curve 2 samples were tested by means of a hyprop test. The air entry value was determined to be 8 kPa. Which corresponds to a silty sand. Moreover, it can be seen that the slope between the residual water content and the saturated state is not flat. This indicated that the soil is well graded. In other words, more suction is needed to decrease the water content further. This suction increase is directly related to pore size by the Young Laplace equation for capillarity 2.9. During the tests the soil samples were saturated by puttting the samples in a layer of water. During this process the samples shrinked due to capillarity. As this happened the samples were topped up again with new material. In the end a relatively dense sample was created. This was also observed in the initial porosity, which was calculated to be 41%.

Figure 3.10 showed that the AEV was approximately 8 kPa. The tangent between VWC 0.40 and 0.05 indicated that in order to desaturate the soil further an increasing amount of suction was needed. This phenomenon is mostly observed for fine grained soils, which corresponds to the particle size distribution in figure 3.3.
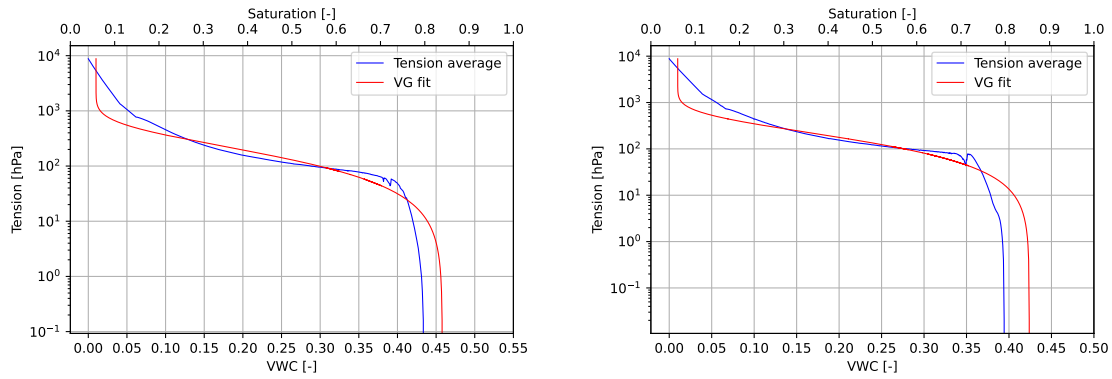
Figure 3.10: Water retention curves for sample 1 (left) and sample 2 (right). The AEV was found at 80 hPa (8kPa) at an initial porosity of 41%

In combination with the hyprop, the same two samples were also tested on saturated conductivity. The average saturated conductivity ($K_{sat,25°}$) was found to be 5.65E-7 m/s. Which corresponds to a silty sand. It should be noted that these results do not represent the conductivity during the actual test. The saturation and the porosity change over time, which both have an influence on the actual hydraulic conductivity.

Table 3.3: Results Ksat tests. Saturated hydraulic conductivity of the soil, normalised for 25 degrees Celsius

| Series | Test # | $K_{soil}$ [E-07 m/s ] |
|--------|--------|------------------------|
| 1 | 1001 | 15.8 |
|   | 1002 | 16.6 |
|   | 1003 | 2.88 |
|   | 1004 | 9.48 |
|   | 1005 | 6.72 |
|   | 1006 | 4.86 |
|   | Average series 1 | 9.39 |
| 2 | 2001 | 3.18 |
|   | 2002 | 2.07 |
|   | 2003 | 1.36 |
|   | 2004 | 1.42 |
|   | 2005 | 1.24 |
|   | 2006 | 2.20 |
|   | Average series 2 | 1.91 |
|   | Average, overall | 5.65 |

# 4
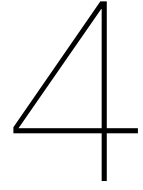
# Phase I: "1m experiments"

Phase I included scaling up from previous research. The set up for this test increased in height from 15cm to 1m. In this chapter the equipment and method for the so called 1m experiments is presented.

## 4.1. Scales and volumes

The masses for these tests were determined with a scale. As the scale had a range from 0 to 600 kg the error, shown on the scale itself, could be as large as 50g. The volumes of water were likewise determined using a scale and assuming a density of 1000 kg/m3. The nutrients were weighed on a smaller scale (range 0 to 2000g). The error on this scale was smaller than 0.1g.

## 4.2. TEROS 12 sensors

During the tests TEROS12 sensors (by Meter group) were used and connected to a data logger. The TEROS12 sensor produced the following data:

- Bulk conductivity of the soil in mS/cm
- Volumetric water content in $m^3/m^3$
- Temperature in $°C$

Based on previous research it was found that EC measurements could provide a close monitoring on the status of the reaction (Young et al. 2021). The nutrients that were added are salts. The bacteria in the soil consume these provided salts. When the EC returns to a control level of salinity the conversion of nutrients was complete. The sensors collect raw data using an electromagnetic field and an alternating current to determine the volumetric water content and the bulk EC. Additionally a thermistor measures the temperature in the surroundings.

The measured bulk EC is always corrected and outputted as the EC at 25°:

$$EC_{25} = \frac{EC_T}{[1 + 0.019(T - 25)]} \tag{4.1}$$

The manual described that in most literature the electrical conductivity is presented in terms of this saturation extract. The reason being that saturation extract can be easily related to soil salinity. The saturation extract is calculated from the pore water EC, which in term is calculated from the bulk EC. After a series of equations the saturation extract is calculated as:

$$\text{Sat extract EC} = \frac{\sigma_p \Theta + \sigma_d(\varphi - \Theta)}{\varphi} \tag{4.2}$$

With:
$\sigma_p$:    The pore water EC in mS/cm
$\Theta$:    The VWC in m3/m3
$\sigma_d$:    The conductivity of distilled water assumed to be 0 mS/cm
$\varphi$:    The porosity (-)

Before testing with the sensors could commence, the sensors were checked whether the output was valid. First the sensors were put in tap water. The results were in line with the prescribed output stated in the manual by Meter group. Furthermore, it was found that after adding the targeted amount of nutrients the salinity was still within range of the factory calibration. Therefore no additional calibration was carried out. For more information regarding the TEROS12 sensors is referred to the manual

## 4.3. Test set up

For each test series three samples were set up, in which 1 sample was untreated and 2 samples were treated. Since this test was only about proof of concept it was assumed that the variability between the big bags was not an issue. To carry out the experiment, three perspex tubes were used with an inner diameter of approximately 9 cm and a volume of 6L. Table 4.1 lists the dimensions of the tubes.

Table 4.1: Dimensions and empty mass of 1m tubes

| m_empty | 160.47 | g | |
|---|---|---|---|
| Di | U1 (cm) | T1 (cm) | T2 (cm) |
| 1 | 8.92 | 8.91 | 8.91 |
| 2 | 8.92 | 8.95 | 8.91 |
| 3 | 8.92 | 8.95 | 8.91 |
| Di,avg (cm) | 8.92 | 8.94 | 8.91 |
| Area,avg (cm2) | 62.49 | 62.73 | 62.35 |
| Volume in 1m (L) | 6.2 | 6.2 | 6.2 |



Figure 4.1: Empty 1m tubes, each with a TEROS12 sensor

## 4.4. Sample placement

### Homogeneous sample

For each test approximately 10 kg of soil was put in a bucket. To be able to place the soil, it was required to mix the soil with a certain amount of water. It was essential that not too much liquid was added, if the slurry became a suspension the fines may segregate, resulting in a layered sample. Similar to previous work, a homogeneous sample was experimented on first before moving on towards more complex, layered, samples. Based on earlier tests a mass ratio of 5:1 soil to water was found to produce the desired viscosity of the slurry. During the first test 2L of water was added and mixed with a concrete mixer until a viscous slurry was produced that could be poured. For the treated tests a certain amount of nutrients as well as an inoculum were added in the mixture. The inoculum was not necessarily required. However this way the bacteria in the soil would not be the limiting factor for gas production. The amount of nutrients that were added depended on the amount of overburden and the volume of gas necessary to desaturate the soil to a targeted saturation. The procedure to calculate the

amount nutrients can be found in Andrag 2017. After the mixture was produced, the perspex tube was tilted and held at an angle of approximately 30 degrees from vertical. The bucket containing the slurry was squeezed together so that, in a continuous motion, the slurry could be poured in. This way a sample with a low initial density and almost no air air inclusions was produced. Lastly, to prevent evaporation of liquid out of the system the tops were sealed using plastic wrap and duct tape[1].



Figure 4.2: Methodology preparing a homogeneous sample. From left to right (1-4): The bucket being filled with water (1), followed by soil (2). Then mixing the slurry (3) and lastly pouring it in the tubes resulting in the final situation (4).

## Layered sample
A layered sample was created by filling the cylinders with 5L of water. For the treated samples the nutrients were mixed in the tube. Sequentially, the material was deposited in the tubes and the suspension was mixed. In this case the ratio soil to water was 1:1. In contrast to the homogeneous sample this was 5 times more diluted, creating a suspension. Due to different settling speeds segregation took place resulting in a layered sample. However the problem with this method was that the actual height of the soil after settling was approximately 3 to 4 times lower than the homogeneous samples.



Figure 4.3: Placement methodology for a layered sample. From left to right (1-4): The water tubes filled with water (1), followed by the nutrients (2). Sequentially the tubes are filled with soil and mixed (3,4)

## 4.5. Compaction technique
The compaction technique included a vibrating needle, often used for concrete. This needle had a power output of 800W. Different ways of compacting the sample were experimented with. During the first experiment the needle was inserted in the tube. Furthermore the expelled water on top was not removed. It was observed that the energy input liquefied the sample. Furthermore, the water on top was reintroduced in the soil system. Thereby creating a slurry with approximately the same density as the initial situation. A lot of the sample was also lost due to spillage as the energy input was too much to compact in a controlled manner.

---

[1]In a later stage the evaporation was measured and found not to be significant.

To provide the energy input in a more controlled manner, the needle was taped to the tube. Furthermore the tube was fitted with dampening cloths to prevent damage on the tubes. The needle was turned on and held firmly against the tube for a time period of five minutes. Based on trial and error it was found that after 5 minutes all gas in the sample was able to get out of the system, this time period was held as a standard. One could argue that this compaction method was not comparable to a real life compaction method. Nonetheless, for this experiment the aim was to find whether the proposed solution would also apply on 1m samples. Therefore the comparison to a real life situation was held out of consideration, the focus was set on the workings of the concept.
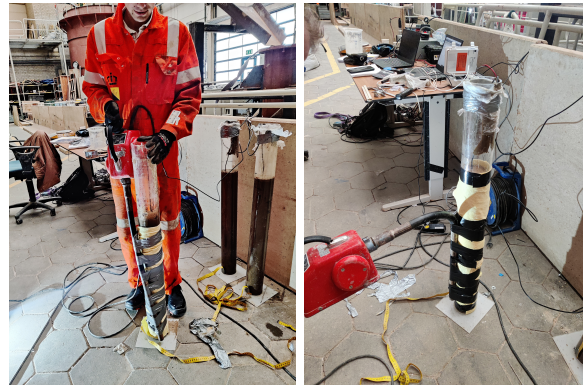


Figure 4.4: Compaction technique 1m experiments

<div style="text-align: right; font-size: 4em;">5</div>

# Phase II: 2.5m experiments

Phase II included the following step, scaling up the test again based on Phase I. An experimental test set up of 2.5m high was developed. This chapter includes the development of the set up and methodology of the so called 2.5m experiments.

## 5.1. Materials and measuring systems

### Load cell

It was anticipated that it would be required to know what the mass of the deposited soil was. In combination with the volume this would lead to the in place (bulk)density of the soil. To determine the mass in the system a load cell was fitted in a lifting crane. This load cell operated similar to a strain gauge and had a range from 0 to 1000 kg. The output of the loadcell was presented on a monitoring station in milliAmpères with a range from 4 to 20 mA. The ranges 0 to 1000 kg and 4 to 20 mA were linearly related. This meant that every mA on the computer represented:

$$Conversion\ factor = \frac{1000 - 0}{20 - 4} = 62.5\ kg/mA \tag{5.1}$$

For good measure the load cell was checked against known masses to verify the conversion factor from mA to kg. This was done by filling known volumes with water.



Figure 5.1: Load cell attached to a big bag

### Big bag dispenser

For the placement method it was required to control the discharge of the soil slurry. A Raimo big bag dispenser, used in agriculture to dispense grain and kettle feed, was used. The tube of the dispenser

was elongated with a pvc tube, the two were assembled to each other with a muffle. During the first tests the dispenser was attached to the big bag as the manual of the dispenser prescribes. However, with this configuration, it was found that tensional forces on the big bag; resulting from pulling on the pvc tube were not distributed well over the big bag. Consequentially the big bag ripped open, thereby covering the entire lab in soil slurry. The configuration was changed, so that the base plate attached to the dispenser was placed inside the big bag. Unfortunately the muffle, connecting the dispenser and the pvc tube broke several times. Both glue and multiple small screws were required to secure this connection. During the last test the small tube of the dispenser itself ripped. This was not resolved, the dispenser was used without any tubes attached to it.

### Sample rings
To determine current in-situ densities, sample rings of volumes 250 and 100 ml were used. In combination with a small scale in the lab the wet densities could be estimated. The sample rings were mainly used to verify the slurry density before placement. Additionally, the rings were used after a test to determine the final density and water content. The results of the samples were compared to the average result of the entire cylinder.

## 5.2. Test set up
The test set up consisted of a frame, with in it a cylinder. The dimensions are specified in figure 5.2, left. To measure the electrical conductivity and the volumetric water content over time, 4 TEROS12 sensors were inserted in this cylinder. The sensors were taped together, with each sensor 40 cm apart. Secondly a prefabricated vertical drain (PVD) was left hanging in the cylinder.

The cylinder had an overflow tube which lead to a container so that the mass balance could be followed narrowly. A perspex window allowed for both visual inspection of the gas production in the sample. Moreover, the height of the soil mass and water column could be measured. This was also monitored by the use of a Brinno TLC 130 timelapse camera, fitted to the frame.

At the bottom of the set up a flange was bolted to the cylinder. In order to the prevent the flange from leaking different sealing techniques were used. First only a liner was used. As some leakage occurred, the following step was to add silicone kit to the liner before bolting the flange back. This worked out, however the liner took great amounts of wear and eventually teared. For the last tests a rubber liner was made which was smeared with petroleum jelly. Even without bolting the flange tightly this already yielded a watertight seal. At the end of a test a 2.5m long and 75mm diameter PVC tube was hammered in the cylinder from above. Sequentially the flange was opened to inspect the results. The pvc tube was closed of from below and samples using sample rings were taken. The PVC tube and sample rings were tested on water content and density. Lastly the cylinder was emptied in a container and processed as waste.

Using the PVD it was hoped for that a situation was created in which drainage would not be the limiting factor. The vibrating engine was assembled to a frame that was welded to the cylinder. Lastly in order to dissipate the energy of the vibrating engine 8 dampening rubbers were installed at the suspension points of the cylinder into the frame (figure 5.4).
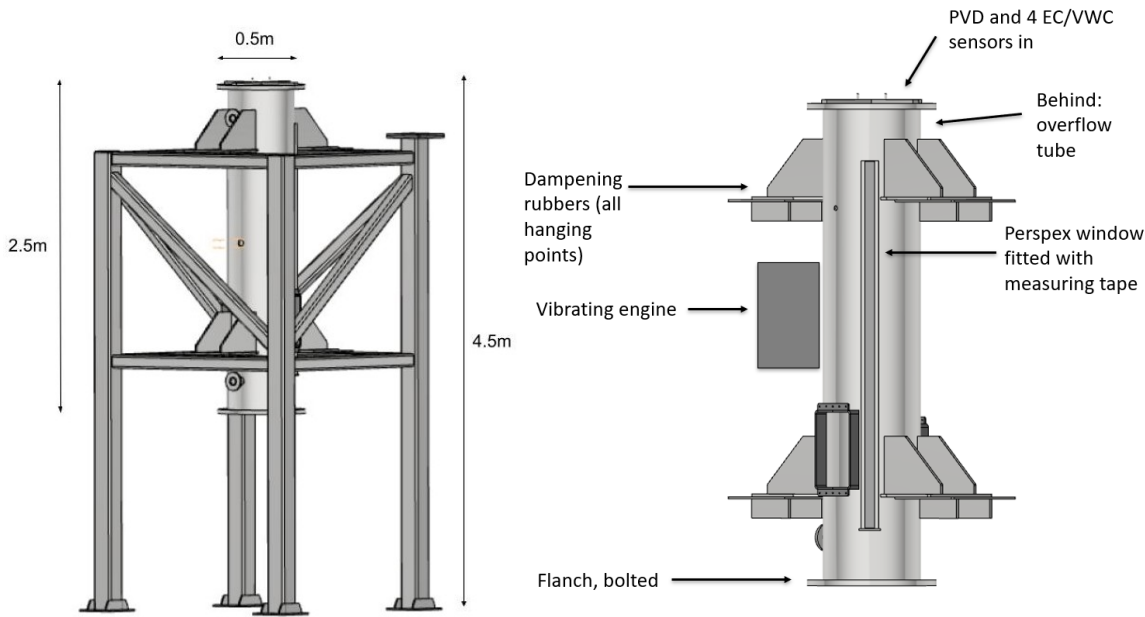
Figure 5.2: Schematics of test set up



Figure 5.3: Images of the set up, note the vibrating engine in yellow and blue

Figure 5.4: Front view of the set up. Up top the cables of the TEROS12 sensors as well as the PVD can be seen. Furthermore 2 dampening rubbers are presented, in total 8 were used for the entire set up

The volume of the cylinder was determined twofold. Firstly it was based on the dimensions of the cylinder. Additionally, the volume was calculated as follows. The discharge of a present fire hose was measured. It was assumed that the measured discharge was constant. Specific heights next to the perspex window were marked. The hose opened and put in the cylinder; at the same time a stopwatch started measuring. At the moment the water level was equal to a marked height, the time was noted. Multiplying the discharge with the time resulted in volumes on the marked heights. These results were crosschecked with the volume at the same heights based on the dimensions. In the end it was found that a diameter of 0.5m was accurate enough.

The discharge was calculated to be

$$Q_{hose} = \frac{V}{t} = \frac{39.35L}{55.5s} = 0.71L/s \tag{5.2}$$

Table 5.1: Volume calculation based on dimensions and constant discharge

| Measurement # | h [cm] | t [s] | V(Q) [m3] | V(dim) (m3) | $\varepsilon_{rel}$ (-) | $\varepsilon_{abs}$ (m3) |
|---|---|---|---|---|---|---|
| 1 | 48.5 | 131.54 | 0.09 | 0.10 | 2% | -0.0020 |
| 2 | 89.5 | 251.37 | 0.18 | 0.18 | -1% | 0.0025 |
| 3 | 125 | 346.47 | 0.25 | 0.25 | 0% | 0.0002 |
| 4 | 171.5 | 471.82 | 0.33 | 0.34 | 1% | -0.0022 |
| 5 | 215 | 590.58 | 0.42 | 0.42 | 1% | -0.0034 |

## 5.3. Sample placement

A method to deposit a homogeneous soil sample was developed. First the sample material had to be prepared. The following images show the steps up to the moment just before filling the cylinder.
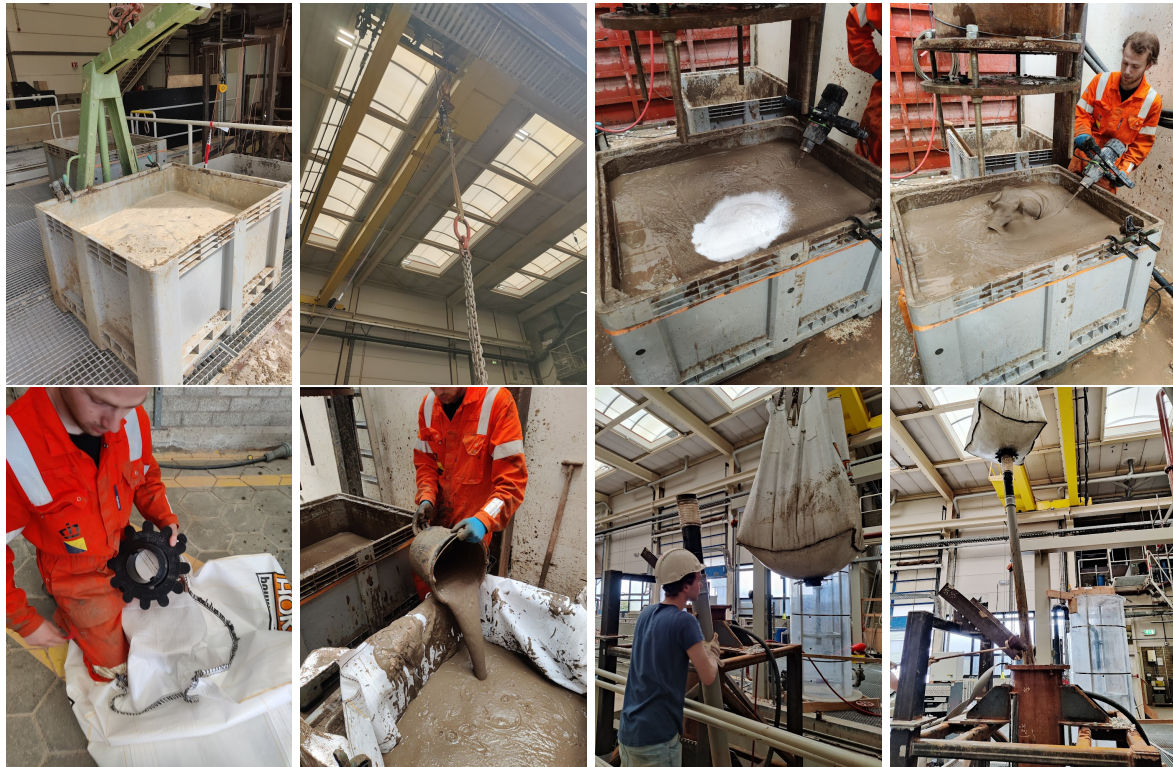
Figure 5.5: Filling procedure for a homogeneous soil sample. From left to right (0-7). Filling container with water and soil (1). The ratio soil to water accurately weighed with a load cell (2). Adding nutrients and mixing of the soil slurry (3,4). Insertion of the dispenser in a big bag (5) and filling this big bag with the slurry (6). The pvc tube connected to the big bag with slurry (7). The big bag with pvc tube being lowered in the cylinder (8) whereafter the placement can start.

A schematic during deposition was produced (figure 5.6). Here it becomes clear why the PVC tube was used. It was hypothesised that the use of the PVC tube would result in a similar depositional process as the hop dobber method (which places underwater concrete accurately). Resulting in a controlled process with low depositional energy. Sequentially being able to produce a desired sample with a low initial density and limited to no air inclusions. During deposition the pvc tube was gradually pulled upwards using the crane. In practice however, it was found that the pressure of the soil slurry was too high in comparison to the back pressure that the deposited soil slurry provided. Due to this, when the dispenser was opened, a turbulent discharge was observed.

It should be noted that the PVC tube still was helpful in terms of control of spillage, resulting in more accurate measurements of the soil mass inserted in the tube.
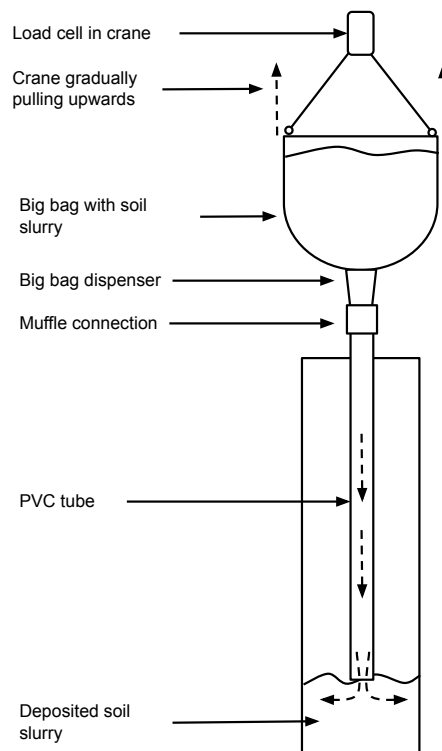
Figure 5.6: Schematic of placement technique, situation just after opening dispenser. The crane is gradually pulled upwards and the mass of the deposited soil is closely monitored with the load cell

For the engine series it was opted to vibrate the sample after deposition. This had two advantages, firstly it was hypothesised that large air pockets in the sample could leave the system. Secondly, if compaction after deposition did not increase the density, this highlighted that an untreated soil with this amount of fines is indeed problematic to compact. Note that, it was assumed that even if a sample was treated, the reaction would not have been able to have any influence on the soil structure in such a short time frame. As the process from mixing with nutrients to deposition maximally took 2 hours (whereas the lag period of the reaction was found to be three days 6.12). Furthermore, the effects of salts on the soil structure were also assumed to be none existent.

## 5.4. Surcharge

After the engine 30 and 100 series described above, it was hypothesised that: If swelling could be avoided, but the same amounts of desaturation and compaction were achieved then a significant gain in density could be achieved. This lead to a test with surcharge (figure 5.7) being developed. The hypothesis was illustrated in figure 5.7.
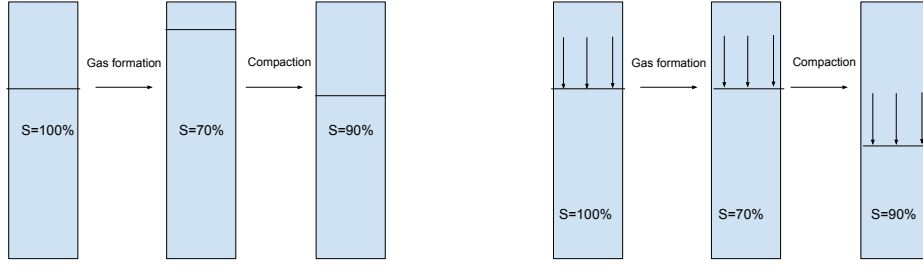
Figure 5.7: Hypothesis, outcome of test with surcharge

After deposition the sample was still a loose consistency. Based on small scale experiments, it was found that the surcharge could sink in the slurry. Additionally, the slurry was able to find its way through the surcharge, so that no extra stress was put on the actual soil sample. These two processes were mitigated, using the following procedure. The surcharge consisted of a multilayered system. First a thin base layer of permeable cloth was put on the slurry. Taking care to cover all edges of the cylinder. The cloth allowed for a layer (10 cm) of drainage sand to be placed carefully on the sample and to fill all around the edges of the cylinder. Sequentially, a layer (30 cm) of gravel was put on top of the drainage sand. Lastly a leaden weight (80 kg) was put on the top. For the gravel and sand a dry unit weight of 1600 kg/m3 was assumed. Incorporating the mass of the leaden weight this lead to a surcharge of 205 kg. With the assumed density of sand this surcharge would be equivalent to an overburden thickness of 65cm of sand (with the assumed density).

$$L_{equivalent} = L_{sand} + L_{gravel} + \frac{\left(\frac{M_{lead}}{\rho_{assumed}}\right)}{\pi * r_{cyl}^2} = 10 + 30 + \frac{\left(\frac{80*10^3}{1.6}\right)}{\pi * 25^2} = 65 \; cm \tag{5.3}$$

Using the equivalent thickness and the unit weight of sand (16 kN/m3). The overburden corresponds to 10.5 kPa. In reality wall friction will play a role in the actual overburden. During swelling of the soil body underneath the overburden may increase due to this friction. Similarly the overburden decreases while the soil body shrinks. In this research this wall friction is not accounted for.

$$L_{equivalent} * \gamma_{assumed} = 0.65 * 16 = 10.5 \; kPa. \tag{5.4}$$

It was anticipated upon that the waterlevel could not be monitored visually. Therefore, after the surcharge was applied, water was added to the level just below the overflow. At the end of the overflow tube an empty container was placed so that all expelled water was, theoretically, collected. The water level was initially 40 cm above the soil slurry level. This means that the effective stress of the surcharge was:

$$\sigma'_{surcharge} = (0.65 * 16) - (0.4 * 10) = 6.5 \; kPa \tag{5.5}$$

Figure 5.8: Set up of surcharge, layering of drainage sand and gravel on top of the soil sample (left). The leaden weight, left with some slack in the crane for safety, notice the waterlevel just below the overflow (right)

## 5.5. Monitoring

Samples were monitored both visually and with a timelapse camera (appendix E. The camera was mounted on the frame next to a construction lamp. The camera set up so that every 30 minutes a picture was taken. For the calculations it was of essence to keep track of the height of both the soil sample and the water column. The TEROS 12 sensors also monitored the sample. The sensors were not used to estimate the degree of compaction, but they provided valuable data with regards to the state of the reaction. During the experiments water pressure meters were also used. A nozzle was put in the side of the cylinder and connected with a tube to a pressure meter. Gas production and clogging of this tube led to a discontinuous water phase in the tube. Consequently, unfortunately, no valid data was produced from these measurements due to this.

## 5.6. Compaction, vibrating needle

After seven days it could be opted to compact using a large vibrating needle (200 Hz). Before actual compaction could take place the expelled water on top of the sample was removed using a bucket and scooping it off. This way, it was prevented that the water would be reintroduced in the system (as observed in the 1m experiments).

The needle was inserted from the top of the cylinder. It should be mentioned that no method to standardize energy input was developed. The needle was lifted up and down, trying to get as much gas out as possible. Since the frame was 4.5m high a safety harness must be worn. Additionally, a platform was constructed next to the cylinder to allow for easy access.

Figure 5.9: Needle compaction, note the safety harness and the platform

## 5.7. Compaction, vibrating engine

A set up for compaction via a vibrating engine was also developed. The power requirements for the engine were determined by reflecting on specifications a vibroflot uses in practice. Essentially this is scaling down from practice. The starting points of the situation/vibroflot are listed as follows:

- A vibroflot compacts 0.5m every 30 s
- A grid of 4x4 is often used (depending on client demands)
- A depth of 10m is assumed
- A specific vibroflot has a power of 202 kW
- A frequency of 28 Hz
- The lab test considers a sample of 2m with a volume of 0.5 $m^3$

For ten meters depth the vibroflot compacts for

$$\frac{10}{0.5} * 30 = 600 \, s$$

During this time the system receives

$$600 * 202000 = 121.2 \, MJ$$

If all energy is equally distributed over the specified volume this results in:

$$\frac{121.2}{4 * 4 * 10} = 757.5 \, kJ/m^3$$

If we scale this to our volume this would mean that a energy of

$$757.5 * 0.5 = 378.75 \, kJ$$

Is put in the lab test sample. If compaction time per m remains the same then for a soil sample of 2m compaction should last for 120 s. That would result in a power of:

$$378.75/120 = 3.2 \, kW$$

From that point a consideration was made between an engine with a power of 3.5 kW or 2.4 kW. The 2.4 kW engine already weighed over 100 kg. It was not known at the time how the whole set up would react to the vibrating engine. Therefore, to be on the safe side, the "lighter" engine of 2.4 kW was chosen. As frequency has no scaling law a similar frequency was held unto.

### Vibrating engine, power variation and energy input

Although by calculations the engine should run on (more than) 100% it was opted to vary with the power output of the engine. This way, it was hypothesised that a conclusion could be drawn about the relationship between energy input and degree of compaction. Additionally, more practically seen, it was not yet known whether the set up would be able to handle the vibrations of the engine. So the lowest setting, 30% of total power, was experimented with first. Additionally, before testing with soil the vibrating engine was tested on a cylinder filled with water only.

Energy input was standardized based on some rules of thumb in the field of vibroflotation (paragraph 5.7). Again, before any compaction took place the expelled water on top of the sample was removed. First, the engine was put on for an interval of 30s and turned off, the height of the soil mass and water column were inspected and measured. This was repeated four times (2m sample with 30s each 0.5). After this series of compaction intervals the engine was left on for 2min continuously to determine whether additional compaction could be achieved. This was worthwhile because it could give an insight in the cost benefit analysis.

## 5.8. Sampling & Calculations

After compaction the cylinder was left untouched for at least one hour to allow for residual settlements. A PVC tube, 75mm in diameter, was inserted from the top to the bottom. By means of a wooden block and a hammer the pvc tube could be driven into the soil if too much resistance was encountered.

Before opening the blind flange, the TEROS12 sensors were given as much slack as possible. This way, when the soil may flow out, the cable of the sensor was less likely to break or tear. Sequentially, the bottom flange was opened. It should be noted that it is of importance to keep the bolts in the blind flange clean. A small quantity of soil between the bolt and nut will prohibit the bolt from getting off, resulting in the bolt having to be sawed through. Cleaning of the bolts was done with a steelbrush in combination with WD40 (or any similar product). Further, the screwthread was kept above the blindflange, as depicted for example in figures 5.10. This prevented most dirt from coming into contact with the bolts.



Figure 5.10: Tests U16N (left) and T16N2 (right), after compaction. Note how the bolts were inserted in the right image to keep the bolts as clean as possible. In the right image a sampling ring can be observed.

When the blind flange was opened, samples were taken using both 100 and 250 ml sampling rings (figure 5.10, right). The samples were tested on the density and water content. After the cylinder had been emptied the PVC tube was lifted slightly using a shovel and a fitting lid was put on the tube so that it could be taken to the lab. In the lab water contents, densities and grain distributions over depth could be determined.

The calculations for the 2.5 m experiments were done in the same way as the 1m experiments. Presented in appendix B.6.

# 6

# Results

This chapter includes the results of the research. For each type of result, a brief explanation in combination with observations is given.

## Performed tests

The performed tests are listed in table 6.2. Every single test was categorised in a specific series based on either the compaction method, or the energy input of the compaction method. Although an effort was made to keep each test the same, this was not always the case. Since the set up kept developing based on current findings not all conditions and characteristics of the test were the same. The conditions and observations regarding all tests can be found in appendix C.

Table 6.1: Test labeling

| Abbreviation | Meaning |
|---|---|
| S | Small, 1m test |
| H/St | Deposition method, homogeneous/stratified. Applies only to 1m tests |
| U/T | Untreated/Treated |
| 16 | Percentage of fines |
| N | Compacted with needle |
| 30/100 | Compacted with vibrating engine. Percentage of total available power |
| Sur | Surcharge |

Table 6.2: Number of tests including their respective series and test ID

| # | Series | TestID |
|---|--------|--------|
| 1 | | U1 |
| 2 | 15cm | T1 |
| 3 | | T2 |
| 4 | | U1 |
| 5 | SH1 | T1 |
| 6 | | T2 |
| 7 | | U1 |
| 8 | SH2 | T1 |
| 9 | | T2 |
| 10 | | U1 |
| 11 | SSt1 | T1 |
| 12 | | T2 |
| 13 | | U16N |
| 14 | Needle | T16N1 |
| 15 | | T16N2 |
| 16 | Engine 30 | U1630 |
| 17 | | T1630 |
| 18 | | U16100 |
| 19 | Engine 100 | T16100 |
| 20 | | T161002 |
| 21 | | T16100sur |

## 6.1. Density over time

### Strain over time

First the plots are presented in terms of strain. The strain was calculated with respect to a settled sample. The advantage of this type of results is that the density can be removed out the equation. An important assumption is made here that the soil behaves in a similar way between tests. In other words, if a soil sample had the same saturation ànd the same volume, the same density could be expected. This way the net gain (or loss) of the method can be easily observed and compared between tests. Positive strain is denoted as compaction. The height over time, on which the strain is based, is given in appendix D

$$\varepsilon_{stage} = \frac{H_{stage} - H_{settled}}{H_{settled}} \tag{6.1}$$

### Dry density vs water content over time

In contrast to the previous results. The dry density shows a more accurate development of the degree of compaction over time. The dry density and corresponding relative density were plotted against the water content (figure 6.2). The markers on the lines represent different moments in time. The plots should be read from right to left. Where the utmost right point is the first moment in time whereas the utmost left point is the last moment in time. Reading from right to left is only valid under the assumption that no additional water is introduced in the system during the test. The saturation contours were included as well. In each plot tests from the same series are presented, where a single line represents one test. It should be noted that the values presented in these plots are averages of the whole sample. Based on the visual inspection and the samples from the final state soil sample, it was found that a gradient of density and water content was present. However the averages could be easily compared and give a fair insight in the global status of the entire sample.

# Phase I: 1m experiments



(a)



(b)



(c)



(d)



(e)



(f)
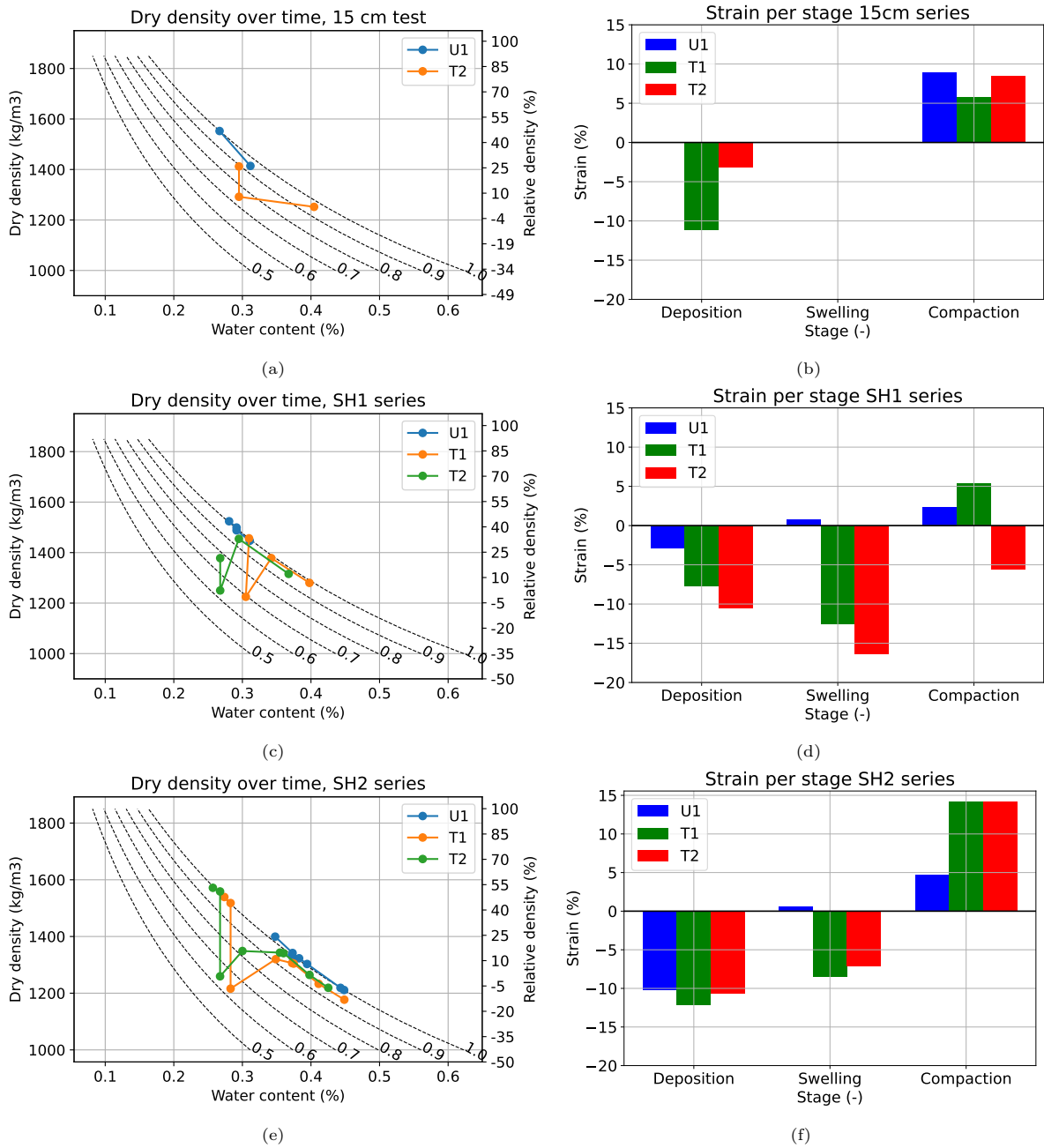
Figure 6.1: Phase I: Dry density and relative density over time, including saturation curves (left column). Percentual strain with respect to settled stage (right column).

# Phase II: 2.5m experiments



(a) Test series: Needle compaction

(b)



(c) Test series: Engine 30

(d)



(e) Test series: Engine 100

(f)
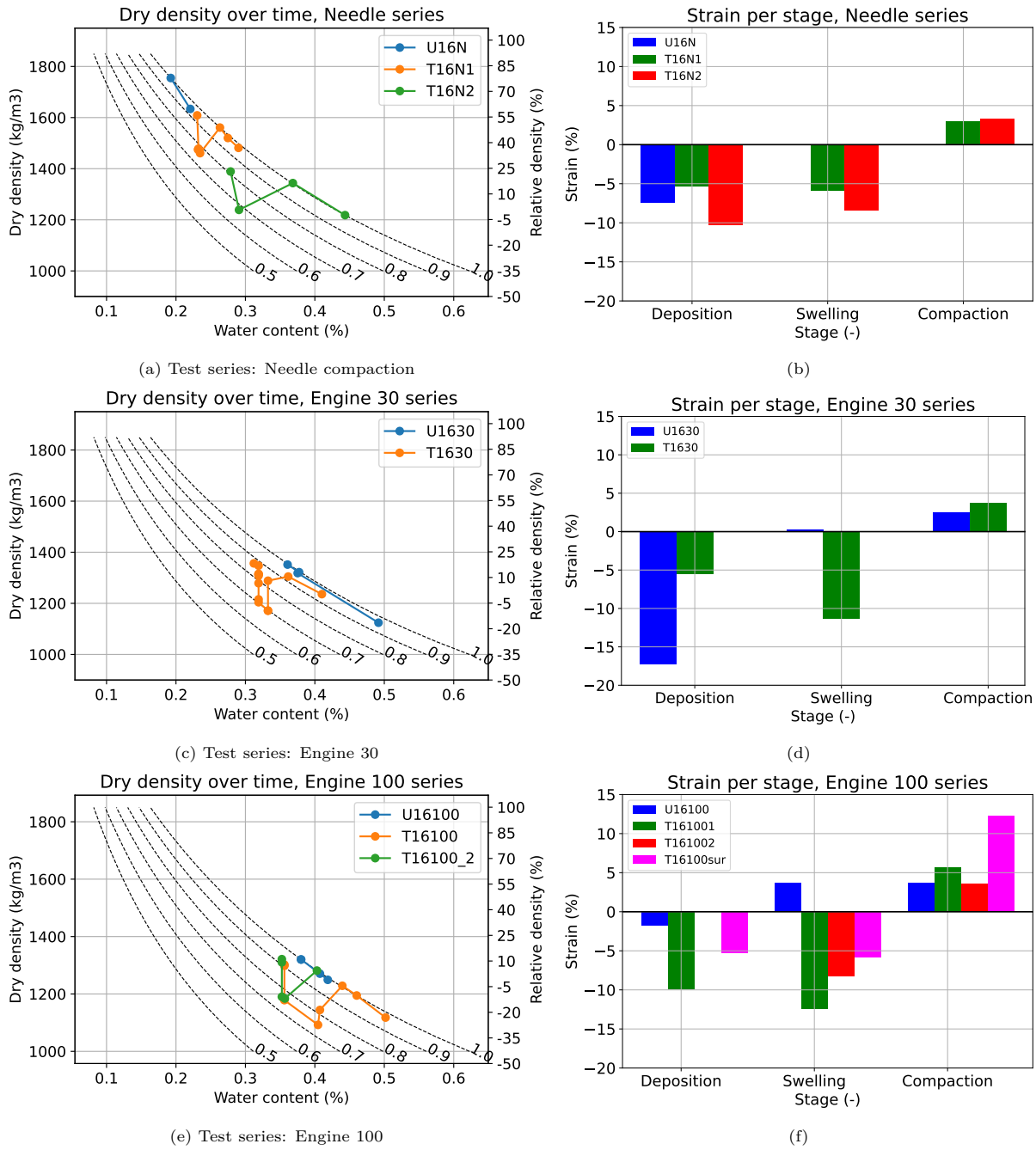
Figure 6.2: Phase II: Dry density and relative density over time, including saturation curves

## 6.2. General observations density over time

Upon testing it was observed that the experiments followed a similar process. The stages a treated test experienced is illustrated in figure 6.3.



Figure 6.3: Schematic of observed phenomena during a treated test. Note, untreated samples do not experience either swelling nor venting

Just after the moment the soil slurry was deposited, the soil began to settle. This was observed for all tests except the small 15 cm test (6.1a). The settled stage is also the stage which is considered as the baseline. Both compaction and swelling are compared to this baseline. The amount of settling depended on the initial density. If a soil slurry was relatively "loose", in comparison to a dense slurry, more settlement was observed. After settling initial densities came closer to each other (Series 6.1e, 6.2c). Initial densities after settling were on average 1200 kg/m$^3$ to 1300 kg/m$^3$

The target saturation was 50% for all tests except T16N2 (35%). Gas production came paired with swelling during all tests except the 15cm series. First a small amount of water was expelled only, whereafter the volume of the sample increased. This is also illustrated in the Appendix "timelapse" E.1. For some samples the swelling was large enough to rise above the perspex window. Due to limitations what the camera could observe, it was not clear what the maximum swelling was when this happened. After the maximum swelling stage, gas would "vent" out of the system. This venting process came paired with a decrease in height of the soil mass. After swelling and venting it was observed that in all cases the soil samples were able to desaturate to, and some below, the optimum water content.

## 15 cm series, vibrating table

This series was carried out on soil from the same project site. However the soil was stored for over 2 years in sealed containers. The slurry for the treated tests was made in the same container. The resulting initial density of the treated tests were almost identical (T1, 1258 and T2 1252 kg/m$^3$). The initial density for the untreated test was significantly higher, being 1414 kg/m$^3$. Some lumps were observed during deposition on this scale heterogeneity's in the slurry may result in larger differences in density.

The reaction stage did not show promising progress. Gas formation took almost two weeks. Indicating a lack of initial biomass in the soil. To add to this effect, no inoculum was used. During the reaction stage it was observed that cylinder T1 leaked at the bottom. That is why T1 has been left out of the plot. T2 desaturated to a water saturation of 75%. No swelling was recorded.

The water on top was removed using a pipet. After that, the samples were compacted for 8 min continuously on a vibrating table of 60 Hz. After one minute of compaction most of the gas had left the sample, however based on the calculations the final water saturation of sample T2 was 90%. In the end, the treated samples showed no gain in terms of degree of compaction opposed to the untreated sample. Furthermore all samples were still in a pour-able, suspension like state. In terms of strain the samples U1 and T2 had a similar amount of compactive strain ( 9%).

## 1m experiments, small needle

Phase I comprised of the 1m experiments. Three series were performed being SH1, SH2 and SSt1.

## SH1

In series SH1 the initial densities after settling were close, being 1488 kg/m$^3$, 1378 kg/m$^3$ and 1454 kg/m$^3$ for U1,T1 and T2 respectively.

The reaction stage desaturated the samples to a water saturation of 70% and 63% for T1 and T2 respectively. All cylinders were closed off using cling film. After a week the cling fill bulged outwards due to the gas. This indicated that not all produced gas could be retained in the sample. The highest amount of swelling was recorded for test T2, with a 16% increase in height corresponding to a swelling of 12.4 cm.



Figure 6.4: SH1 sample T2. Cling film bulging outwards due to gas production

The compaction stage for SH1 comprised of inserting the needle in the sample without draining the columns of the expelled water first. This resulted in a the samples returning to a slurry, as the water was reintroduced in the system. Whereas T1 did return to a fully saturated state but T2 to a water saturation of 76%. Due to the amount of spillage during compaction the mass balance was not correct and with that, the results carry significant uncertainty. The final degree of compaction of the untreated test was 68 kg/m$^3$ and 146 kg/m$^3$ higher than T1 and T2 respectively. The final state in terms of strain showed that U1 had 2.5% compactive strain. In contrast to all other tests T2 ended up in a looser state after compaction. It actually increased in height, with a strain of -5%.

## SH2

For the samples in series SH2 the initial densities after settling were almost identical 1342 kg/m$^3$, 1320 kg/m$^3$ and 1349 kg/m$^3$ for U1 T1 and T2 respectively.

During the reaction stage the treated samples showed a similar desaturation path. The saturation after the reaction stage was 64% for both treated samples. The desaturation phase resulted in 9% and 7% percentual swelling for T1 and T2 respectively.

Due to the spillage of the previous series a non intrusive way of compacting with the needle was carried out 5.9. Additionally, the sample was drained of water first and compacted for 5min. This lead to all samples returning to the fully saturated state. Furthermore, it was found that the both treated tests had a higher final dry density than the untreated test. The profit in terms of dry density was 139 kg/m$^3$ and 172 kg/m$^3$ for samples T1 and T2 respectively. This test experienced the highest amount of compactive strain being 14% for both T1 and T2. The final RD of the treated tests was at least two times higher than the final RD of the untreated test. (50% and 56% RD vs 24% RD).

## SSt

In this series a stratified sample was created. Due to the depositional method a small sample of only 20 cm was created. It was observed that gas formation mostly occurred in the coarser (lower) layers and not in the silt. The sample was not compacted.

## 2.5m experiments, Needle compaction

Based on the plot initial densities during the needle series differed significantly. Furthermore an established soil to water ratio was used. However the initial water content was not taken into account, resulting in the large variations presenting in the different slurry's. During deposition of U16N and T16N1 a large mass balance error occurred during the deposition due to spillage. For U16N the error could not be estimated. For T16N1 an error of maximally 120 kg ($\approx$ 2 mA) can be expected. The initial density after settling was 1344 kg/m$^3$ for T16N2. The mass error can be estimated such that the initial after settling density is approximately the same as T16N2. This lead to an error of 50 kg for both U16N and T16N1. The dry density was re-plotted figure 6.6.

The reaction stage for T16N2 desaturated the sample to a water saturation of 68%. T16N1 showed the least amount of percentual swelling of all 2.5m tests, being 5.8%. The swelling of T16N2 was 8.4%. Furthermore, for this test it was found that gas production took place on all depths of the treated sample. This was a qualitative observation based on visual inspection of the perspex window (figure 6.5). The gas distribution seemed homogeneous over depth for both the 1m and the 2.5m tests. The gas pockets at the perspex window were of similar size, ranging from 0.1mm to 2.5mm, and occurred with the same frequency.



Figure 6.5: Gas bubbles in test T16N2, viewed through the perspex glass of the set up. From bottom (left) to top (right)

The needle series was compacted with a 200 Hz vibrating needle (plot 6.2a). The needle was inserted in the cylinder and lifted up and down throughout the compaction stage. This method of needle compaction required a significant amount of time to get all gas out of the system. Test T16N1 was compacted for over 20 min. However this did lead to an almost fully saturated state again. Test T16N2 was compacted for 12 min, as the vibroflot would also compact for only 2 minutes for this volume of soil, it was deemed that this was enough time. It was observed that a large amount of residual gas was still present in the soil for T16N2. T16N2 ended with a final dry density of 1389 kg/m$^3$ and a water saturation of 81%. For both T16N1 and T16N2 a compactive strain just over 3% was recorded. It should be noted that in 6.6 a significant gain in density could be made if T16N2 was able to get back to a fully saturated state.
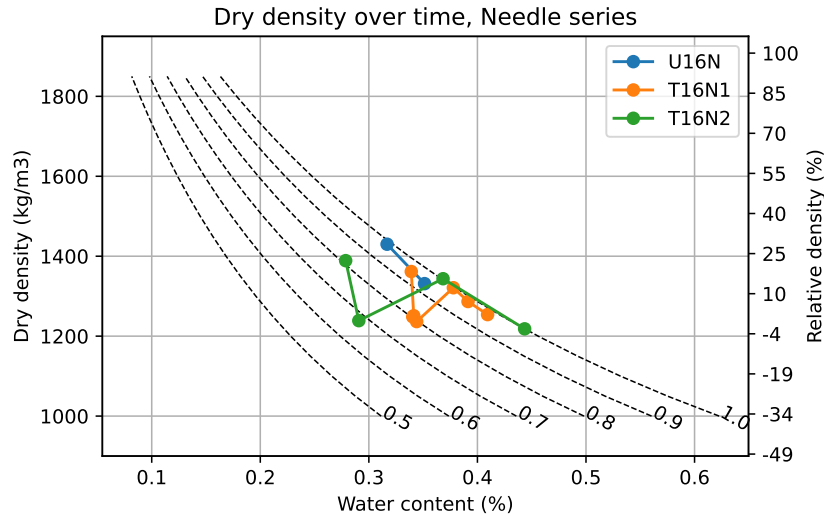
Figure 6.6: Dry density vs water content over time for the needle series. Corrected for initial density after settling being 1350 kg/m$^3$.

Eight sample rings were taken, mostly from the bottom of the cylinder. The average dry density of these samples was 1576 kg/m$^3$, almost 200 kg/m$^3$ higher than the average of the whole cylinder.

## Engine compaction 30%

During the engine tests the method was more controlled and standardized. The initial densities after settling were 1318 kg/m$^3$ and 1305 kg/m$^3$ for U1630 and T1630 respectively. Nonetheless, the maximum amount of settlement was found for this test. The settling for U1630 was 31.5cm, -17%, opposed to the 11cm settlement, -5%, for test T1630. As mentioned in the methodology, this test series was compacted right after deposition. It was found that no increase in density was found for this compaction interval. This indicated that the soil was indeed difficult to compact under saturated conditions. Although no initial compaction was recorded, the deposited soil did settle (figures 6.2c,6.2e).

After venting had occurred, sample T1630 was desaturated to a water saturation of 70%. T1630 experienced a percentual height increase due to swelling of 11%.

For the treated test the compaction process went as follows. After the first interval of 30s compaction a suspension of approximately 4cm height was created on top. Without this 4cm suspension the first interval accounted for 72.5% of the total height decrease. The second interval lead to a marginal decrease of height of 0.75%. The third and fourth interval did not account for any extra decrease in height. After the fifth interval of 2min continuously and allowing the sample to settle for at least an hour the remaining decrease in height of 20% was recorded. The treated test was not able to get back to a fully saturated state, the final average saturation was found to be 87%. The final dry density of the untreated test was almost identical to the treated test, with 1352 kg/m$^3$ for the untreated test and 1356 kg/m$^3$ for the treated test. The tests experienced compactive strain, being 2.5% and 3.8% for U1630 and T1630 respectively.

Three sample rings were taken from the bottom of the cylinder. The average dry density of the samples was 1389 kg/m$^3$ and the saturation was 82%.

Figure 6.7: PVC samples after compaction. Left side is the lower part of the cylinder and right side the top of the cylinder. Test T1630

## Engine compaction 100%
### T16100 & T16100_2

The initial densities after settling of this series were 1271 kg/m$^3$, 1229 kg/m$^3$ and 1281 kg/m$^3$ for U16100, T16100 and T16100_2 respectively. It can be observed that in terms of reproducibility the final depositional method proved that for 5 separate tests (both engine series) a difference after settling less then 100 kg/m$^3$ (6.2c,6.2e) was present. Similar to the engine 30 series, the sample was compacted right after deposition. The same result was found that no increase in density was found.

After the reaction stage and venting the saturation was 75% for T16100 and 76% for T16100_2. The percentual increase due to swelling was 12.5% and 8.2% for T16100 and T16100_2 respectively.

For the treated tests the compaction process showed that more effort led to faster release of the initial amounts of gas. For the treated tests, the first 30s compaction interval led to 97% and 87% of the total height decrease. However,it did not lead to higher degrees of compaction in comparison to lower energy inputs. Still a similar final saturation of 91 and 93% was present compared to the final saturation of 87% of the engine 30 series. The final result in terms of density was similar to the engine 30 series. The final dry densities and corresponding compactive strain were 1320 kg/m$^3$, 3.7%, 1302 kg/m$^3$, 5.7% ,1321kg/m$^3$ and 3.6% for U16100, T16100 and T16100_2 respectively. Similarly the final RD was 10%, 7% and 10%.

It was found that the bottom flange leaked during test T16100. In figure 6.8 it can be seen that the bottom flange leaked. A clear distinction in moisture content could be observed as well as a well compacted zone.
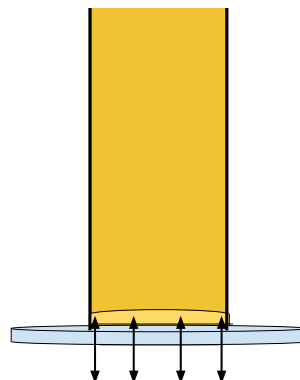


Figure 6.8: Pore fluid and air interchanging, creating an unsaturated, well compacted, zone in the lowest part of the cylinder

Considering test T16100, four sample rings were taken from the bottom of the cylinder. Adding to that, 6 samples were taken from the pvc tube. For T16100 the average dry density of the samples from the pvc tube was 1530. Corresponding with figure 6.9 a density gradient was present, where the bottom had a dry density of 1675 kg/m$^3$ and the top 1464 kg/m$^3$.

In figure 6.10 a sample of T16100_2 after compaction is presented. The sample showed a clear gradient where most of the residual gas was present in the lower parts of the cylinder.



Figure 6.9: PVC samples after compaction. Left side is the lower part of the cylinder and right side the top of the cylinder. Test T16100



Figure 6.10: PVC samples after compaction. Left side is the lower part of the cylinder and right side the top of the cylinder. Test T16100_2, note the gas volume that is still present in the lower part of the sample

### Surcharge test

The initial dry density after settlement for the surcharge test was 1224 kg/m$^3$. This corresponded with a relative density of -4%.

During the reaction phase the surcharge could not inhibit the swelling process of the sample. A decrease in density to 1176 kg/m$^3$ was recorded, corresponding to a swelling of 5.8%. This test had the lowest amount of swelling along with test T16N1.

The surcharge test was only compacted for 2 intervals of 30s. Both the vibrating engine and the frame did not feel safe to continue. Furthermore, after compaction some degree of mixing between the soil sample and the surcharge occurred. This made it made it difficult to take note of the interface where the height of the soil was. After compaction 31 cm height decrease had taken place. Of all the 2.5m tests this was both relatively, in terms of strain, but also in absolute terms the highest amount of compaction. The vertical strain was 12.4% compared to the settled stage. The final dry density was 1420 kg/m$^3$. This density corresponded with a RD of 28%. In comparison to the final RD of U16100 (10% RD) the surcharge test had a final RD of 2.8 times higher[1].

The final saturation could not be determined due to the leakage, however it was observed that a certain amount of residual gas was still present. This can be seen in figure 6.11.

---

[1]U16100 was not compacted with a surcharge, so comparison might not be representative.

Figure 6.11: PVC samples after compaction. Left is the lower part of the cylinder and right the top of the cylinder. Test T16100sur, gas is still present in the lower part of the sample

## 6.3. EC and VWC over time

The electrical conductivity, expressed in saturation extract, was plotted against time (figure 6.12).
Considering phase I only a single series was monitored using the EC sensors. In plot 6.12a, each sensor
represented a different sample being untreated (U1) or treated (T1,T2). As only a single plot of phase
I was produced the results of both phases were merged.

For the tests of phase II, each plot shows the results of a single test. During such a test multiple sensors
over depth could be used. With port 1 being the deepest and port 4 the shallowest. Initially, a spacing
of 40cm was present between each sensor. Note that in plot 6.12h the y-scale is differs from the other
plots.

Similarly the volumetric water content was plotted against time (figure 6.13).

(a) SH2

(b) T16N1

(c) T16N2

(d) U1630

(e) T1630

(f) U16100

(g) T16100

(h) T161002, note different y-scale (0-16 mS/cm)
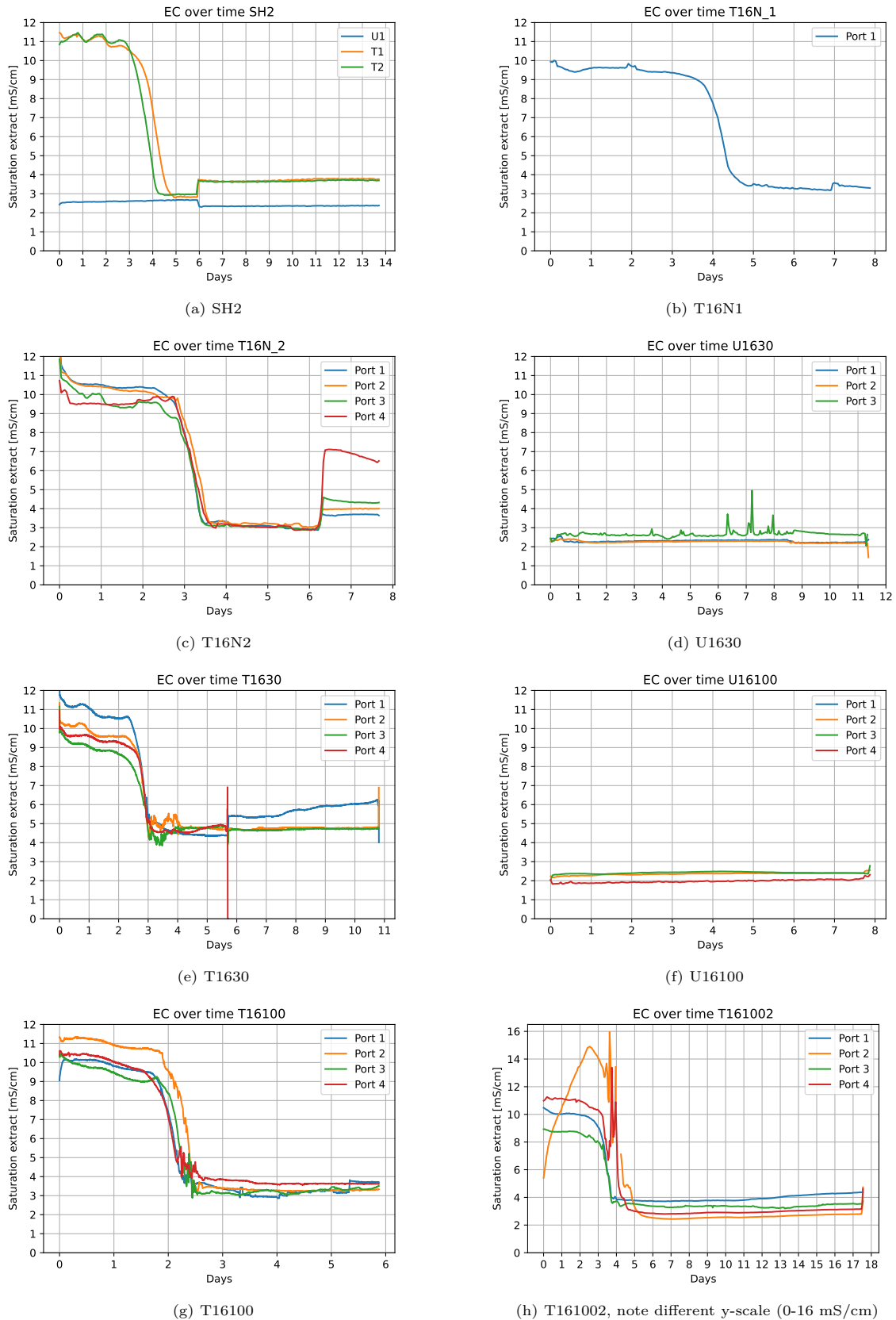
Figure 6.12: Electrical conductivity over time, expressed in saturation extract
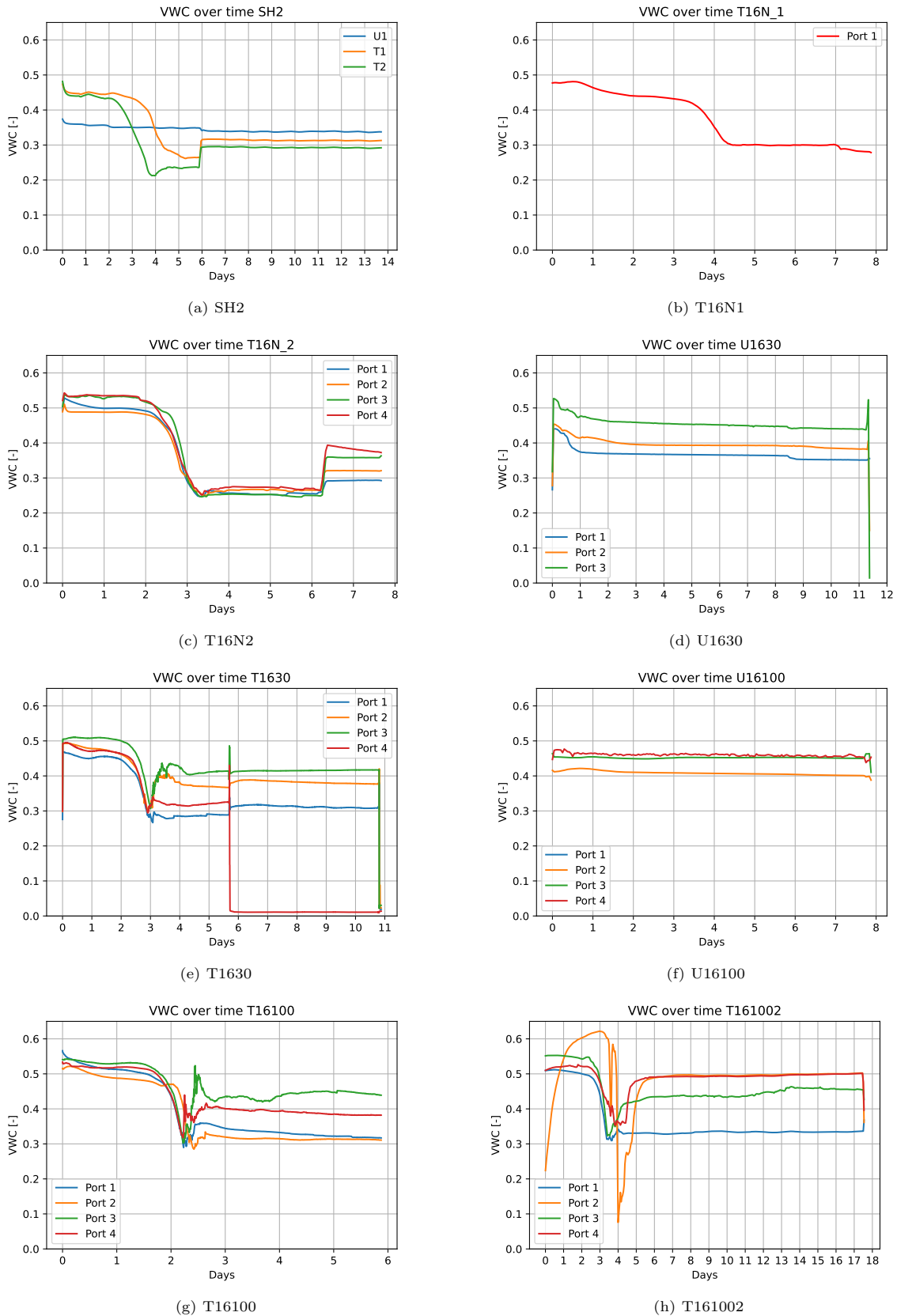
Figure 6.13: Volumetric water content over time

## 6.4. Observations EC/VWC measurements

As soon as the bacteria came into contact with the nutrients, the reaction commenced. The tests started with a conductivity of about 10 to 12 mS/cm. The tests with a target saturation had an initial concentration of nitrate was 60mM and the initial concentration of acetate was 80mM. All monitored tests presented consistent lag period of 3 days before the conductivity returned to a control level of 3 to 4 mS/cm. The drop in salinity occurred within half a day (figure 6.12 and 6.13).

For untreated tests the conductivity stayed at a constant level of 2 to 3 mS/cm. Tests with multiple sensors over depth showed little difference (<0.2 mS/cm) between the output of the sensors.

The TEROS 12 sensors also measured the VWC over time. Again, the same trend appears for both treated and untreated samples. In general, all samples are deposited with a VWC of approximately 0.5. For the treated tests this often decreased to a value of 0.3. After the compaction stage the treated samples go up in volumetric water content. The untreated samples did not show large differences over time.

During the tests the sensors were not held firmly into place. The swelling was able to displace the sensors, during test T16100.2 sensor 1 and 2 came up. In all cases it was not determined what the displacement of these sensors was. In figures 6.12h, 6.13h it was both observed and seen in the figures that sensor of port 2 came up and floated in the water column. This may explain the high EC and VWC. The VWC also drops to 0 were it probably just got out of the water.

| Initial salinity ≈12 mS/cm and VWC ≈0.5 | Lag period ≈3 days | Nutrient consumption ≈0.5 day | Final salinity ≈3 mS/cm and VWC≈0.3 | Compaction stage |

Figure 6.14: Schematic of observed phenomena during a treated test in terms of conductivity and VWC

# 7

# Discussion

This chapter discusses the results. Suggestions on how and why certain results were acquired are made. Moreover, a model is presented based on literature and compared to the findings in this research.

The main objective of this research was to increase in degree of compaction. Although the degree of compaction depends on many factors such as soil type and compaction method, in this research these parameters were tried to keep equal between untreated and treated tests. A treated test distinguishes itself based on gas behaviour. In term, it is argued that gas behaviour is responsible for the outcome of the degree of compaction.
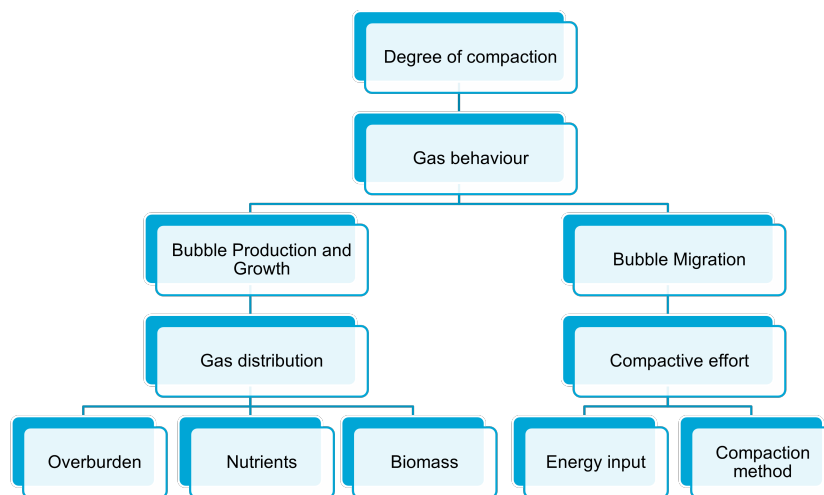


Figure 7.1: Relationship discussion points

## 7.1. Uncertainties in the research

The first uncertainty was the deposited mass. Inherently leading to errors in the calculated density. Additionally, a mistake could be made in the volume estimation. However this would only lead to a biased result as the volume is constant. In contrast to spillage, where only 50 kg can have great influence on the results (figure 6.6). By presenting the results in terms of relative density this error is enlarged. Under the assumption that the soil has the same density for a given volume and saturation a comparison can be made using the calculated strain (or absolute height).

During the tests leakage was observed directly, by means of visual inspection. However it was also observed indirectly based on the water level of the water column. During the settlement process three mechanisms were recognized:

- Only the soil slurry decreased in height not the water column
- Only the water level decreased in height, not the soil slurry
- Both the soil slurry and the water column decreased in height

It was deduced that if the soil slurry only decreases in height, then self-weight consolidation was the only applied mechanism. When only the water level decreased then the cylinder experienced leakage or air bubbles are interchanged with the same volume of water. Whenever the soil slurry ànd the water column decreased then a combination of the two above would be present. In figure 7.2, both the settlement process can be observed as well as a slight decrease in water level.
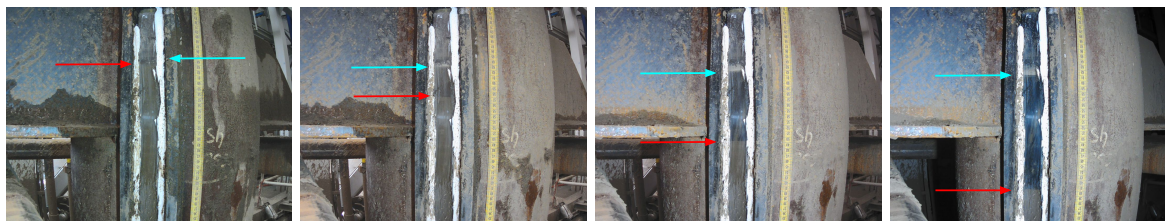


Figure 7.2: Settlement process, timelapse from test U16.30, The soil slurry level is indicated using red arrows. The blue arrows denote the water level.

In all tests where leakage took place, the confinement of the test was compromised. This results in different boundary conditions. This was especially the case for test T16N1. The travelling distance to the atmosphere for the gas was halved in this situation. The combination of a leak at the bottom of the cylinder and the overlying overburden may enhance the compaction significantly.

Although in the surcharge test also leakage occurred it is argued that this was a different case. The reason being that leakage only initialized after gas production started picking up. Apparently there was an interplay between the overburden and gas pressure. This might be an indication that the overburden indeed suppresses swelling. It is suggested that the leakage only had an effect on the desaturation process, not on the compaction process. Leakage was a problem since it resulted in an error in the mass balance. In the case of leakage, the average water content could not be determined with certainty anymore. This was also the reason why T16100sur was not plotted in the dry density vs water content. During the surcharge test it was observed that as gas production commenced water started pushing the sealing layer of kit away, resulting in large leakage throughout the test. It was not recorded what the exact amount of leakage was. However based on the initial conditions the measured heights, could still be related to dry densities. Although one might argue that the compaction mechanism for a different drainage/boundary conditions cannot be compared.

Figure 7.3: Leakage induced by gas pressure

Pressure sensors were installed in the set up but unfortunately did not work. In order to actually have certainty on the water and gas pressures these might clear up a lot of the mechanisms that occurred. During the gas phase this might show how the desaturation over depth takes place. During the compaction stage it can be observed how much of the stresses are taken up by the water.

Another uncertainty is the energy input. In this research 4 methods of compaction were applied, all with their respective power and frequency. In T16N1 20min of intrusive compaction with a 200 Hz needle was used. Opposed to the non-intrusive engine series which was maximally compacted for 4 minutes on 30 Hz. Furthermore the amplitude greatly differed. Wheras the needle was highly frequent on a low amplitude, the engine was low frequent with the whole frame vibrating with 2 to 3 mm. It cannot be said with certainty which compaction part of a specific method led to the acquired results. Thereby clouding whether something was the result of the energy input or the method of energy input.

## 7.2. Bubble Production & Growth, Shear strength dependency

In the review of literature it was noted that the nucleation of bubbles depends on the equilibrium of pressure and concentration according with Henry's law (2.8). Furthermore, in line with the ideal gas law, the increase of pressure due to the overburden would result in smaller volumes of gas being present. This hypothesis was also partly based on the findings of Stals 2020 and Pham 2017. Pham 2017 used CT-scans in which it could be easily observed that gas volume was related to depth. In Stals 2020 the visual inspection also lead to this observation.



Figure 7.4: Sample showing gas distribution of treated sample, by: Stals 2020
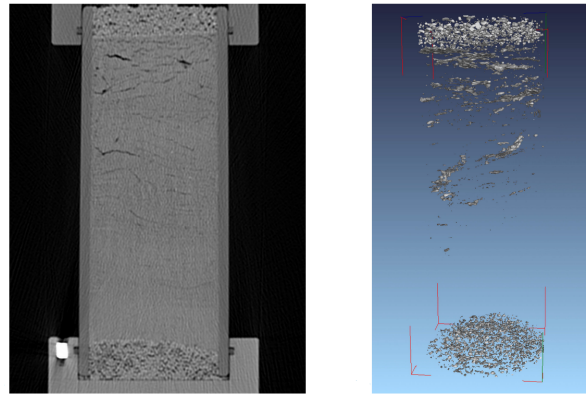
Figure 7.5: CT scan of a treated sand sample (left) and a contstructed 3D image from: Pham 2017. Note the gradient of the gas volume over depth.

In contrast to previous findings, this research found a relatively homogeneous gas distribution. Furthermore the test samples were a factor 6 times higher (opposed to the samples of Stals 2020). Multiple reasons for the relatively homogeneous gas distribution are proposed:

- The boundary conditions of previous work resulted in the distribution of less gas near the lower boundaries not necessarily the pressure increase
- Local compaction due to bubble growth is less pronounced for larger samples, under the assumption of rigid boundaries
- The increase in pressure due to the overburden only has a marginal effect on the gas production and nucleation process
- In this research supersaturation reached a such a high point where nucleation happened rather homogeneous
- The gas retention characteristics of this researched material allow for homogeneous gas production over depth

The first point refers to preferential flow paths along which the gas can migrate.
Kessel 1998 highlighted the effect of bubbles locally compacting the soil during growth. Relatively speaking, when the sample size increases there is a higher volume of soil which can deform, opposed to the rigid boundaries of the set up. Therefore it is suggested that as the sample increases, there is more room for bubbles to develop.
An important difference in the presented experiments of Pham 2017 was that the tests were on sand. Because of the low relatively low AEV of sands, it is suggested that the gas capacity at a specific pressure is lower as for silty sands. Based on Henry's law in combination with the ideal gas law, the gas volume over depth was calculated and plotted for different initial concentrations of NO3 by Pham 2017.
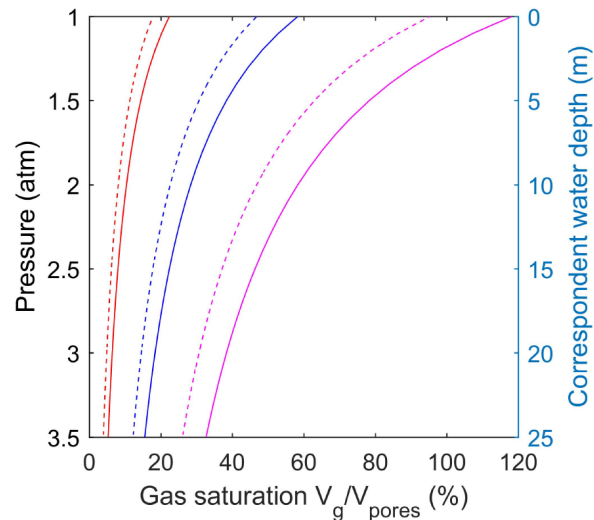
Figure 7.6: "The gas saturation induced by denitrification as a function of pore pressure, calculated for the stoichiometry of maximal growth (dashed lines) and pure maintenance or zero growth (continuous lines), for three different concentrations consumed NO3-: 20 mM (-), 50 mM (-) and 100 mM (-). Pham 2017"

In this research an average concentration of $NO_3$ was used of 60 mM. Suppose the blue line can be used (50 mM), then the difference in gas saturation for 2m of water pressure (assuming that the gas pressure is equal to that) would only be 10%. However, based on the results it is suggested that a continuous gas phase starts to occur at a gas saturation of approximately 40% and higher. For the blue line the intersection of 40% gas saturation is at 5m water depth. As the sample is only 2m it is argued that, in this case, the continuous gas phase is the limiting factor regarding the gas saturation rather than the overburden. If one were to increase the concentration of nitrate to 100 mM then the found gas saturation would still be 25% (Sw=75%) at 25m water depth. It is argued that even at this pressure the overburden is not the limiting factor to achieve the optimum water saturation. Based on a qualitative visual inspection a relatively homogeneous gas distribution was found.

Following Henry's law, the concentration of dissolved nutrients needs to increase for larger depths. It is suggested that the feasibility of desaturation through nutrients can be assigned to two aspects. Firstly, the costs of the nutrients and secondly, whether the nutrients can be homogeneously mixed over a soil body. In this research an inoculum was used to ensure that biomass would not be the limiting factor. The inoculum was easily produced and it is suggested that in the unlikely chance of no biomass in the soil this inoculum can be easily added whilst mixing of the nutrients with the soil.

Both Pham 2017 and Stals 2020 carried out tests on soils with low to no amounts of clay. Based on the above it is suggested that pressure difference plays a larger role for more coarse materials regarding gas distribution.

Based on the swelling of the samples the bubble growth follows mechanism I (the bubbles deform the soil matrix, paragraph 2.3). Vane tests showed a shear strength of 0 to 1 kPa. However it should be mentioned that the vane tests were not done in-situ. When assuming a shear modulus of approximately ten times the undrained shear strength, a limit pressure that the bubbles needs to grow in a sludge can be calculated (equation (2.10)). This resulted in:

$$\Delta p_{r \to \infty} = \frac{4}{3} * 1(1 + ln(\frac{1000}{1})) = 10.54 \, kPa \tag{7.1}$$

In the last test a surcharge of 6.5 kPa effective stress was added. Based on the formula by Kessel 1998 it was expected that swelling would occur. The results are in line with the formula, however it is argued that the original formula might not be relevant for large depth as no depth dependency is present in the formula ((i)). In reality, for unconsolidated soils, the $\tau$ is dependent on depth following the Mohr-Coulomb criterion.
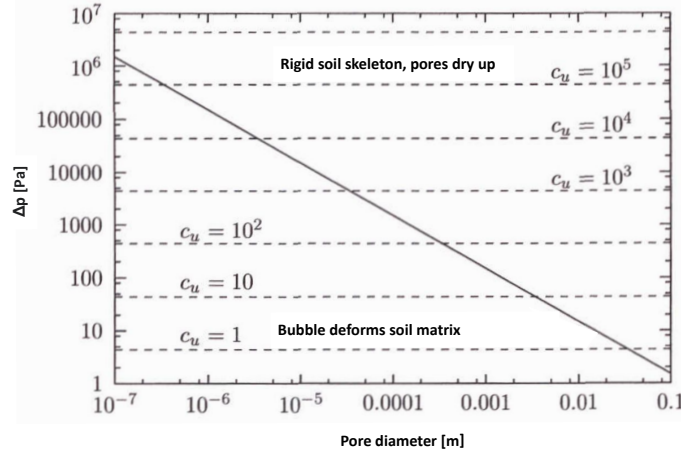
Figure 7.7: Criterium for two proposed mechanisms: Either the bubble deforms the soil matrix, or the bubble moves through the pores according with the rigid soil skeleton mechanism (from: Kessel 1998, translated)

$$\tau = \sigma \, tan(\phi) + c \qquad (7.2)$$

In figure it can be observed that the mechanism that is present depends on the shear strength and the bubble radius. If the shear strength increases then, for the same bubble radius, the change from mechanism I to mechanism II can be observed. This research showed that the amount of swelling was partly suppressed due to a surcharge. It is suggested that the surcharge increased the shear strength of the soil, resulting in less mobilisation of the soil skeleton (mechanism I). Furthermore, with the soil skeleton providing a higher resistance, more gas drive will expel more water out of the soil. If enough resistance of the soil skeleton is present, the so-called rigid skeleton mechanism will take place. Here fluids move trough the porous media without deformation of the grains. It is therefore suggested that if swelling may be mitigated more water may driven out due to the gas pressure. Similarly for an increasing bubble radius but the same shear strength the same process may occur.

An additional reason why the swelling was less in the surcharge test was that that part of the upward pressure dissipated by leakage. In Kessel 1998 it was stated that when bubbles grow in a loose soil the bubbles may locally compact the soil. This adds to the effect of an increase of $\tau$ and thus less swelling over depth.

In some cases the water managed to displace fine grained material during water migration to the top. This corresponds to the observation of siffosion. It was observed that little to no drainage via the drain was achieved. Due to depositional processes, lateral conductivity is often higher than vertical conductivity. This means that in reality either higher degrees of desaturation can be expected and lower amounts of swelling. The optimum water content was reached in all tests, it can be said that water expulsion was not necessarily a problem. However it is yet to be established how desaturation will take place with radial drainage possible. Especially with focus on the swelling.

## 7.3. Bubble migration, Saturation dependent gas conductivity

In this mechanism it is suggested that the gas conductivity is dependent on the saturation state of the sample. It is suggested that when gas saturation is high in combination with a loose state of the soil a continuous gas phase may along which gas can quickly escape. As bubbles merge and a flow path is created. When this happens, the gas bubbles come into contact with the atmosphere. Consequently, the gas pressure instantaneously becomes equal to the atmospheric pressure. Equation (2.9) becomes:

$$p_c = -p_w \qquad (7.3)$$

Analogue to the proctor test the capillary pressures actually aid in the compaction process when this mechanism is present. This is also illustrated by the arrows and the schematic of the pore throat in figure 7.8. This mechanism clearly outlines how increasing the scale is essential in the gas behaviour. As the scale of the set up increases the chance to create a continuous gas phase becomes lower. As

the height increases, the distance to the surface increases. Similarly as the diameter of the cylinder increases the distance to the wall (and drain) along which a preferential flow path may easily occur. It is suggested that this mechanism was present at the following observations.

It is suggested that the reason series SH2 yielded successful results was because a continuous gas phase was present. The 1m set up only had a diameter of 9 cm. Vibrating against the side of the side of the cylinder allowed for the gas to escape via this boundary. Resulting in a fully saturated, compacted state.

When the bottom flange was opened after test T16100sur it was qualitatively observed that a radial gradient of compaction was present. The soil was more compacted at the drain side opposed to other side. It is suggested that the drain worked as a preferential flow path along which gas could escape.
When bubbles are largest they are able to migrate faster through the porous medium, more importantly, bubbles are also connected easier. The loose state of the soil in combination with the vibrations of the compaction method resulted in a continuous gas phase. This also explained why the initial intervals of compaction also resulted in the largest decrease in height.
Lastly, the observation of leakage in figure 6.8. The leakage allowed for a flow path for gas. It is suggested that the overburden in combination with a short flow path led to a well compacted soil. One could argue that in figure 6.8 segregation of fines and sand was the cause of the colour change not leakage. Other tests however showed that, based on grain distrbutions, the deposition process of the 2.5m test resulted in a homogeneous sample.
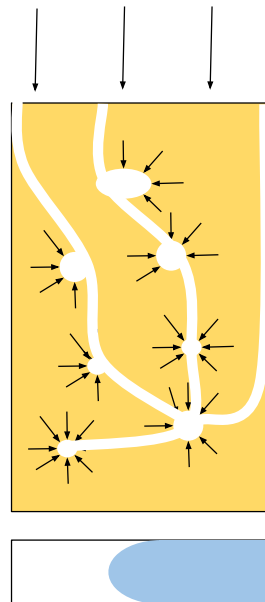


Figure 7.8: Schematic of proposed bubble migration with a continuous gas phase

A model was produced based on the input conditions and literature (Appendix G). The model assumes an initial rate of the nitrate consumption as well as an initial concentration of biomass. Using a saturation dependent gas conductivity the amount of swelling and occluded gas was calculated.

The initial concentration of nitrate used in the tests was known. In the model the average of 60 mM was used. Furthermore, as the saturation extract can be directly linked to concentration, a normalisation from saturation extract to concentration was used to fit the model. Knowing that the EC starts and ends at a saturation extract of 11 mS/cm to 3 mS/cm the normalisation was done by focusing on the lag period and the non-linear consumption of the nutrients.
As the reaction takes place, initially, dissolved nitrogen is produced. Keeping the stoichiometry of max growth in mind. Based on Young La Place law of capillarity, Henry's law and the ideal gas law the volume of nitrogen gas is computed. Although Henry's law works both ways, it was forced that gas could not dissolve again.

In figure 7.9 can be seen that as the biomass grows the concentration of nitrate decreases. After a lag period of approximately three days the reaction rate increases exponentially. The rate of the reaction was assumed to be a product of the initial rate and the biomass. A Monod-term was included to make the transition smooth (7.4). Over time dissolved nitrogen is produced. As the concentration of dissolved nitrogen increases, gas starts to nucleate and nitrogen gas is produced. When the reaction is over the amount of dissolved nitrogen returns to 0 as all is converted to nitrogen gas.

$$r_{reaction} = r_0 * [X] * \frac{[NO_3]}{(K_m + [NO_3])} \tag{7.4}$$

In which:

| | |
|---|---|
| $r_{reaction}$ | Rate of nutrient consumption [mol/(kg*X*hr)] |
| $r_0$ | Initial rate of nuntrient consumption [mol/(kg*X*hr)] |
| $[X]$ | Concentration of biomass [mol/kg] |
| $[NO_3]$ | Concentration of nitrate [mol/kg] |
| $K_m$ | Constant for asymptotic condition [-] |
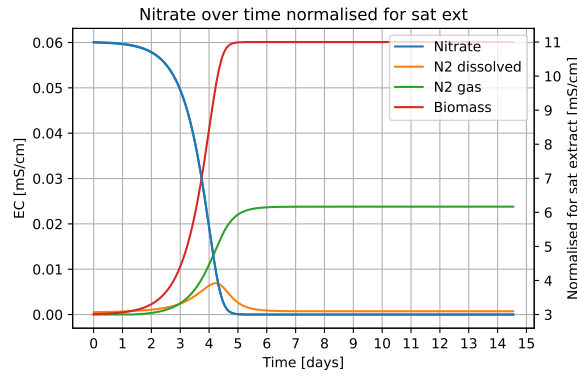


Figure 7.9: Concentration and Normalised saturation extract agains time.

Based on the tests the residual gas saturation was estimated to be 10%. Without taking into account hysteresis the residual water saturation was assumed to be the same. Using a modified Stone equation presented in Mahabadi and Jaewon Jang 2014 a saturation dependent relative gas conductivity was computed with equation 7.5. The saturated gas conductivity was estimated to be the saturated hydraulic conductivity times a factor ten. The saturated hydraulic conductivity was retrieved from the Ksat tests (5.65E-7 m/s).

$$k_{rw} = \left( \frac{S_{gas} - S_{gas,residual}}{1 - S_{wat,residual}} \right)^{n_g} \tag{7.5}$$

In which:

| | |
|---|---|
| $k_{rw}$ | relative permeability [-] |
| $n_g$ | Fitting paramater (2.0 in this research) [-] |

The actual gas conductivity for that specific saturation was then found by:

$$k_i = k_{sat} * krw \tag{7.6}$$
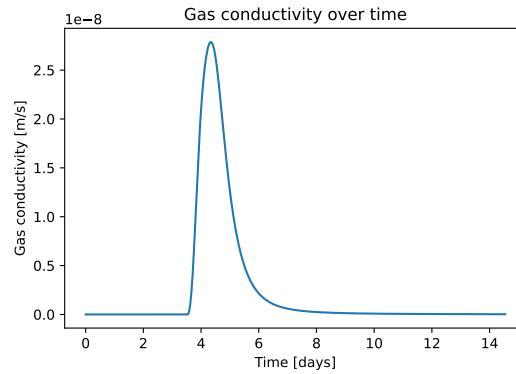
Figure 7.10: Gas conductivity over time

Using a specific conductivity in time a flux out of the system was calculated by Darcy's law. With the flux known the amount of occluded and vented gas were computed.

$$J_i = K_i * A_{cyl} * \frac{dH}{dz} \tag{7.7}$$

Based on the occluded and vented gas the amount of swelling over time was computed.
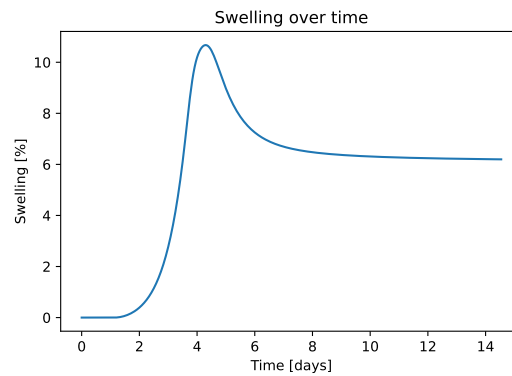


Figure 7.11: Modelled swelling over time

It can be seen that the swelling was maximally 10%. After venting however the swelling was 6%. Although only 1 simulation was carried out, this result does show potential as the result is within range of the tests in this research. This simulation only ran for a specific case. Apparently, for this case, the Modified Stone's equation gives a fair insight in the gas migration process. The model might prove useful to estimate expected amounts of gas in a soil body. If one were able to measure the gas pressure over time, also during compaction, the model could be used to determine the gas volumes after compaction as well.

## 7.4. Liquefaction

If bubbles cannot form a continuos gas phase anymore it is suggested that during compaction individual bubbles move through the soil body according with Stoke's law. Stoke's law. Stoke's law may be applied for spheres in fluids. This leads to the first assumption that, during compaction the entire soil sample is liquefied. Secondly, a bubble is a sphere with a constant radius. It does not deform during migration. Multiple tests showed a significant amount of residual gas still present in the sample after compaction. This was observed in the samples but also based on the calculations. Stoke's law can be used to estimate the bubble migration velocity. In order to do this the average bubble radius needs to be assumed as well as the viscosity of the liquefied soil.

Based on the observations the average bubble radius was assumed to be 2.5 mm. Alba and Ballestero 2006 did research on the viscosity of liquefied sands (figure 7.12). In order to get a maximum velocity the lowest viscosity is used of $50\,Pa \cdot s$.
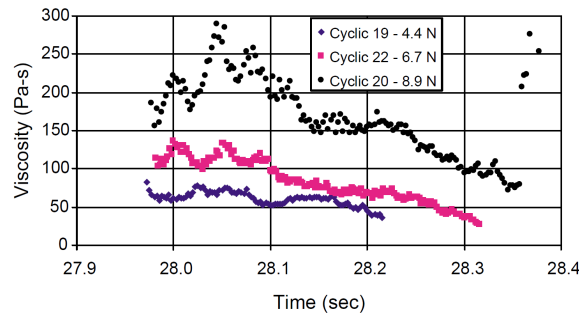


Figure 7.12: Apparrent viscosity of liquefied sand versus time from: Alba and Ballestero 2006

This results in a bubble velocity of:

$$v = \frac{2 \cdot (1850 - 1251) \cdot 9.81 \cdot (2.5 * 10^{-3})^2}{9 \cdot 50} = 0.50\,m/s \qquad (7.8)$$

The engine compacts for four minutes. The bubble would then have travelled a distance of:

$$0.5 * 240 = 120\,mm$$

This corresponds to the observation of residual gas still being present in the samples. Furthermore if this bubble would be located at the bottom of the sample, then in order to get it out one should compact for:

$$\frac{2000}{0.5} \approx 66\,minutes$$

This methodology can be worked out for a range of bubble radii. Resulting in a relationship between the bubble radius and the time it would take for that bubble to travel 2m through a liquefied medium ($\mu = 50\,Pa \cdot s$).
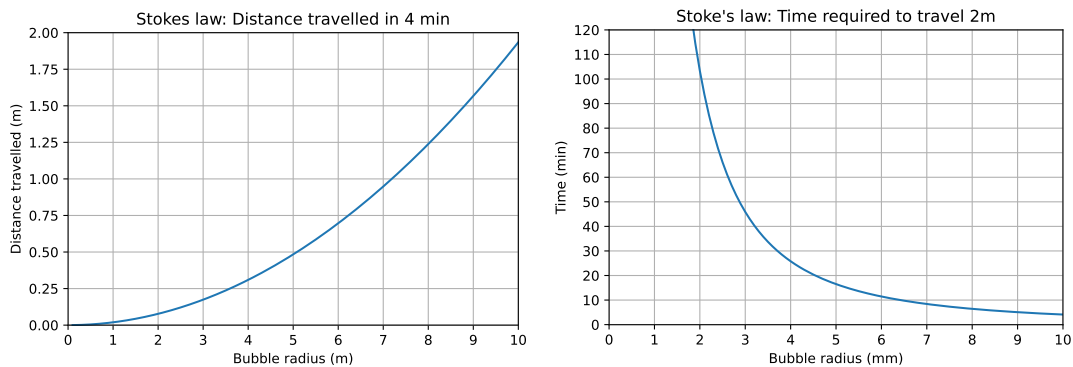


Figure 7.13: Travel distance of a bubble after 4minutes (standardized compaction time), left. Time required for a bubble to travel 2m (largest travelling distance), right

Figure 7.13 showed that only bubbles of 10mm would be able to travel the full length of the cylinder. Additionally it can be seen that bubbles lower than 2mm only exit the system after an almost infinite amount of time. Visual inspection of the samples figures 6.9, 6.10 showed that after compaction bubbles with radii larger than 10mm were still present in the sample. This approach of applying Stoke's did assume the viscosity and without knowing whether the soil actually liquefies may explain why the calculation is not in line with the found result.

Similarly one could vary for a range of viscosities. As we saw that a bubble of 10mm was still present in one of the samples. To give a more clear insight an average radius of 5mm was used to produce figure 7.14.
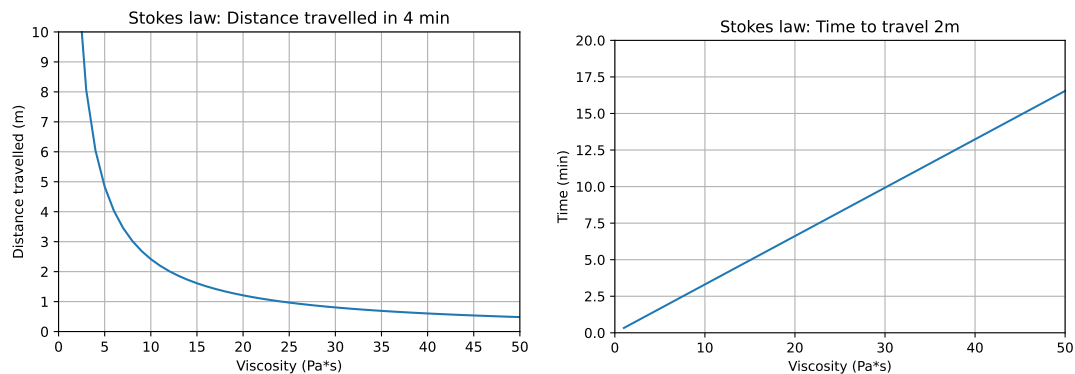


Figure 7.14: Travel distance of a bubble after 4minutes for various viscosities,left. Time required for a bubble to travel 2m for varying viscosities, right. Both plots assume a constant bubble radius of 5mm.

It was observed that in order to get all 5mm radius bubbles out of the system a viscosity of $12\,Pa\cdot s$ is required. This is 4 times more viscous than the assumed $50\,Pa\cdot s$.

Based on the above liquefaction may be the solution to remove all gas out of the system. However, based on Nicholson 2014 (figure 2.9). Showed that the liquefied zone was not ideal for compaction purposes. In this research the vibrating engine was not adjusted radially to account for the distance to acquire the optimum particle acceleration.

## 7.5. Residual gas, Occluded gas bubbles

For all 2.5m tests it was observed that a residual amount of gas was present. The actual mechanism after the first few intervals of compaction is suggested to be the occluded gas mechanism. In this case the gas pressure is the sum of the capillary pressure, the water pressure and the atmospheric pressure. In this case the meniscus in the pore throat flips. For this application this mechanism is undesired. The gas in the system essentially works like a spring and dampens incoming compactive forces. The residual gas may inhibit further compaction. This effect however is desired for earthquake mitigation. As Tsukamoto et al. 2002 stated 10% gas saturation already increases the CRR drastically. This research showed that gas bubbles are able to stay in the system after 4 minutes of compaction with a vibrating engine. Liquefaction mitigation and physical modelling of earthquakes was out of the scope of this research, although results of residual gas are promising for this application.
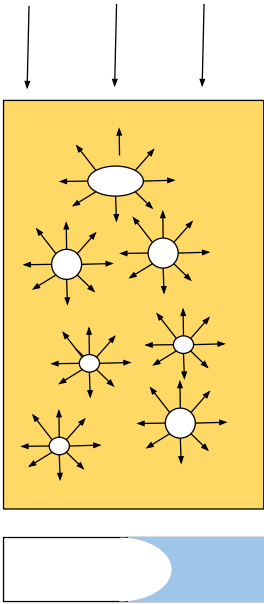
Figure 7.15: Schematic of state residual gas bubbles

# 8

# Techno-economical analysis

This chapter combines the results and a future field trial. The impact of the acquired results is discussed.

Hall et al. 2022 published a techno-economic analysis (TEA) for the application: MID as a solution for liquefaction mitigation. Although a different application the same approach for the analysis will be held onto. First a hypothetical case will be set up. Sequentially a plan to realise MID for increased degrees of compaction is set up with corresponding estimated costs. Lastly a comparison to a replacement technique will be carried out.

## 8.1. Hypothetical field test and input conditions

In order to make a TEA, a hypothetical field trial is set up. The input conditions largely coincide with the experimental tests. Starting with the geological profile, this includes a case in which a soil body with a thickness of 5m and an area of 100 $m^2$. The soil body will consist of a homogeneous silty sand with 16% fines (similar to the used test material in this research). Nutrients will be injected and extracted using drains. Depending on the hydraulic conductivity the maximum injection rate can be determined. Practically, it was found that mixing of the nutrients was easier with calcium nitrate tetra-hydrate ($Ca(NO_3)_2 \cdot 4H_2O$), opposed to regular calcium nitrate. Lumps of material were produced that were difficult to dissolve. This may be of relevance for the injection/extraction purposes



Figure 8.1: Mixing of Yara Calcinit, resulting in lupms of nutrients

The optimal configuration of injection and extraction wells is yet to be established, however two possible

configurations are proposed based on Zeng et al. 2021 and Hall et al. 2022. In Zeng et al. 2021 an injection well is placed in the middle of other extraction wells. Furthermore a center to center distance of 3.5m was used. Hall et al. 2022 proposed a simpler configuration in which a single head gradient pulls the nutrients from one side of the treated area to the other.
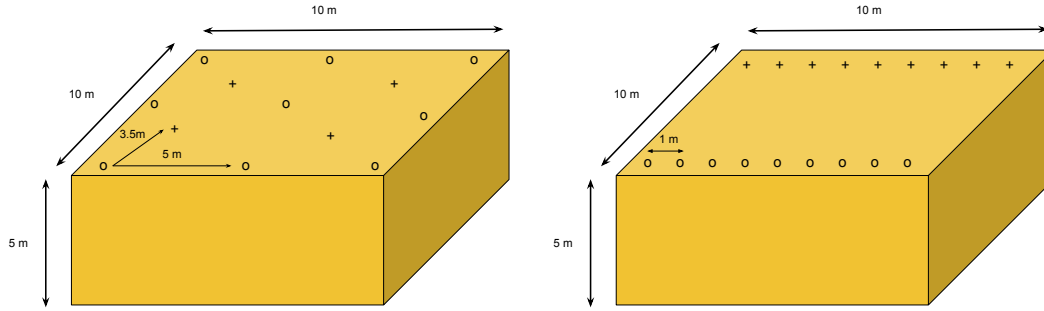


Figure 8.2: Schematic of proposed hypothetical case. Including preliminary configuration of extraction wells (o) and injection wells (+). Left a configuration based on Zeng et al. 2021 and right from Hall et al. 2022.

The distribution process off flushing nutrients is known to be a rather unpredictable process due to the heterogeneous nature of a soil body. Consequently, the amount of flushes and corresponding amount of nutrients will be an unknown. Therefore to keep the analysis simple the. The amount of nutrients will be set to a target saturation of 50% under the assumption that mixing of the nutrients with the soil will distributed evenly. With the boundaries of the target areas being no-flow boundaries, i.e. all injected nutrients stay in the system. Although this research did show that less nutrients can be used, this was not yet optimised. Therefore the amount is kept the same (accounting for the difference in pressure due to increased depth) as in the research as this is known to desaturate the soil to the OWC.

## 8.2. Nutrients, estimated price per cubic meter

In practice nutrients can be bought in bulk. For this research this was obviously not necessary. That is why prices per cubic meter for the nutrients may vary. In this research Niacet Calcium Acetate was used as an organic carbon source. The price €2.5 per kg was based on earlier research Hall et al. 2022. Secondly Calcinit Calcium Nitrate was bought in a farmers store. The price was approximately €1.50 per kg, this corresponds to the estimated costs in Hall et al. 2022. For a target saturation of 50%, a in-situ soil mass of 1900 kg/m3 and a water depth of 4m (phreatic water level of -1m below surface assumed). The amount of nutrients per $m^3$ is calculated to be approximately 2.8 kg of Acetate and 3.4 kg of nitrate (calculation sheet by: Andrag 2017). Resulting in a total cost of €12.10 per cubic meter of soil. The calculations are summarised in the following table 8.1.

Table 8.1: Nutrient costs per m3

| Product | price | unit | kg/m3 | price per m3 |
|---|---|---|---|---|
| Nitrate (Yara liva Calcinit) | € 1.50 | kg | 3.4 | € 5.10 |
| Acetate (Niacet Calcium Acetate) | € 2.50 | kg | 2.8 | € 7.00 |
| | | | Total | € 12.10 |

## 8.3. Stone columns

In Bouassida and Hazzar 2008, it was stated that a price for stone columns would be approximately €105 per linear m of column. It was assumed that the area of the columns covers 10 to 15 percent of the area. Assuming a diameter of 600mm for the stone columns and a square grid this would lead to a center to center distance of:

$$A = \sqrt{10 * (\pi * 0.3^2)} \approx 1.68m \tag{8.1}$$

For the hypothetical field this would lead to $\approx 35$ stone columns.

## 8.4. Cost comparison
For the hypothetical case this would lead to the following cost comparison:

Table 8.2: Cost comparison MIDP and Stone columns

| MIDP and Compaction | | | | Stone columns | | | |
|---|---|---|---|---|---|---|---|
| Item | Price per unit | Units | Costs | Item | Price per unit | Units | Costs |
| Nutrients | € 12.10 | (10*10*5) m3 | € 6,050.00 | Stone columns | € 105.00 | (35*5) m | € 18,375 |

No cost estimate for impact compaction and installation of drains were taken into account in the analysis. The comparison therefore may not be representative. Furthermore, costs highly depend on in-situ conditions and costs of personnel. This cost comparison presents only a shallow insight in the costs a possible field trial will have. Large unknowns are still present. As described, the injection of nutrients and the actual desaturation process may not yield the required amount of desaturation. In the end the question remains whether the proposed solution achieves the desired results in terms of densification.

## 8.5. Impact of results
The relationship between this research and the field trial is made. This is done by analysing the results and extrapolating the impact they have on possible field conditions

### 8.5.1. Desaturation
Flushing of nutrients. Flushing of nutrients is a well researched practice for carbonate precipitation. In practice soil bodies are never homogeneous. Test SSt1 showed that gas production took place in the coarse layers. It is expected that the sandy layers will desaturate first based on Young Laplace equation of capillarity.

### 8.5.2. Impact compaction
The hypothetical field trial had a depth of approximately 5 to 10m, an relatively cheap method for compaction is impact compaction. Assuming that the gas formation stage is successful, it can be expected that, similar to this research, during the first few hits the larger bubbles may form a continuous gas phase. The initial amounts of compaction will be largest. However because of the nature of the gas bubbles, the first few hits will also be dampened the most. The reach of the stress waves may increase over time as more bubbles are vented out of the system. In this research a residual gas saturation of 10% is found. As the depth increases it is expected that the residual gas saturation is at least the same, or higher.

After no continuous gas phase can be realised anymore it is expected that the stress waves of the compaction method will be taken up mostly by the occluded bubbles. Gas is compressible. After a hit, the occluded gas bubbles decrease in volume instantaneously and with that the soil skeleton may rearrange itself. The decrease in volume is directly related to an increase in gas pressure according with the Ideal gas law. One could argue that the bubble will increase in volume again displacing back to its original state before the hit. However it is expected that this is not a fully reversible process. As the grains get closer to each other the undrained shear strength may also go up. Thereby the pressure the bubble needs to mobilise the skeleton may not be large enough anymore. As suggested in this research in figure 7.7 it can be seen that the mechanism may change to a situation in which the gas moves through the pore throats. As the pressure of the gas is higher, more gas drive can be expected. Two things may happen. First of all the gas may increase in volume by dividing itself over multiple pores. Additionally more water is expelled towards the drains. If the gas pressure is higher than the AEV of the drains the gas may vent out. If the undrained shear strength is increased drastically the gas pressures may also keep increasing. According with the equilibrium of Henry's law the gas may also dissolve in the water again. However it is expected that this will not be the leading mechanism, due to heterogeneity there will always be a suitable nucleation spot. Over time more gas gets out of the system and the zone of

influence of the CDC increases as the stress waves are able to travel further through stiffer material. If the pressures in the soil can be measured, then a possibility would be to further implement the gas migration model based on a Modified Stone's equation.

### 8.5.3. Vibroflotation

A second possibility is the use of a vibroflotation compaction method. Usually this method is applied from 7m depth. It may not be viable to produce gas at such high overburden pressures as the required nutrients keep increasing over depth. Although vibroflotation locally liquefies the soil, the gas around the soil is not expected to migrate move according with Stoke's law. It is suggested that the fluidized zone is too turbulent for this to apply. Still, it is expected that the vibroflotation probe creates a preferential flow path similar to the intrusive vibrating needle in this research. Along the probe gas may be easily vented out of the system. As mentioned multiple zones, characterized by their soil response, were identified. In the plastic and compaction zone (figure 2.9) it is expected that due to occluded gas bubbles more power may be required to achieve the same particle accelerations. Similarly, the zone of influence will be smaller due to this dampening effect. The grid spacing might need to be decreased accordingly. In the case of vibroflotation dephts it is expected that the limiting factor will be the costs of gas production and not gettting out the gas.

# 9

# Conclusion

In this follow up research the feasibility of MIDP as a pretreatment for compaction was researched. Two test set ups and their corresponding methodology were developed, scaling up from previous work. All treated tests, including 1m and 2.5m tests, showed a similar process. After deposition the samples settled first before swelling and venting. After venting the compaction stage was initiated. When scaling up the research question was stated:

- What are the scale effects, when scaling up from previous work?

After settling initial densities varied. This was due to uncertainties regarding the mass in the set up. In the end a reproducible depositional method was developed that resulted in an initial dry density after settling of approximately 1200 to 1300 kg/m$^3$.

It was concluded that, after mixing the nutrients with the soil, a consistent lag period of 3 days was found before significant gas production commenced. This conclusion can be drawn under the assumption that saturation extract is directly linked to nutrient consumption. The target saturation of treated samples was 50% with the exception of a single test that had a target saturation of 35%. It was concluded that all samples were able to desaturate to, and even below, the optimum water saturation of 75%.

The production and growth of bubbles caused swelling of all samples. A surcharge of 10.5 kPa could not mitigate the swellling process. It was suggested that the surcharge suppressed the swelling. This cannot be said with certainty as one test showed similar degrees of percentual swelling without the surcharge. It was suggested that whether a bubble deforms the soil matrix (swelling) or moves through it during growth is dependent on the undrained shear strength. Sequentially as the shear strength can be dependent on the overburden the first scale effect was identified.

Gas nucleation happened heterogeneously. As expected smaller bubbles and larger bubbles were both present in the sample. This observation was in line with the expected behaviour based on a combination of Henry's law and Young Laplace. By the same reasoning, and adding to the effect of heterogeneity, the bubbles grow instead of nucleate. A qualitative visual inspection, however did not indicate a strong relationship between overburden and gas distribution. It was argued that this scale effect was present, only on the scale of 2m a 10% difference in gas saturation was to be expected. Furthermore it was suggested that for a continuous gas phase occuring at 40% gas saturation the overburden will not be the limiting factor to achieve the optimum water saturation.

The samples were not able to retain all produced gas resulting in a venting process. A saturation dependent model was presented based on a modified Stone's equation. The underlying mechanism being a continuous gas phase that may occur at high gas saturations. Sequentially increasing the gas conductivity. It was concluded that the model could be promising in the sense that swelling and venting were well approximated for a single case. With pressure data during compaction the model may be extended to a model that may possibly be applied to estimate gas volumes after the compaction stage as well. It was argued that, similarly to the proctor test, this was a desired mechanism as the capillary forces aid in the compaction of the soil. The occurrence of a continuous gas phase did not only depend on the saturation.

Scaling up resulted in a larger travelling distance the gas bubbles had to overcome. Radially, towards the boundary of the cylinder and vertically, where the sample comes into contact with the atmosphere. Along the boundaries of the cylinder a preferential flow path may be encountered. The travel distance towards this boundary increases as the diameter increases. Similarly, assuming that there is no leakage, the height of the sample causes the travelling distance to the atmosphere to be larger. It was therefore suggested that boundary and scale effects have the largest effect on the continuous gas phase.

Four different compaction methods were experimented with. It was suggested that an intrusive compaction method, such as a vibrating needle, may allow for preferential flow paths such that all gas may be removed out of the system. Compaction with the vibrating, non-intrusive, engine led to a residual gas saturation of approximately 10%. For the vibrating engine higher amounts of energy input led to faster, but not more release of gas. The occluded gas bubbles were argued to work against the compaction method, dampening incoming compactive stresses. MIDP as an application to mitigate liquefaction is promising as the occluded gas was still found after the compaction stage.

The main question stated:

- Can MIDP be used as a pretreatment to increase the compactibility of silty sands

Phase I consisted of the 1m experiments. One series, SH2, had promising results in terms of degree of compaction. The final dry density was 139 kg/m$^3$ and 172 kg/m$^3$ higher opposed to the untreated, control, test. The final relative density of both treated tests was at least two times higher than the relative density of the untreated test.

Phase II consisted of the 2.5m experiments. Based on the results no gain in density was found for any of the tests, however some comments of uncertainty have to be placed here. Taking into account uncertainty of the initial density and the assumption that all gas could be removed with enough effort. A significant gain in dry density could be made using an intrusive needle compaction. In this case a linear extrapolation was applied to the results. Secondly, during a test with surcharge the set up started leaking. Although this changed the boundary conditions, during compaction leakage was not an issue. The results of the surcharge test were promising. One of the lowest amount of strain in the swelling stage was observed and the highest amount of compactive strain was found of all Phase II tests. The final dry density was 1420 kg/m$^3$, which is 100 kg/m$^3$ higher than the untreated test, which was compacted twice as long. The final relative density the treated test was 2.8 times higher than the relative density of the untreated test.

Although assumptions on uncertainty have to be made, it is concluded that the proposed method holds promising results, especially compaction methods with higher vertical forces (or overburden) are applied.

As the test was never done before and newly developed it can be said that, scaling up the test was successful. Taking into account the uncertainties it was concluded that the results still are promising. There are indications that MIDP is suitable as a pretreatment to compact silty sands.

# 10

# Recommendations

The first recommendation point are pressure sensors. It is strongly advised to do some measurements regarding pressure. In this research tubes filled with water were attached to a pressure meter. Leakage, clogging and gas production led to a discontinuous water phase in these tubes. Consequently leading to wrong measurements. If a stable method can be developed to measure pressure in the sample over time multiple recommendations are made:

- Vary the overburden, moreover, develop a no displacement boundary on top of the sample. What is the maximum produced gas pressure and compare to AEV.
- Relate in-situ pressures to the amount of swelling do gas pressures exceed overburden pressures
- Relate pressure to in-situ $c_u$, then compare to the equation presented by Kessel 1998 to see whether swelling was expected
- Relate pressures to gas migration. One could even extend the presented model based on Stone's equation and Darcy based on the pressures

Kesteren, Cornelisse, and Kessel 1998 modelled gas production in sludge. Based on linear elastic expansion theory, combined with crack initiation conditions and analysis on stress distributions in bubbles, gas behaviour was modelled. One could try to extend and apply the model to soft soil slurry's and validate with the results.

In this research the total swelling was calculated. A depth dependency was related to the swelling. A possible advise is to deposit marker layers during the deposition. This way the swelling over depth can be determined. For the described depositional method this will be difficult to achieve. A different depositional method is recommended. Possibly the usage of concrete-slurry pump can be utilized.

The results in this research were mostly focused on degree of compaction. The main parameter to estimate this was the density. As highlighted in this research a lot of uncertainties may present itself on this scale focusing on this parameter. Therefore it is recommended to validate results of the proposed method using a CPT after deposition and after compaction. Every test can be reliably compared and empirical relationships can be used to determine the relative density. This practice also narrowly connects to practice.

The compaction method has come a long way. From static loading to implementing vibrations. The next step is to compact in a similar way as the proctor test. The surcharge test simulated this in a sense, but a compaction method comparable to impact compaction is advised. This research scaled up the compaction method based on the vibratory table used by Stals 2020 and made the connection with a vibroflotation compaction method. However it makes more sense to connect the current hypothetical case to a lab test. As the hypothetical case presented the depth on which the proposed solution is applied will not be deeper than 7m. The most used compaction method for this depth range is impact compaction. Scaling down from this case one could opt to do the small scale tests with a compaction method representative of impact compaction. Not only does this comply better with reality it also

relates better to the the proctor test, from which this proposed method was derived. A further note on impact compaction method is related to the present residual amounts of gas in the treated tests. A flow problem does not necessarily have to be present in the case of impact compaction. In principle nitrogen is compressible. When a impact compaction is applied the nitrogen may possibly dissolve again in the pore water. However one could argue that over time the gas will nucleate and displace the entire soil body in a "looser" state again.

It was suggested that boundary conditions play a major role in the gas behaviour. One could opt to carry out similar tests with varying diameter and height. This way a better insight in the mechanisms of continuous gas phases and occluded gas bubbles can be attained.

During this research only one type of soil was experimented upon. In comparison to previous research, which yielded promising results, this soil had a higher clay content. It is recommended to vary soils.The optimum range of fines lies somewhere between 10 to 20%. The role of plasticity is not yet known. Furthermore it was not found out whether soil type was the reason the tests did not yield the same results as Stals 2020 or that the set up was not adequate for the aspired results. Small scale testing on the soil on which an actual the field trial will take place is highly recommended.

For future experiments in the lab it is recommended to scale down from the 2.5m experiments. The 2.5m experiments took a long time to prepare and each took a week before another test could be prepared. In this research relatively much work has been put in development and preparations of a test, resulting in initial conditions varying and standardization only becoming a factor in a late stage (engine 30 and 100 series). To put the amount of work into perspective: The amount of soil prepared in a container for a single 2.5m test could be as much as 700 kg with a density of 1850 kg/m$^3$. This corresponds to a volume of 380L. Considering 8L in each 1m test this would lead to more than 45 tests that can be prepared. With more tests and a standardized approach, a large data set can be produced where the reliability of the outcome drastically increases as both control and treated tests are in abundance. Furthermore different parameters can be more easily varied.

# References

[1] Pedro de Alba and Thomas P Ballestero. "Residual strength after liquefaction: A rheological approach". In: Soil Dynamics and Earthquake Engineering 26.2-4 (2006), pp. 143–151.

[2] G M Andrag. Compaction of silty sands through biogenic gas desaturation pretreatment. 2017. URL: http://repository.tudelft.nl/.

[3] Alberto Arab, Isam Shahrour, and Laurent Lancelot. "A laboratory study of liquefaction of partially saturated sand". In: Journal of Iberian Geology 37.1 (2011), pp. 29–36.

[4] Mounir Bouassida and Lassaad Hazzar. "Comparison between stone columns and vertical geodrains with preloading embankment techniques". In: paper 7 (2008), pp. 11–18.

[5] Delwyn G Fredlund and Hendry Rahardjo. Soil mechanics for unsaturated soils. John Wiley & Sons, 1993.

[6] Caitlyn A Hall et al. Techno-Economic Assessment of Liquefaction Mitigation by Microbially Induced Desaturation. 2022.

[7] J Hopman. Denitrification-based pretreatment for the compaction of silty sands. 2018. URL: http://repository.tudelft.nl/.

[8] Junbong Jang, Zhonghao Sun, and J Carlos Santamarina. "Capillary pressure across a pore throat in the presence of surfactants". In: Water Resources Research 52.12 (2016), pp. 9586–9599.

[9] Keller. Deep vibro techniques 10-02e brochure. n.d.

[10] T. Van Kessel. "Belinitiatie en Belgroei in Sliblagen.pdf". In: (1998).

[11] van Kesteren, J.C. Cornelisse, and T. Van Kessel. "Scheurvorming en gasvorming in slib". In: (1998).

[12] T Hamed Khodadadi et al. "Bio-grout materials: A review". In: Geotech. Spec. Publ (2017), pp. 1–12.

[13] Klaus Kirsch and Fabian Kirsch. Ground improvement by deep vibratory methods. Taylor & Francis, 2017.

[14] Nariman Mahabadi and Jaewon Jang. "Relative water and gas permeability for gas production from hydrate-bearing sediments". In: Geochemistry, geophysics, geosystems 15.6 (2014), pp. 2346–2353.

[15] Nariman Mahabadi, Xianglei Zheng, et al. "Gas bubble migration and trapping in porous media: pore-scale simulation". In: Journal of Geophysical Research: Solid Earth 123.2 (2018), pp. 1060–1071.

[16] QD Nguyen and DV Boger. "Measuring the flow properties of yield stress fluids". In: Annual Review of Fluid Mechanics 24.1 (1992), pp. 47–88.

[17] Peter G Nicholson. Soil improvement and ground modification methods. Butterworth-Heinemann, 2014.

[18] Mitsu Okamura and Yasumasa Soga. Effects of pore fluid compressibility on liquefaction resistance of partially saturated sand. 2006.

[19] Pham. Bio-based ground improvement through Microbial Induced Desaturation and Precipitation (MIDP). 2017. DOI: 10.4233/uuid:3997066a-0ad6-4de2-9c79-e5e474bae20f. URL: https://doi.org/10.4233/uuid:3997066a-0ad6-4de2-9c79-e5e474bae20f.

[20] VR Raju and W Sondermann. "Ground improvement using deep vibro techniques". In: Elsevier Geo-Engineering Book Series. Vol. 3. Elsevier, 2005, pp. 601–638.

[21] GJ Schotmeyer. "Stability of growing gas bubbles in sediments". In: GeoDelft report 373350/18 (1998).

[22] ASTM Committee D-18 on Soil and Rock. Standard Test Method for Particle-Size Distribution (Gradation) of Fine-Grained Soils Using the Sedimentation (Hydrometer) Analysis. ASTM International, 2009.

[23] ASTM Committee D-18 on Soil and Rock. Standard test methods for liquid limit, plastic limit, and plasticity index of soils. ASTM international, 2010.

[24] ASTM Committee D-18 on Soil and Rock. Standard test methods for particle-size distribution (gradation) of soils using sieve analysis. ASTM International, 2009.

[25] M Stals. Verdichten van siltig zand met behulp van een biologische voorbehandeling Bachelor scriptie. 2020.

[26] Karl Terzaghi, Ralph B Peck, and Gholamreza Mesri. Soil mechanics in engineering practice. John Wiley & Sons, 1996.

[27] Yoshimichi Tsukamoto et al. "Resistance of partly saturated sand to liquefaction with reference to longitudinal and shear wave velocities". In: Soils and foundations 42.6 (2002), pp. 93–104.

[28] T Van Kessel and WGM Van Kesteren. "Gas production and transport in artificial sludge depots". In: Waste Management 22.1 (2002), pp. 19–28.

[29] Jun Yang, Stavros Savidis, and Matthias Roemer. "Evaluating liquefaction strength of partially saturated sand". In: Journal of Geotechnical and Geoenvironmental Engineering 130.9 (2004), pp. 975–979.

[30] Elizabeth G. Stallings Young et al. "Microbial-Induced Desaturation in Stratified Soil Conditions". In: International Journal of Geosynthetics and Ground Engineering 7 (2 June 2021). ISSN: 21999279. DOI: 10.1007/s40891-021-00276-9.

[31] Chen Zeng et al. "Experimental and Numerical Analysis of a Field Trial Application of Microbially Induced Calcite Precipitation for Ground Stabilization". In: Journal of Geotechnical and Geoenvironmental Engineering 147 (7 July 2021), p. 05021003. ISSN: 1090-0241. DOI: 10.1061/(asce)gt.1943-5606.0002545.

# A
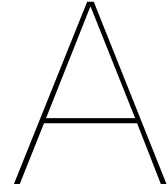
# Sieving analysis

This appendix includes the results of the sieve analysis.

Table A.1: Data grain size distribution for samples up,mid and low from big bag 6

| Grain size distribution BB6 | Samples | | |
|---|---|---|---|
| Sieve aperture ($\mu m$) | Up | Mid | Low |
| 2000 | 99.33% | 97.68% | 99.06% |
| 1000 | 98.84% | 96.76% | 98.29% |
| 500 | 96.17% | 93.73% | 94.89% |
| 250 | 74.87% | 73.07% | 74.74% |
| 125 | 38.80% | 38.26% | 36.05% |
| 63 | 17.67% | 17.29% | 16.95% |
| 33.4 | 11.79% | 12.27% | 12.54% |
| 21.7 | 10.96% | 10.77% | 11.23% |
| 12.7 | 9.64% | 10.02% | 9.48% |
| 9.1 | 9.02% | 9.35% | 9.26% |
| 6.5 | 8.67% | 8.90% | 8.75% |
| 3.2 | 7.63% | 7.44% | 7.73% |
| 1.4 | 6.18% | 6.28% | 6.34% |

Table A.2: Diameters corresponding to percentage passing, including Coefficients of uniformity and curvature

| | Sample | | |
|---|---|---|---|
| | Up ($\mu m$) | Mid ($\mu m$) | Low ($\mu m$) |
| $D_{90}$ | 409 | 441 | 423 |
| $D_{80}$ | 295 | 315 | 300 |
| $D_{70}$ | 228 | 235 | 230 |
| $D_{60}$ | 188 | 193 | 192 |
| $D_{50}$ | 155 | 158 | 160 |
| $D_{40}$ | 128 | 129 | 134 |
| $D_{30}$ | 94 | 95 | 101 |
| $D_{20}$ | 68 | 69 | 70 |
| $D_{10}$ | 10 | 10 | 10 |
| $C_u$ | 18.79 | 19.27 | 19.20 |
| $C_z$ | 4.70 | 4.72 | 5.27 |

$$B$$

# Measurements and calculations

This appendix includes the derivation of equation B.6. As this is the starting point of the calculations the derivation is given. Following this starting point the step wise procedure of calculations is presented. The initial mass of the system is defined as:

$$m_{ini,wet} = m_s + m_w + m_a \tag{B.1}$$

The mass of air was neglected as the mass of air was not significant for the calculation.

$$m_{ini,wet} = V_s * \rho_s + V_w * \rho_w \tag{B.2}$$

Knowing that:

$$V_{voids} = n * V_{tot} \,|\, V_w = S * V_{voids} \,|\, V_w = n * S * V_{tot} \tag{B.3}$$

and

$$Vs = (1 - n) * V_{tot} \tag{B.4}$$

$$m_{ini,wet} = (1 - n) * V_{tot} * \rho_s + n * S * V_{tot} * \rho_w \tag{B.5}$$

Rewriting gives:

$$n = \frac{\frac{m_{ini}}{V_{tot}} - \rho_s}{-\rho_s + S\rho_w} = \frac{\rho_s - \rho_{wet}}{\rho_s - S\rho_w} \tag{B.6}$$

## B.1. Initial situation

After placing the soil the first measurement considered the wet mass deposited in the tube. Secondly, with the resulting height of the slurry and the area of the tube, the volume of the slurry was determined. With these variables the wet density was calculated by:

$$\rho_{wet,ini} = \frac{m_{wet,ini}}{V_{wet,ini}} \tag{B.7}$$

During earlier trials the methodology of Stals 2020 was carried out. In his methodology a soil sample was taken of the slurry to determine the water content, and thus also the dry density.

For this methodology it was assumed that a small sample may not be representative as clumps of clay and/or rock could lead to a large error in the water content. Another approach was adopted to determine what the initial situation included. The following starting assumptions were made to be able to carry out the calculations:

(i) After deposition ànd settling the soil was fully saturated ($S_r = 1$)

(ii) The grain density ($\rho_s$) was assumed to be $2650\,kg/m^3$ and the density of water ($\rho_w$) $1000\,kg/m^3$

The initial porosity is calculated by:

$$n_{ini} = \frac{\rho_s - \rho_{wet}}{\rho_s - S\rho_w} \tag{B.8}$$

With the porosity known the initial water content was calculated:

$$w_{ini} = \frac{n_{ini} * \rho_w}{(1 - n_{ini}) * \rho_s} \tag{B.9}$$

The initial water content lead to the dry mass in the tube:

$$m_{dry} = \frac{m_{wet}}{1 + w_{ini}} \tag{B.10}$$

The dry mass was the most important variable that was calculated during the initial state. Using dry mass the dry density was could be calculated. Dry density excludes the amount of water in the sample, making it easy to compare results between tests. The calculations in the following paragraph can be looped and are based on the ones above. This is also the reason that they were separately discussed.

## B.2. Measurements and calculations during the experiment

During the experiment two variables were monitored manually, namely the height of the slurry and the height of the water column. The height of the water column lead to the mass of the water expelled. The new wet mass of the sample could be calculated as well as the new water content.

$$m_{wet,j} = m_{wet,j-1} - m_{expwater} \tag{B.11}$$

$$w_j = \frac{m_{wet,j} - m_{dry}}{m_{dry}} \tag{B.12}$$

The height of the slurry lead to both the dry and wet density at a certain time step. By either dividing the dry mass over the sample volume, or using the current water content.

$$\rho_{dry} = \frac{m_{dry}}{V_{sample,i}} = \frac{\rho_{wet,j}}{1 + w_j} \tag{B.13}$$

The dry density can be presented in terms of relative density. This way differences in densities over time were highlighted as the results are expressed in a set range (from 1267 g/cm3 to 1809 g/cm3):

$$RD = \frac{\rho_j - \rho_{min}}{\rho_{max} - \rho_{min}} \tag{B.14}$$

Additionally,the porosity was calculated:

$$n_j = 1 - (\frac{\rho_{dry,j}}{\rho_s}) \tag{B.15}$$

The void ratio was defined as:

$$e_j = \frac{n_j}{1 - n_j} \tag{B.16}$$

The saturation:

$$S_{r,j} = \frac{w_j * G_s}{e_j} \rightarrow S_g = 1 - S_r \tag{B.17}$$

Aside from manual measurements the TEROS12 sensors monitored the bulk conductivity and volumetric water content over time. The volumetric water content measured could be compared to the calculated water content. The volumetric water content was calculated using the water content as:

$$\Theta = n * S_r = \frac{e}{1 + e} * \frac{wG_s}{e} = w \frac{G_s}{1 + e} \tag{B.18}$$

# C
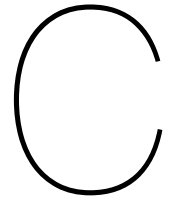
# Logbook

This appendix holds the logbook for all tests.

## Compaction rating

After each test a visual inspection of the results was performed. During the visual inspection the flange on the bottom was opened. In some cases the soil slurry came flowing out in other cases it was able to remain its shape. In order to give a qualitative analysis of the visual inspection table C.1 was created. This chart is based on the maximum and minimum results that were encountered. A "well compacted" soil does not represent a specific density, nor the maximum relative density of the soil.

Table C.1: Compaction grading

| Term | Explanation | Mark |
|---|---|---|
| Well compacted | The soil is able to remain its shape, or slightly deforms | 8-10 |
| Medium compacted | The soil is not able to remain its shape, but does not flow out | 6-8 |
| Weakly compacted | Some structure, soil does flow out. Often a foamy consistency where small gas bubbles are still present in the soil | 3-6 |
| Slurry | No structure, water like behaviour | 0-3 |

## 15 cm series

| | |
|---|---|
| Date start/end: | 10-03-2022 22-03-2022 |
| Conditions | • Target saturation 50%<br>• Nutrients: 5.30 g/L Ac and 6.35 g/L Nit. 1.5 L of water used on 10 kg of soil.<br>• No inoculum used<br>• Test set up: Three 15 cm cylinders, same set up as Stals 2020.<br>• Compaction method: Vibrating table, 8 min continuously. Amplitude 0.3 mm.<br>• Drainage before compaction |
| Visual inspection |  |

Samples after 10 days, left U1. Right T2 and T1

| | |
|---|---|
| Compaction rating | Slurry |
| Observations | • Rocks/cobbles clogged the deposition process, initial densities differed<br>• Cylinder T2 experienced leakage<br>• Lag period more than 5 days, old soil and no inoculum<br>• Little to no gas bubbles after desaturation process, again old soil and no inoculum<br>• Little to no swelling of the treated samples |
| Sampling results | • Initial water content U1: 0.37<br>• Initial Water content T1/T2: 0.45 |

## SH1 series

| | |
|---|---|
| Date start/end: | 21-03-2022 to 08-04-2022 |

| | |
|---|---|
| Conditions: | • Target saturation: 50%<br>• Nutrients: 5.8 g/L Ac and 6.89 g/L Nit. 2.5 L water used. 14.4 g of Ac and 17.23 g Nit<br>• No inoculum used<br>• Test set up: Three 1m cylinders.<br>• Deposition method: Tilting cylinder and pouring slurry in<br>• U1 had a thicker slurry upon deposition than T1/T2. U1 soil to water ratio 10kg:2.5L. T1/T2 soil to water ratio 10kg:2L<br>• Compaction method: Small vibrating needle inserted in the cylinder<br>• No drainage before compaction |

| | |
|---|---|
| Visual inspection | <br>Bulging of sealing cap (left). Gas distribution in sample T2 (upper part middle and lower part right) |

| | |
|---|---|
| Compaction rating | Slurry |
| Observations | • More settling observed for T1 and T2 than U1<br>• Desaturation process good, homogeneous gas distribution with no depth gradient.<br>• Sealing cap on top started bulging outwards, venting of gas out of sample<br>• Compaction method was trial and error based, results may be sensitive to large errors<br>• During compaction water was reintroduced to system, back to initial situation slurry like consistency<br>• A lot of spillage, energy too much for sample, again error increases<br>• The densities did not increase significantly. Additionally, using a ruler was inserted in each tube. The density was then estimated based on resistance. For T1 the density was highest, for U1 and T2 the density based on feel was more or less the same. |

# SH2 series

| | |
|---|---|
| Date start/end: | 21-03-2022 to 08-04-2022 |

| | |
|---|---|
| Conditions: | <ul><li>Target sat 0%</li><li>Nutrients: Nutrients: 11.6 g/L Ac and 13.78 g/L Nit. 2.5 L water used. 29 g of Ac and 34.45 g Nit</li><li>Inoculum was used</li><li>Test set up: Three 1m cylinders.</li><li>Depositional method: Tilting cylinder and pouring slurry in</li><li>EC sensor in each cylinder</li><li>Compaction method: Small needle held against tubes from the side, non intrusive. Vibrating for 5 min continuously</li><li>Drainage before compaction</li></ul> |

Visual inspection



Visual inpsection of samples after compaction. Untreated sample left and right the result of a treated sample

| | |
|---|---|
| Compaction rating | Treated samples: Well compacted, Untreated sample medium compacted |
| Observations | <ul><li>Initial densities similar, especially after settling.</li><li>Desaturation process good, however saturation after reaction phase similar to target saturation 50%. No need for extra nutrients</li><li>Controlled compaction method. Almost all gas able to get out of the system</li><li>Densities of treated samples higher than untreated sample</li></ul> |

## SSt3 series

| Date start/end: | |
| --- | --- |
| Conditions: | • Target sat 50% for T1 and 0% for T2<br>• Nutrients:<br>• Inoculum was used<br>• Test set up: Three 1m cylinders.<br>• Depositional method: Wet pluviation method. Soil to water ratio 1kg :1L<br>• EC sensors in<br>• Not compacted |
| Visual inspection |  |
| Observations | • Gas production only occured below the silt layer<br>• No difference in gas volume produced based on visual inspection |

## U16%N

| | |
|---|---|
| Date start/end: | 26-04-2022 to 03-05-2022 |

| | |
|---|---|
| Conditions: | <ul><li>Test set up: Single 2.5m cylinder</li><li>Depositional method: Using big bag and dispenser</li><li>Compaction method: Large needle inserted in the tube from the top. Vibrating strategy was still trial and error. Vibrated until point of no change 10 min continuously</li><li>Drainage before compaction</li></ul> |

| | |
|---|---|
| Visual inspection: |  |

| | |
|---|---|
| Compaction rating | Medium to weakly compacted |
| Observations | <ul><li>Loss of soil on the ground during deposition, mass in tube has a large error and thus densities as well</li><li>Compaction did not increase density.</li></ul> |

# T16%N1

| | |
|---|---|
| Date start/end: | 04-05-2022 to 11-05-2022 |

| | |
|---|---|
| Conditions: | <ul><li>Target saturation 50%</li><li>Nutrients: 1400g Ac and 1700g Nit</li><li>Compaction method: Large needle inserted from the top. Vibrated and moved around needle until no bubbles came out, 20 min continuously.</li><li>Drainage before compaction</li></ul> |

| | |
|---|---|
| Visual inspection |  |

| | |
|---|---|
| Compaction rating | Well compacted |
| Observations | <ul><li>Spillage during deposition, 2 mA (125 kg) error is possible</li></ul> |

## T16%N2

| Date start/end: | 17-05-2022 to 23-05-2022 |
|---|---|

| Conditions: | • Target saturation 35%<br>• Nutrients: 1850g Ac and 2250g Nit<br>• Inoculum used<br>• Drainage before compaction<br>• Compaction method: Large needle inserted from the top. Compacted for 15 min continuously, stopped vibrating prematurely. Bubbles were still surfacing |
|---|---|

| Visual inspection |  |
|---|---|

| Compaction rating | medium compacted |
|---|---|

| Observations | • Not fully compacted. Still a lot of gas in the system<br>• The initial density after settling differed more than 200 kg/m3 compared to the untreated test of the same series. |
|---|---|

Sample results

Table C.2: Sample results T16N2, sample rings were taken after compaction and taken from the bottom where the flange was opened

| number | container (g) | wet (g) | dry | wc | rhowet g/cm3 | rhodry | RD |
|---|---|---|---|---|---|---|---|
| 1 | 9.8 | 481.56 | 391 | 24% | 1.887 | 1.525 | 48% |
| 2 | 9.87 | 491.5 | 399.5 | 24% | 1.927 | 1.559 | 54% |
| 3 | 9.82 | 521.88 | 424 | 24% | 2.048 | 1.657 | 72% |
| !4 | 9.82 | 500.94 | 401 | 26% | 1.964 | 1.565 | 55% |
| 5 | 9.81 | 507.56 | 408.5 | 25% | 1.991 | 1.595 | 60% |
| 6 | 9.81 | 518 | 420.5 | 24% | 2.033 | 1.643 | 69% |
| 7 | 9.67 | 479 | 382 | 26% | 1.877 | 1.489 | 41% |
| Averages | | | | 24% | 1.961 | 1.576 | 57% |

## U16%30 (explosion)

| Date start/end: | 30-05-2022 to 30-05-2022 |
| --- | --- |
| Observations | • The PVC dispenser was too long, in order to get the pvc tube in the cylinder too much tension was put on the big bag. This resulted in the big bag ripping open and covering the entire lab in slurry. In future tests the base plate of the dispenser was put in the big bag instead of outside in contrast to the manual of the Raimo dispenser. |

## U16%30

| Date start/end: | 01-06-2022 to 02-06-2022 |
|---|---|
| Conditions: | • Compaction method: Engine on 30% of power. The engine was put on for four intervals of 30s whereafter the engine was left on for 2 min continuously |

| Visual inspection |  |
|---|---|

| Compaction rating | Medium to Weakly compacted |
|---|---|
| Observations | • First time, using the engine |

Sample results

Table C.3: Sample results U1630, sample rings were taken after compaction and taken from the bottom where the flange was opened

| Samples | container (g) | wet (g) | dry (g) | wc | rhowet g/cm3 | rhodry | RD |
|---|---|---|---|---|---|---|---|
| Akkerbuis | 437.6 | 3414.37 | 2821.49 | 25% | 2.143 | 1.716 | 83% |
| Steekring (100ml) | 9.74 | 213.22 | 174.82 | 23% | 2.035 | 1.651 | 71% |

# T16%30

| Date start/end: | 03-06-2022 to 09-06-2022 |
|---|---|

| Conditions: | <ul><li>Target saturation 50%</li><li>Nutrients: 1400g Ac and 1700g Nit</li><li>Compaction method: Engine on 30% of power. Engine put on for four intervals of 30s and one interval of 2 min continuously</li><li>Drainage before compaction</li></ul> |
|---|---|

| Visual inspection |  |
|---|---|

| Compaction rating | slurry to weakly compacted |
|---|---|

| Observations | <ul><li>Came out flowing after opening</li><li>Had been standing for 5 days before opening tube</li><li>Smelled like manure, it was suggested that this was degrading biomass</li></ul> |
|---|---|

Sample results

Table C.4: Samples T1630

**3 steekringetjes gemeten vanaf onderkant**

|  | height | l | n | rhowet | rhodry | n | e | S |
|---|---|---|---|---|---|---|---|---|
| onder | 10.00 | 102.78 | 276.67 | 1.739 | 1.382 | 0.48 | 0.92 | 0.75 |
| mid | 85.00 | 100.25 | 285.54 | 1.853 | 1.433 | 0.46 | 0.85 | 0.91 |
| high | 140.00 | 103.01 | 277.05 | 1.740 | 1.354 | 0.49 | 0.96 | 0.79 |

**3 steekringetjes water content (andere container)**

|  | l | n | d | wc |
|---|---|---|---|---|
| onder | 1.92 | 166.38 | 132.60 | 0.26 |
| mid | 1.92 | 176.38 | 136.81 | 0.29 |
| high | 1.92 | 170.24 | 132.85 | 0.29 |

# T16%100

| Date start/end: | 14-06-2022 to 21-06-2022 |
|---|---|

| Conditions: | <ul><li>Target saturation 50%</li><li>Nutrients: 1600g Ac and 2000g Nit</li><li>Compaction method: Engine with 100% of available power. Three intervals of 30s.</li><li>Drainage before compaction</li></ul> |
|---|---|

| Visual inspection |  |
|---|---|

| Compaction rating | Well compacted |
|---|---|

Sample results

Table C.5: Samples T16100

| | H (cm) | net wet mass | rhowet | l | n | d | wc | rhodry | RD | n | e | S |
|---|---|---|---|---|---|---|---|---|---|---|---|---|
| pvc1 | 5 | 200.9 | 2.009 | 1.92 | 200.3 | 167.4 | 0.20 | 1.676 | 0.75 | 0.37 | 0.58 | 0.91 |
| pvc2 | 30 | 191.1 | 1.911 | 1.92 | 115.5 | 92.8 | 0.25 | 1.529 | 0.48 | 0.42 | 0.73 | 0.90 |
| pvc3 | 50 | 192.9 | 1.929 | 1.92 | 127.1 | 100.4 | 0.27 | 1.518 | 0.46 | 0.43 | 0.75 | 0.96 |
| pvc4 | 70 | 196.6 | 1.966 | 1.92 | 104.7 | 81.6 | 0.29 | 1.524 | 0.47 | 0.42 | 0.74 | 1.04 |
| pvc5 | 90 | 192.3 | 1.923 | 1.92 | 89.9 | 69.6 | 0.30 | 1.479 | 0.39 | 0.44 | 0.79 | 1.00 |
| pvc6 | 106 | 196.2 | 1.962 | 1.92 | 100.1 | 75.2 | 0.34 | 1.464 | 0.36 | 0.45 | 0.81 | 1.11 |

| | H ongeveer | l | n | d | wc | rhowet | rhodry | RD | | n | e | S |
|---|---|---|---|---|---|---|---|---|---|---|---|---|
| 1steek | onder in cylinder | 9.3 | 461.6 | 389.9 | 0.19 | 1.8092 | 1.522 | 0.47 | | 0.43 | 0.74 | 0.67 |
| 2steek | ook onder | 213.3 | 704.7 | 627 | 0.19 | 1.9656 | 1.655 | 0.72 | | 0.38 | 0.60 | 0.83 |
| 3steek | slurry | 216.3 | 706.6 | 604.6 | 0.26 | 1.9612 | 1.553 | 0.53 | | 0.41 | 0.71 | 0.99 |
| 4steek | slurry | 209.3 | 705.7 | 594.2 | 0.29 | 1.9856 | 1.540 | 0.50 | | 0.42 | 0.72 | 1.06 |

# U16%100

| | |
|---|---|
| Date start/end: | 04-05-2022 to 11-05-2022 |
| Conditions: | • Target saturation 50%<br>• Nutrients: 1400g Ac and 1700g Nit<br>• Compaction method:<br>• Drainage before compaction |
| Visual inspection |  |
| Compaction rating | Weakly compacted |
| Observations | •<br>• |
| Sample results | |

Table C.6: Samples U16100

| height (0 is bottom) | l | n | d | rhowet [kg/m3] | wc | rhodry | d (after 63 mu) | fines |
|---|---|---|---|---|---|---|---|---|
| 0 | 9.4 | 370.8 | 301.72 | 1849 | 0.23 | 1496 | 255.88 | 0.152 |
| 35 | 9.4 | 373.4 | 292.08 | 1982 | 0.29 | 1539 | 248.95 | 0.148 |
| 120 | 9.4 | 344.6 | 264.97 | 1831 | 0.31 | 1396 | 221.72 | 0.163 |

# T16%100.2

| | |
|---|---|
| Date start/end: | 04-05-2022 to 11-05-2022 |

| | |
|---|---|
| Conditions: | <ul><li>Target saturation 50%</li><li>Nutrients: 1400g Ac and 1700g Nit</li><li>Compaction method:</li><li>Drainage before compaction</li></ul> |

| | |
|---|---|
| Visual inspection |  |

| | |
|---|---|
| Compaction rating | Weakly compacted, almost slurry |
| Observations | <ul><li></li><li></li></ul> |

# T16%100.sur

| Date start/end: | 04-05-2022 to 11-05-2022 |
|---|---|

**Conditions:**
- Target saturation 50%
- Nutrients: 1400g Ac and 1700g Nit
- Compaction method: Engine put on 100% of power. Three intervals of 30s
- Drainage before compaction

**Visual inspection**



| Compaction rating | On one side weakly compacted to slurry like. On the other side medium compacted |
|---|---|

**Observations**
- At the drain side the sample seemed more compacted compared to the opposite side. A radial gradient in terms of density was present.
- At the top the sample held less gas than at the bottom.
- The density seemed to increase with height. A depth gradient was also present. Where the top had a higher density than the bottom.

**Sample photo**

# T16%100.sur

Sample results

Table C.7: Samples T16100 sur

| Sample rings | | l | n | d | deksel | wc | rhowet | rhod | RD |
|---|---|---|---|---|---|---|---|---|---|
| 1 | small ds | 9.4 | 305.9 | 171.02 | 101.9 | 0.20 | 2040 | 1694 | 78.83% |
| 2 | ds1 | 9.3 | 494.2 | 402.42 | 214.8 | 0.23 | 1976.8 | 1603 | 61.93% |
| 3 | ds2 | 9.3 | 524 | 435.81 | 221.7 | 0.21 | 2096 | 1737 | 86.69% |
| 4 | ws1 | 9.3 | 498.3 | 397.01 | 221.2 | 0.26 | 1993.2 | 1580 | 57.81% |
| 5 | ws2 | 9.3 | 508.6 | 408.75 | 215.3 | 0.25 | 2034.4 | 1628 | 66.52% |

| PVC | h (cm) | l | n | d | | wc | | | RD |
|---|---|---|---|---|---|---|---|---|---|
| | | | | | | | | | 70.36% |
| 1 | 10 | 9.4 | 188.5 | 152.67 | | 0.25 | 1885 | 1508 | 44.45% |
| 2 | 20 | 9.4 | 196.2 | 156.19 | | 0.27 | 1962 | 1542 | 50.69% |
| 3 | 30 | 9.4 | 194 | 154.21 | | 0.27 | 1940 | 1522 | 47.02% |
| 4 | 40 | 9.4 | 193 | 154.48 | | 0.27 | 1930 | 1525 | 47.62% |
| 5 | 50 | 9.4 | 194 | 157.67 | | 0.25 | 1940 | 1558 | 53.73% |
| 6 | 60 | 9.4 | 199.6 | 162.89 | | 0.24 | 1996 | 1611 | 63.42% |
| 7 | 70 | 9.4 | 203.6 | 168.24 | | 0.22 | 2036 | 1665 | 73.48% |
| 8 | 80 | 9.4 | 203.5 | 167.81 | | 0.23 | 2035 | 1661 | 72.66% |
| 9 | 90 | 9.4 | 205.3 | 169.41 | | 0.22 | 2053 | 1677 | 75.62% |
| 10 | 100 | 9.4 | 199.1 | 165.56 | | 0.21 | 1991 | 1639 | 68.63% |
| 11 | 110 | 9.4 | 197.4 | 164.77 | | 0.21 | 1974 | 1631 | 67.23% |

# D
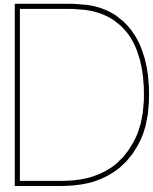
# Height over time

The most straightforward way to present the results is the height over time. For each test the height at a certain stage is plotted. It must be noted that comparing different tests with each other may lead to a wrong comparison. Initial densities may differ, meaning that an equal height between tests does not represent the same degree of compaction. Therefore the plots should be read per test only. Tests of the same series are presented in the same plot however.
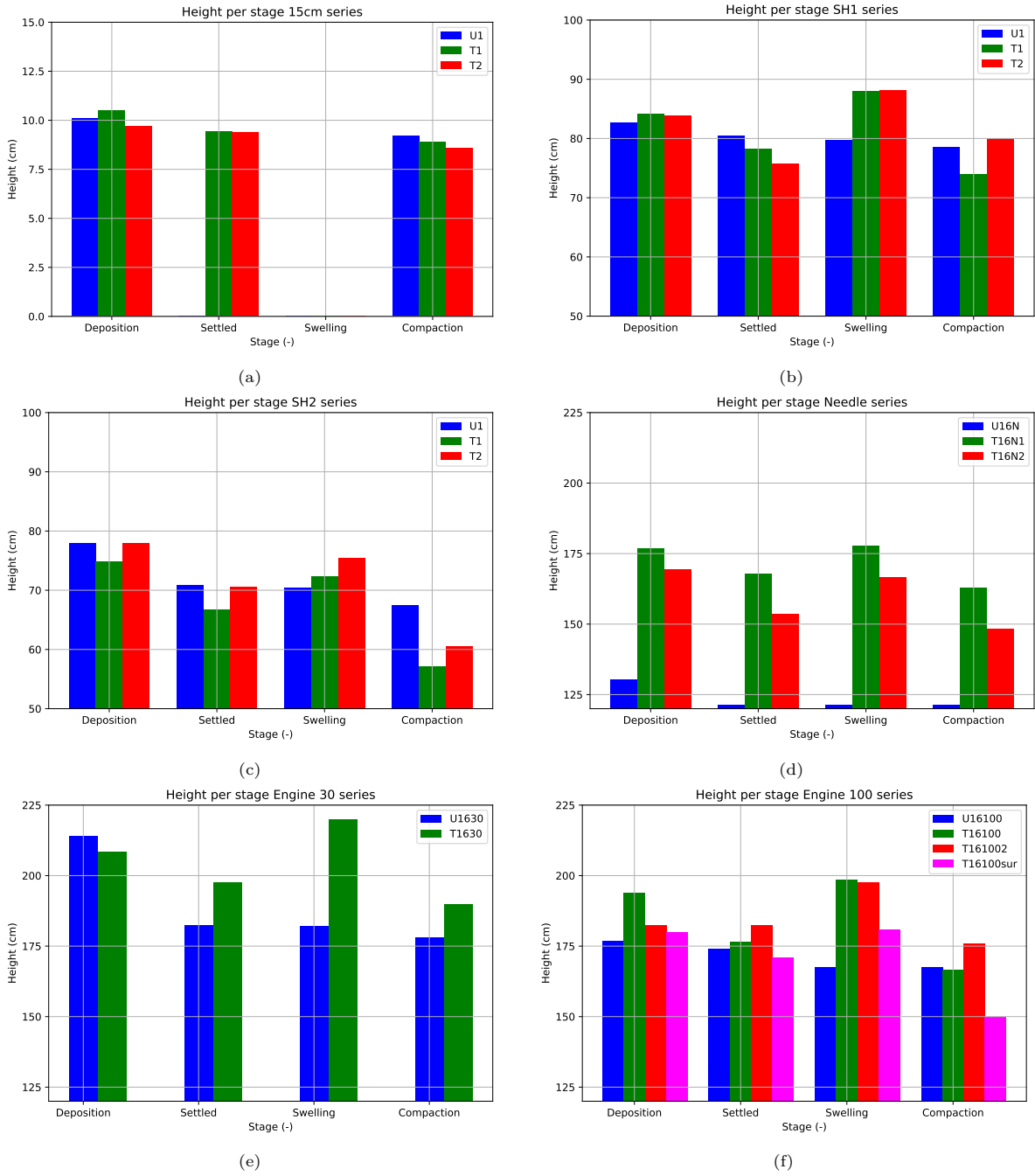
Figure D.1: Height per stage

# E
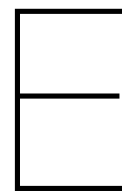
# Timelapse T161002

This chapter holds highlights of a produced timelapse. The photo's of the timelapse are edited with arrows that denote the water level (blue arrows) and the soil slurry level (red arrows). Timelapses of test series engine 30 and engine 100 are also available upon request.

(a) Initial situation

(b) After settling

(c) Water expulsion

(d) Start swelling

(e) Swelling continued

(f) Swelling maximum

(g) Venting of sample

(h) Venting continued
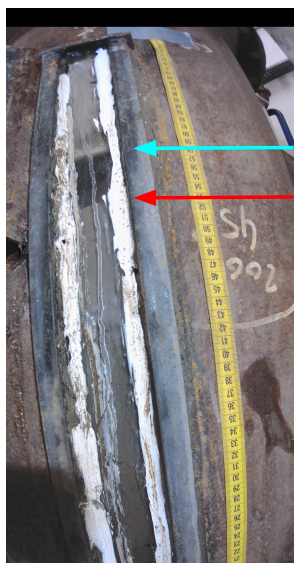
(i) Situation before compaction

Figure E.1: Highlights timelapse test T16100.2

# F

# Vibrating engine

The specifications of the vibrating engine are given in this appendix.

**BRECON**
smart vibration technology

## BRECON external vibrator - BIG series

Type: 18 151 102
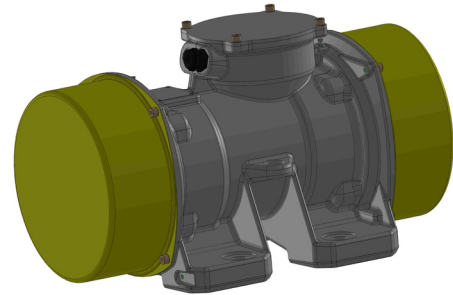
## Technical Data

| | |
|---|---|
| Centrifugal force [kN] | 39,2 |
| Working moment [kN] | 316 |
| Frequency [Hz] | 50 |
| Rotational speed [rpm] | 1.500 |
| Voltage 3 ~ [V] | 220-240/380-415 |
| Power [kW] | 2,40 |
| Nominal current [A] | 8,70/5,00 |
| Protection | IP 65 |
| Weight [kg] | 118,0 |
| Comments | without cable |

## Dimensions

| | |
|---|---|
| External dimensions [mm] L x B x H | 568 x 330 x 331 |
| Length of the base g [mm] High of the base h [mm] Width of the base e [mm] | 360 35 330 |
| Mounting pattern [mm] Distance between bolts l Distance between bolts b Diameter of the drills d | 155 255 4x Ø25 |
| Heigth of the shaft m [mm] | 150 |

## Schema



**BRECON Vibrationstechnik GmbH - smart vibration technology**
Stolberger Straße 393 · 50933 Cologne · Germany
Phone: +49 221 9544270 · Fax: +49 221 9544277
www.brecon.de · info@brecon.de

# G
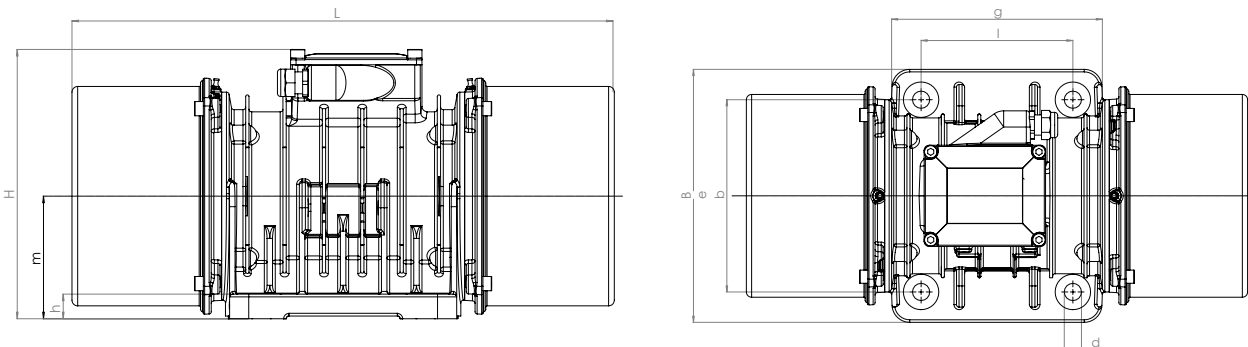
# Kinetic Batch model

```python
import numpy as np
import math as m
import matplotlib.pyplot as plt

#%%
def fluxdepth(z,A,K,pc):
    rhow=1000                               #density water
    dz=0.01                                 #discretization distance =1cm
    zvec=np.arange(0,z,dz)                  #depth vector discretized on 1cm
    pwvec=zvec*rhow*9.81/(100000)           #water pressure at each depth
    dH=pwvec+pc                             #pressure difference at each depth
    Fluxes=np.zeros(len(dH))
    for i in range(len(dH)):
        Fluxes[i]=K*A*dH[i]*dz*10*1000*3600#flux dependent on gas conductivity and pressure difference at specific depth
    Totflux=sum(Fluxes)
    return Totflux


###################################INPUT VARIABLES #####################################

# Initial concentrations per kg solvent (water) in:
NO3_ini = 0.06                              #Nitrate  mol/kg (M)
X_0     = 0.0001                            #Biomass  mol/kg (M)
N2_0    = 0.00052                           #Nitrogen mol/kg (M)


r_0     = 0.09                             #mol/(kg.X.hr) #Initial rate of reaction
K_h     = 0.00065                          #mol/(kg.bar) Henry's constant for nitrogen
dt      = 1                                #hr timestep
patm    = 1                                #bar pressure of atmosphere
pN2     = 0.8                              #Partial pressure nitrogen in air

Y_N2    = 0.40                            #[mol-N2/mol-NO3] coefficient max growth, stoichiometry
Y_X     = 1.00                            #[mol-Biomass/mol-NO3] coefficient max growth, stoichiometry
Km      = 0.02                            #[mol kg-1] condition
kLA     = 0.10                            #[hr-1]

zw      = 1                               #[m] water depth
rho_w   = 1000.00                         #[kg/m3] density water
pw      = zw*rho_w*9.81/(100000)          #[bar] water pressure
sigma   = 0.074                           #[N/m] surface tension water
r_bubble= 1.00E-04                        #[m] radius bubble, assumed
pc      = ((2*sigma)/r_bubble)/100000     #[bar] capillary pressure
pg      =  pc+pw+patm                     #[bar]gas pressure


CN2_hen = K_h*pg                         #[molkg-1] concentration of nitrogen (based on henry)
T       = 273                            #[K] Temperature
R       = 8.31                           #[J/mol K] Gas constant
rho_d   = 1200                           #[kg/m-3] Dry density (from tests)
rho_s   = 2650                           #[kg/m-3] Grain density
n       = 1-rho_d/rho_s                  #[-] porosity
Vs      = 1-n                            #[m3-S/m3-T] Volume solids per
Vw      = n                              #[m3-w/m3-T]

Sw_tres = 0.80                           #Saturation at which venting starts (based on observations)
Kws     =5.65E-07                        #[m/s] average saturated hydraulic conductivity
Kgs     =Kws*10                          #[m/s] average saturated gas conductivity (reference?)
ng      =2.00                            #[-] power Stone's equation (reference van leon)
Srg     =0.10                            #[-] Residual gas saturation
Srw     =0.10                            #[-] Residual water saturation
```

```
r_cyl    =0.25                                        #Radius of set up cylinder
A        = m.pi*r_cyl**2                              #[m^2] Area 2.5m cylinder


######################################INITIALIZE CONCENTRATION VECTORS#########################################


t_hr=np.arange(0,351,dt)                              #time in hours (arbitrary number)
t_day=t_hr/24                                         #time in days
NO3=np.zeros(len(t_hr))                               #[mol/kg] Vector with concentrations of nitrate
X=np.zeros(len(t_hr))                                 #[mol/kg] Vector with concentrations of biomass
r=np.zeros(len(t_hr))                                 #[mol No3/hr] Vector with the rate over time, this changes because biomass grows
N2_aq=np.zeros(len(t_hr))                             #[mol/kg] Vector with concentrations of nitrogen dissolved in water
CdiffN2=np.zeros(len(t_hr))                           #[mol/kg] Vector with concentration difference based on henry's law
r_gt=np.zeros(len(t_hr))                              #[mol/(kg*hr)]Vector with gas transfer over time
N2_gas=np.zeros(len(t_hr))                            #[mol/kg] Vector with concentrations of nitrogen in gas state
Sw=np.zeros(len(t_hr))                                #Vector with water saturations


for i in range(len(t_hr)):
    if i==0:
        NO3[i]=NO3_ini
        X[i]=X_0
        r[i]=r_0*X[i]*NO3[i]/(Km+NO3[i])
        N2_aq[i]=N2_0
        N2_gas[i]=0                                   #Initially no gas in sample
        CdiffN2[i]=N2_aq[i]-CN2_hen
        if CdiffN2[i]>0: r_gt[i]=CdiffN2[i]*kLA
                                                      #calculate concentration of gas transport
        else: r_gt[i]=0                               #Note only one way is forced. Gas does not dissolve again
                                                      #if according to henry gas will dissolve then gas tranport is zero
    else:
        NO3[i]=NO3[i-1]-(dt*r[i-1])                   #calculate next nitrate concentration based on current rate
        X[i]=X[i-1]+(dt*r[i-1]*Y_X)                   #calculate next biomass concentration based on current rate and stoichiometry
        r[i]=r_0*X[i]*NO3[i]/(Km+NO3[i])             #calculate rate based on calculated nitrate and biomass
                                                      #use Km to create a dampening effect
        N2_aq[i]=N2_aq[i-1]+r[i-1]*dt*Y_N2-r_gt[i-1]#Concentration of nitrogen in water based on current rate, gas transport and

        CdiffN2[i]=N2_aq[i]-CN2_hen
        if CdiffN2[i]>0: r_gt[i]=CdiffN2[i]*kLA
        else: r_gt[i]=0
        N2_gas[i]=N2_gas[i-1]+r_gt[i]*dt


#################################SATURATIONS VENTING AND SWELLING#####################

Vgvw=np.zeros(len(t_hr))
Vgvent=np.zeros(len(t_hr))                            #Volume vented gas/kg
Vgoccl=np.zeros(len(t_hr))                            #Volume occluded gas/kg
Sw=np.zeros(len(t_hr))                                #water saturation
Sg=np.zeros(len(t_hr))                                #gas saturation
Kg=np.zeros(len(t_hr))                                #[m/s] gas conductivity
Jg=np.zeros(len(t_hr))                                #[L/hr] Flux out of system

Vgvw=(N2_gas*R*T)/(pg*100000)*1000                    #[L/kg] Ideal gas law nRT/P=V note n= in mol/kg
Sw[0]=1                                               #Initially fully saturated
Vgoccl[0]=Vgvw[0]-Vgvent[0]                           #Occluded gas is difference between total and vented


for i in range(len(t_hr)-1):
    Vgoccl=Vgvw-Vgvent
    Sw[i+1]=1-Vgoccl[i]/(1+Vgoccl[i])                 #The next water saturation from the occluded gas
    Sg=1-Sw#the gas saturation

    if Sg[i]<Srg:                                     #if gas saturation is lower than residual gas then no gas
        Kg[i]=0
    else:
        Kg[i]=Kgs*((Sg[i]-Srg)/(1-Srw))**ng          #gas conductivity based on Mod. Stone's equation
    #Jg[i]=Kg[i]*A*(pg-patm)*10*1000*3600             #flux dependent on gas conductivity and
                                                      #pressure difference at specific depth
    Jg[i]=fluxdepth(zw,A,Kg[i],pc)
    Vgvent[i+1]=Jg[i]*dt+Vgvent[i]                    #Amount of gas vented based on flux

Swell=Vgoccl*Vw




##########################################PLOTTING#############################################

fig1,ax1=plt.subplots()
ax1.plot(t_day[:-1],Swell[:-1]*100)
ax1.set(title="Swelling over time",
        xlabel="Time [days]",
```

```
            ylabel="Swelling [%]")

fig2,ax2=plt.subplots()
ax2.plot(t_day[:-1],Vgvw[:-1]*100,label="Vgvw")
ax2.plot(t_day[:-1],Vgvent[:-1]*100,label="Volume gas vented")
ax2.plot(t_day[:-1],Vgoccl[:-1]*100, label="Volume gas occluded")

ax2.set(title="Gas volumes over time",
        xlabel="Time [days]",
        ylabel="[%]")
ax2.legend()

fig3,ax3=plt.subplots()
ax3.plot(t_day[:-1],Kg[:-1])
ax3.set(title="Gas conductivity over time",
        xlabel="Time [days]",
        ylabel="Gas conductivity [m/s]")

fig4,ax4=plt.subplots()
ax4.plot(t_day[:-1],NO3[:-1] ,label="Nitrate")
ax4.plot(t_day[:-1],N2_aq[:-1],label="N2 dissolved")
ax4.plot(t_day[:-1],N2_gas[:-1],label="N2 gas")
ax4.plot(t_day[:-1],X[:-1],label="Biomass")
ax4.legend(loc=4)

ax4.set(title="Gas conductivity over time",
        xlabel="Time [days]",
        ylabel="Concentration per kg solvent (water) [mol/kg]")

fig5,ax5=plt.subplots()
ax5.plot(t_day[:-1],Sg[:-1]*100 ,label="Gas saturation")
ax5.plot(t_day[:-1],Sw[:-1]*100,label="Water saturation")

ax5.set(title="Saturation over time",
        xlabel="Time [days]",
        ylabel="Saturation [%]")
ax5.legend()


NO3norm=NO3*((11-3)/0.06)+3

fig4,ax4=plt.subplots()

ax11=ax4.twinx()
ax4.plot(t_day[:-1],NO3[:-1] ,label="Nitrate")
ax11.plot(t_day[:-1],NO3norm[:-1])


ax11.set_ylabel('Normalised for sat extract [mS/cm]')

ax4.plot(t_day[:-1],N2_aq[:-1],label="N2 dissolved")
ax4.plot(t_day[:-1],N2_gas[:-1],label="N2 gas")
ax4.plot(t_day[:-1],X[:-1],label="Biomass")
ax4.legend(loc=1)
ax4.grid()

ax4.set(title="Nitrate over time normalised for sat ext",
        xlabel="Time [days]",
        ylabel="EC [mS/cm]")
ax4.set_xticks(np.arange(min(t_day),max(t_day)+1,1))


fig33,ax33=plt.subplots()

ax33.plot(Sg,Kg)
ax33.set(title="k v sat",
        xlabel="satg []",
        ylabel="krel []")
ax33.legend()


fig1.savefig("Swell v time.pdf",format='pdf')
fig2.savefig("Gas vol v time.pdf",format='pdf')
fig3.savefig("Cond v time.pdf",format='pdf')
fig5.savefig("Sat v time.pdf",format='pdf')
fig4.savefig("Nit v time norm.pdf", format="pdf")
```